Aus der

Universitätsklinik für Allgemeine, Viszeral- und Transplantationschirurgie

Positive effect of obesity on rapamycin-induced prolongation of allograft survival associated with induction of myeloid-derived suppressor cells and regulatory T cells

Inaugural-Dissertation

zur Erlangung des Doktorgrades

der Medizin

der Medizinischen Fakultät

der Eberhard Karls Universität

zu Tübingen

vorgelegt von

Deißler, Astrid Alena

2022

Dekan:	Professor Dr. B. Pichler
1. Berichterstatter:	Professor Dr. A. Königsrainer
2. Berichterstatter:	Professor Dr. U. Settmacher
3. Berichterstatter:	Privatdozentin Dr. M. Witte

Tag der Disputation: 19.09.2022

Contents

List of figures 7

List of tables 9

List of abbreviations 10

1. Introduction 13

1.1 Clinical background 13

1.1.1 Obesity 13

1.1.2 Clinical impact of obesity in transplantation medicine 14

1.2 Cells involved in the immune response 14

1.2.1 MDSCs 14

1.2.1.1 Subsets of MDSCs 15

1.2.1.2 Origin and generation of MDSCs 16

1.2.1.3 Immunosuppressive activity of MDSCs 18

1.2.2 T cells 19

1.2.2.1 Th1 cells 21

1.2.2.2 Th2 cells 21

1.2.2.3 Th17 cells 22

1.2.2.4 Tregs 22

1.2.3 Macrophages 23

1.2.3.1 M1 macrophages 23

1.2.3.2 M2 macrophages 24

1.2.3.3 M2-like macrophages 25

1.3 Effect of obesity on the immune response 25

1.3.1 Obesity-related chronic inflammation 25

1.3.2 Effect of obesity on an alloimmune response 28

1.4 Post-transplantation immunosuppressive therapy with rapamycin 28

1.4.1 Rapamycin’s mechanisms of action 29
1.5 Aim of the study and experimental approach 31
2. Materials and methods 32
2.1 Outline of the experimental approach 32
2.2 Animals 32
2.3 Materials 32
2.3.1 Reagents, enzymes and proteins 32
2.3.2 Consumables 33
2.3.3 Drugs and diets 34
2.3.4 Cell culture medium, supplements and buffers 34
2.3.5 Kits 35
2.3.6 Antibodies used for flow cytometric analyses 36
2.3.7 Primers for qPCR 37
2.3.8 Laboratory equipment 38
2.3.9 Software 38
2.4 Methods 39
2.4.1 Surveying of allograft survival in obese recipients treated with rapamycin 39
2.4.1.1 Mouse model of diet-induced obesity 39
2.4.1.2 Skin allograft transplantation 39
2.4.1.3 Administration of rapamycin 40
2.4.1.4 Collection of tissue and blood samples 41
2.4.2 In vitro analyses of immune cells 42
2.4.2.1 Determination of cell numbers 42
2.4.2.2 Preparation of single cell suspensions from spleen and blood ... 42
2.4.2.3 Phenotyping of immune cells by flow cytometry 43

2.4.2.4 Cell isolation from single cell suspensions by magnetic-activated cell sorting 48
2.4.2.5 Assessing the immunosuppressive activity of MDSCs 50
2.4.2.6 Analyses of MDSCs' relative expression of specific messenger RNAs by quantitative real-time PCR 52
2.4.2.7 Measuring the concentrations of cytokines and chemokines in plasma 56
2.4.3 Statistical analyses 58
3. Results 59
3.1 Skin allograft survival was prolonged by rapamycin treatment particularly favoring obese recipients 59
3.2 Number of splenic M-MDSCs and their relative abundance was increased by rapamycin in obese allograft recipients 59
3.3 The immunosuppressive activity of M-MDSCs was enhanced by rapamycin in obese allograft recipients 61
3.4 Rapamycin treatment changed expression of mRNAs encoding relevant proteins by M-MDSCs and PMN-MDSCs from obese mice 66
3.5 Rapamycin treatment enlarged the Treg population in obese mice 69
3.6 Numbers of pro-inflammatory M1 macrophages remained constant during rapamycin treatment 72
3.7 The CXCL2 concentration in blood of obese mice was increased by rapamycin treatment 74
4. Discussion 77
4.1 Suitability of the murine model used to study obesity and allograft transplantation 77
4.2 Allograft survival 78
4.3 Immune cells and proteins involved in the alloimmune response 79
4.3.1 Effect of obesity 79

4.3.2 Impact of mTOR inhibition by rapamycin on immune response and allograft survival 82
4.4 Clinical relevance and outlook 90
4.5 Conclusion 92
5. Abstracts 93
5.1 English abstract 93
5.2 German abstract / deutsche Zusammenfassung 94
6. Bibliography 96
7. Declaration of own contribution / Erklärung zum Eigenanteil 106
8. Publication 107
9. Acknowledgments 108
10. Appendix 110

List of figures

Figure 1: Origin of MDSCs……..17

Figure 2: Differentiation of T cell subsets……..…...20

Figure 3: Differentiation into main macrophage subtypes……....24

Figure 4: Mechanism of mTOR inhibition by rapamycin……30

Figure 5: Schematic overall illustration of the experimental approach……32

Figure 6: Skin allograft transplantation……40

Figure 7: Gating strategies for flow cytometry data……47

Figure 8: Gating strategy to measure proliferation with the CFSE assay..……52

Figure 9: Rapamycin-induced extension of skin allograft survival was more pronounced in obese recipients……59

Figure 10: Number of splenic M-MDSCs from obese mice increased during rapamycin treatment……60

Figure 11: Representative histograms of CFSE-stained $CD4^+$ T cells co-cultivated with M-MDSCs……62

Figure 12: Representative histograms of CFSE-labeled $CD4^+$ T cells co-cultivated with PMN-MDSCs..……...63

Figure 13: Rapamycin increased the suppressive effect of M-MDSCs on T cell proliferation……64

Figure 14: From POD 3 until POD 11, rapamycin only slightly altered the effects of M-MDSCs and PMN-MDSCs on T cell proliferation……..65

Figure 15: Rapamycin treatment induced M-MDSCs to differently express mRNAs relevant to their function……...67

Figure 16: Rapamycin treatment induced PMN-MDSCs to differently express mRNAs relevant to their function……...68

Figure 17: Rapamycin treatment increased the abundance of Tregs in obese mice……69

Figure 18: Rapamycin treatment shifted the T cell population in obese mice towards expansion of Tregs……70

Figure 19: Rapamycin treatment increased the number of Tregs in obese mice from POD 3 to POD 11……71

Figure 20: The splenocyte subpopulation of M2-like macrophages was increased by rapamycin treatment of lean allograft recipients……..72

Figure 21: Rapamycin only slightly altered numbers of macrophages assessed in the period from POD 3 until POD 11……73

Figure 22: Rapamycin treatment resulted in a lower relative abundance of pro-inflammatory M1 and M2 macrophages in favor of anti-inflammatory M2-like macrophages, M-MDSCs, PMN-MDSCs and Tregs……..74

Figure 23: Rapamycin treatment of obese mice increased their plasma concentration of CXCL2……..75

Figure 24: CXCL1 and IL-6 plasma concentrations were positively correlated with PMN-MDSC numbers.....76

List of tables

Table 1: Classification of obesity……..……13

Table 2: Monoclonal antibodies specific for mouse proteins…….……36

Table 3: Forward and reverse primers used to quantify transcripts by qPCR...37

Table 4: Basic compositions of HFD and LFD……39

Table 5: Markers used for immunophenotyping of distinct cell types……..44

Table 6: CFSE proliferation assay: Numbers and ratios of MDSCs and $CD4^+$ T cells…..……...……51

Table 7: qPCR conditions…….……..55

Table 8: Postoperative monitoring score…….……..110

List of abbreviations

7-AAD	7-aminoactinomycin D
AKI	acute kidney injury
ANOVA	analysis of variance
APC	allophycocyanin
APCs	antigen-presenting cells
Arg-1	arginase-1
ATP	adenosine triphosphate
BMI	body mass index
BSA	bovine serum albumin
CCL	CC-chemokine ligand
CCR	C-C chemokine receptor
CD	cluster of differentiation
cDNA	complementary DNA
CFSE	carboxyfluorescein succinimidyl ester
COX-2	cyclooxygenase-2
CSF	colony-stimulating factor
C_T	threshold cycle
CXCL	CXC-chemokine ligand
CXCR	C-X-C motif chemokine receptor
Cy7	cyanine 7
DEPTOR	disheveled, egl-10 and pleckstrin domain containing mTOR interacting protein
DMSO	dimethyl sulfoxide
DNA	deoxyribonucleic acid
dNTP	deoxyribose nucleoside triphosphate
dsDNA	double-stranded DNA
EDTA	ethylendiaminetetraacetic acid
FBS	fetal bovine serum
FC	flow cytometry
FITC	fluorescein isothiocyanate
FKBP12	FK506 binding protein 12

FoxP3	forkhead box P3
FSC	forward scatter
G-CSF	granulocyte CSF
GM-CSF	granulocyte/macrophage CSF
GvHD	graft-versus-host disease
HEPES	2-(4-hydroxyethyl)-1-piperazineethanesulfonic acid
HFD	high fat diet
IDO	indoleamine 2,3-dioxygenase
IFN-γ	interferon gamma
IL	interleukin
IMCs	immature myeloid cells
iNOS	inducible nitric oxide synthase
JAK	Janus kinase
LFD	low fat diet
LOX-1	lectin-type oxidized lipoprotein receptor 1
LPS	lipopolysaccharide
MACS	magnetic activated cell sorting
M-CSF	macrophage CSF
MDSC	myeloid-derived suppressor cell
MFI	median fluorescence intensity
MHC	major histocompatibility complex
mLST8	mammalian lethal with Sec13 protein 8
M-MDSC	monocytic MDSC
mRNA	messenger RNA
mSin1	mammalian SAPK interacting protein 1
mTor	mammalian target of rapamycin
mTORC	mTOR complex
NADPH	nicotinamide adenine dinucleotide phosphate
NF-κB	nuclear factor kappa-light-chain-enhancer of activated B cells
NO	nitric oxide
PAMPs	pathogen-associated molecular patterns
PBMCs	peripheral blood mononuclear cells

PBS	phosphate buffered saline
PCR	polymerase chain reaction
PE	phycoerythrin
PerCP	peridinin-chlorophyll-protein
PGE2	prostaglandin E2
PMN-MDSC	polymorphonuclear MDSC
POD	postoperative day
PRAS40	proline-rich Akt substrate of 40 kDa
Protor	protein observed with Rictor
PW	permeabilization wash
qPCR	quantitative PCR
Raptor	regulatory protein associated with mTOR
RBC	red blood cell
RELM-β	resistin-like molecule beta
Rictor	rapamycin insensitive companion of mTOR
RNA	ribonucleic acid
ROS	reactive oxygen species
RPMI	Roswell Park Memorial Institute
RT	reverse transcription
SD	standard deviation
SSC	side scatter
STAT3	signal transducer and activator of transcription 3
TCR	T cell receptor
TGF-β	transforming growth factor beta
Th	T helper
TLR	Toll-like receptor
TNF-α	tumor necrosis factor alpha
Tregs	regulatory T cells
VEGF	vascular endothelial growth factor
VHC	vehicle
xMAP	multi-analyte profiling
YM1, CHI3L3	chitinase-3-like protein-3

1. Introduction

1.1 Clinical background

1.1.1 Obesity

Clinically, obesity is defined as "*abnormal or excessive fat accumulation that may impair health*" with a body mass index (BMI) of ≥ 30 kg/m² for adults (Table 1) (World Health Organization 2020). The obesity prevalence nearly tripled during the past four decades finally evolving into a global epidemic that affected about 650 million adults (13% of the entire population) worldwide in 2016 (World Health Organization 2020). In 2013, about one third of the US population was obese (Ng et al. 2014). Although genetic factors such as mutation of the melanocortin-4-receptor expressed in the hypothalamus, diseases of the endocrine system (e.g. Cushing's disease or hypothyroidism), or brain tumors can lead to obesity, overnutrition and low physical activity resulting in an imbalance of energy intake and consumption, an unhealthy lifestyle, or mental stress may account for more than 90% of the cases. Manifestation of the metabolic syndrome including insulin resistance or type 2 diabetes, arterial hypertension, dyslipoproteinemia and hyperuricemia are typical co-morbidities resulting from obesity. Other associated complications include cardiovascular diseases, malignancies, non-alcoholic fatty liver disease, sleep apnea syndrome, and hormone disorders (Herold 2017). Therefore, obesity is not only a severe health problem associated with significantly increased mortality and morbidity concerning the individual patient, but also a great burden for the health care systems worldwide (Herold 2017, Tremmel et al. 2017).

Table 1: Classification of obesity
(Herold 2017). *BMI* body mass index.

BMI (kg/m²)	weight class	
< 18.5	underweight	
18.5 – 24.9	normal weight	
25.0 – 29.9	overweight	
30.0 – 34.9	obesity	class I
35.0 – 39.9		class II
≥ 40.0		class III

1.1.2 Clinical impact of obesity in transplantation medicine

A continuous increase in the number of obese allograft donors and recipients with a higher risk of surgical complications, perioperative infections and prolonged hospitalization and surgical procedures was observed during the last three decades (Heinbokel et al. 2013, Quante et al. 2015, Yang et al. 2016). A recent study showed not only an increased risk of renal allograft loss in obese graft recipients, but also that these patients were more likely affected by delayed graft function, graft rejection, and even death after transplantation due to systemic chronic inflammation and related co-morbidities (Heinbokel et al. 2013, Hill et al. 2015, Wu et al. 2019, Yang et al. 2016). In addition, allografts from obese donors were frequently attributed with lower overall graft quality (Heinbokel et al. 2013, Yang et al. 2016).

1.2 Cells involved in the immune response

On the cellular level, a large number of different players are involved in the immune response to an allograft and their functions or activities might not only be specifically altered in obese individuals but could also be modulated by immunomodulatory therapeutics, e. g. rapamycin. The study presented here was focused on cell types which are known to play an important role in alloimmune response: Immunosuppressive myeloid-derived suppressor cells (MDSCs) and their potential beneficial role in allograft acceptance, T cells and macrophages.

1.2.1 MDSCs

MDSCs, a heterogeneous group of immature myeloid cells, express their strong immunosuppressive properties mainly by inhibiting T cell activity and proliferation (Gabrilovich et al. 2009). In addition to their role in the immune response to allografts, many diseases and also normal physiological processes have been identified, in which MDSCs are crucially involved. They were first described as cells with a tumor-promoting potential resulting from inhibition of the anti-tumor immune response that might support tumor growth and angiogenesis and cause

T cell dysfunction (Talmadge et al. 2013). In pregnancy, MDSCs support adaption of the maternal immune system towards the semi-allogenic fetus to avoid its rejection and thereby ensure a successful pregnancy. MDSCs are also important to limit the negative effects of an overshooting immune system, e.g. tissue damage caused by pro-inflammatory mediators in acute and chronic infections or autoimmune diseases, by restricting effector T cell responses and inducing immune tolerance, which also lessens disease-associated symptoms (Budhwar et al. 2018, Pawelec et al. 2019). Accordingly, inflammatory conditions such as chronic infections, asthma, and obesity, or autoimmune diseases like inflammatory bowel disease, cryopyrin-associated periodic syndromes and ankylosing spondylitis have been found to be associated with increased numbers of MDSCs (Ballbach et al. 2016, Kontaki et al. 2017, Liu et al. 2018, Pawelec et al. 2019). After allograft transplantations, MDSCs have been reported to improve allograft survival by inducing immune tolerance towards the graft (Nakamura et al. 2018, Zhang et al. 2018). Their numbers were found to be increased after full major histocompatibility complex (MHC) -mismatched heart transplantation and their immunosuppressive activity likely prolongs allograft survival upon adoptive cell transfer (Lee et al. 2020). The beneficial promotion of allograft survival by MDSCs has also been confirmed by experiments based on various animal models of organ transplantation: Cardiac (Nakamura et al. 2015, Zhao et al. 2018), corneal (Wei et al. 2018), skin (Yang et al. 2019), lung (Heigl et al. 2019), renal (Luan et al. 2013, Meng et al. 2014), intestinal (Okano et al. 2018) and islet allograft transplantation (Arakawa et al. 2014).

1.2.1.1 Subsets of MDSCs

In mice, MDSCs used to be defined as cluster of differentiation (CD) $11b^+$ and $Gr\text{-}1^+$ (with the two epitopes Ly-6C and Ly-6G) cells. Nowadays, two main MDSC subgroups can be identified based on their phenotypical similarities to monocytes and neutrophils: Monocytic (M-) and polymorphonuclear (PMN-) MDSCs. Murine M-MDSCs are characterized by the expression pattern $CD11b^+$ $Ly\text{-}6G^-$ $Ly\text{-}6C^{high}$ and PMN-MDSCs by $CD11b^+$ $Ly\text{-}6G^+$ $Ly\text{-}6C^{low}$, whereas human M-MDSCs are defined as $CD11b^+$ $CD14^+$ $HLA\text{-}DR^{-/low}$ $CD15^+$ cells and PMN-MDSCs as $CD11b^+$

$CD14^-$ $CD15^+$ or $CD11b^+$ $CD14^-$ $CD66b^+$ cells. Due to their heterogeneity, distinguishing MDSCs from monocytes and neutrophils only by techniques based on expression of specific marker molecules, e.g. cell surface proteins, is not possible. However, clear discrimination requires additional characterization by functional assays to assess their immunosuppressive activity (Bronte et al. 2016). Of note, a recent study described the lectin-type oxidized lipoprotein receptor 1 (LOX-1) to be a more specific cell surface marker useful to characterize PMN-MDSCs. As LOX-1 is present on macrophages (and endothelial and smooth muscle cells), but not on neutrophils, it can be used to distinguish PMN-MDSCs from this cell type (Condamine et al. 2016).

1.2.1.2 Origin and generation of MDSCs

Common myeloid progenitor cells develop from hematopoietic stem cells and differentiate *via* immature myeloid cells (IMCs) into myeloid cells including granulocytes, monocytes, dendritic cells, red blood cells, thrombocytes and mast cells (Fig. 1). Two signals are required to interrupt this sequence of differentiation and stimulate the proliferation of MDSCs. Under certain pathological conditions (see 1.2.1) associated with chronic inflammation, the first signal stimulates hematopoiesis and simultaneously down-regulates the differentiation of IMCs into mature myeloid cells. This leads to an expansion of IMCs, which then need to be activated and converted into immunosuppressive MDSCs by the second signal. Many MDSCs can be found in the bone marrow (up to 30% of all cells) but only 2-4% of splenocytes show the characteristics of MDSCs (Gabrilovich et al. 2009).

Factors involved in the regulation of proliferation and activation of MDSCs include granulocyte-macrophage (GM-) colony-stimulation factor (CSF), granulocyte (G-) CSF, macrophage CSF, prostaglandins, interferon gamma (IFN-γ), transforming growth factor beta (TGF-β), vascular endothelial growth factor, and interleukins (ILs) like IL-1β, IL-6 and IL-10. These are mainly generated and secreted by activated T cells or macrophages (Gabrilovich et al. 2009). Expansion of MDSCs is mainly regulated by the signal transducer and activator of transcription 3 (STAT3, encoded by *Stat3*). The Janus kinase (JAK) 2/STAT3 pathway and

downstream signaling is activated by GM-CSF, G-CSF or IL-6 (Gabrilovich et al. 2009, Li et al. 2016, Peng et al. 2016, Thorn et al. 2016). Up-regulation of STAT1 and STAT6 by IFN-γ or IL-4 and IL-13, respectively, is necessary to activate

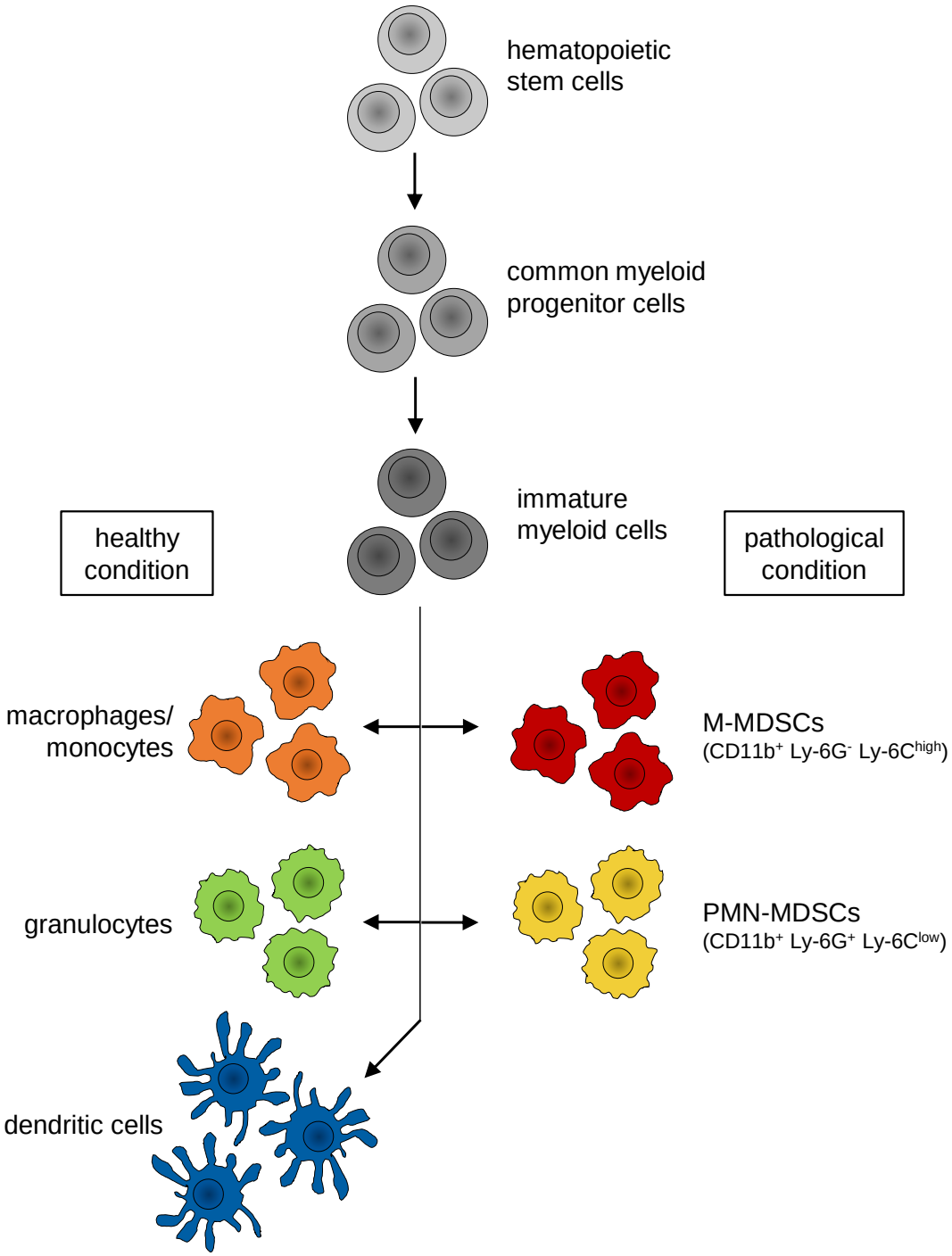

Figure 1: Origin of MDSCs.
In normal hematopoiesis, monocytes, granulocytes, dendritic cells, red blood cells, thrombocytes and mast cells (some not shown) develop from hematopoietic stem cells *via* myeloid progenitor cells and immature myeloid cells. Under certain pathological conditions (e.g. an inflammation), the differentiation of IMCs is interrupted and immature, immunosuppressive monocytic (M-) and polymorphonuclear (PMN-) myeloid-derived suppressor cells (MDSCs) are generated. Figure adapted from Gabrilovic and Nagaraj (2009).

MDSCs, thereby inducing expression of arginase-1 (Arg-1, encoded by *Arg1*), inducible nitric oxide synthase (iNOS, encoded by *Nos2*), synthesis of reactive oxygen species (ROS), as well as the release of immunosuppressive TGF-β by these cells (Condamine et al. 2015, Gabrilovich et al. 2009, Mundy-Bosse et al. 2011). Furthermore, pro-inflammatory mediators like Toll-like receptor (TLR) ligands, IL-1β, IL-12, the cyclooxygenase 2 (COX-2) product prostaglandin E2 (PGE2) or tumor necrosis factor alpha (TNF-α) induce the immunosuppressive activity of MDSCs through the nuclear factor kappa-light-chain-enhancer of activated B cells (NF-κB) pathway (Choi et al. 2019, Hu et al. 2011, Porta et al. 2020, Schroder et al. 2018, Tannenbaum et al. 2019, Tu et al. 2008). In addition, epigenetic modifications seem to play a role in activation and proliferation of MDSCs (Budhwar et al. 2018). After generation of MDSCs, chemokines are responsible for their recruitment from the bone marrow to their site of action through interaction with the corresponding G-protein coupled chemokine receptors on the cells. The following are considered the most important ligand-receptor combinations: Chemokine (C-X-C motif) ligand (CXCL) 1/CXCL2/CXCL5 – C-X-C motif chemokine receptor (CXCR) 2 and chemokine (C-C motif) ligand (CCL) 2 – C-C chemokine receptor (CCR) 2 (Chang et al. 2016, Taki et al. 2018). In particular, the CXCR2 seems to be essential for MDSC recruitment (Han et al. 2019, Katoh et al. 2013, Sun et al. 2019).

1.2.1.3 Immunosuppressive activity of MDSCs

The immunosuppressive activity of MDSCs, namely inhibiting the effector T cell response, is mediated through different mechanisms. Converting L-arginine either into urea and L-ornithine or in L-citrulline and nitric oxide (NO), or metabolizing tryptophan by MDSC-expressed enzymes Arg-1, iNOS or indoleamine 2,3-dioxygenase (IDO, encoded by *Ido1* and *Ido2*), results in depletion of the amino acids from the microenvironment. Since these amino acids are crucially required in T cell metabolism, T cell functions and their proliferation are hampered as a consequence (Budhwar et al. 2018, Gabrilovich et al. 2009, Yu et al. 2013). NO, one of the products of amino acid conversion, itself suppresses T cell proliferation by blocking essential signaling pathways and can even induce apoptosis

(Gabrilovich et al. 2009). Nitration of the specific T cell receptor by peroxynitrite, resulting from a reaction of NO with the superoxide anion, impedes its ability to bind its specific antigen and trigger an immune response (Nagaraj et al. 2007). In addition, ROS – produced by MDSC-expressed nicotinamide adenine dinucleotide phosphate (NADPH) oxidase – suppresses T cell function by damaging cellular structures and thereby inducing apoptosis (Ohl et al. 2018).

MDSC also induce and recruit regulatory T cells (Tregs) in a cell-cell contact-independent manner by secreting the cytokines IFN-γ, IL-10 and TGF-β, and the enzyme IDO, leading to suppression of effector T cell proliferation (Dilek et al. 2012, Gabrilovich et al. 2009, Yu et al. 2013, Zhang et al. 2016). IL-10 produced by MDSCs also induces anti-inflammatory M2 macrophages and auto-stimulates further proliferation of the MDSCs (Budhwar et al. 2018).

Interestingly, the underlying mechanisms of inhibition of T cells seem to be differently utilized by the MDSC subsets: Suppression of effector T cell response by M-MDSCs is mainly achieved through action of Arg-1 and iNOS (→ production of NO) and secretion of IL-10, whereas PMN-MDSCs generate high levels of ROS, peroxynitrite and also of Arg-1 (Budhwar et al. 2018, Raber et al. 2014, Youn et al. 2008, Zhang et al. 2016).

1.2.2 T cells

In concert with B cells, T cells form the adaptive immune system responsible for the elimination of specific pathogens. In contrast to the innate immune system, fast reactivation of immune cells, triggered by memory cells derived from T and B cells, allow a quick immune response to subsequent contacts with the same pathogen. The most important function of activated T cells is the stimulation of macrophages and B cells. Naïve $CD4^+$ and $CD8^+$ T cells specifically recognize their distinctive antigen presented on MHC receptors by antigen-presenting cells (APCs) through contact with their T cell receptor (TCR) (Baumann 2015). Antigens of intracellular (viral) pathogens and cellular proteins are presented on MHC-I molecules and recognized by $CD8^+$ T cells, whereas $CD4^+$ T cells

recognize antigens of processed extracellular pathogens presented on MHC-II receptors (Graefe 2016). Binding of co-factors such as CD28 on T cells and of CD80 or CD86 on APCs is necessary for activation of the specific T cells, which then secrete IL-2 and express the IL-2 receptor. These specific T cells proliferate as a consequence of the autocrine IL-2 stimulation and convert into effector T cells of different subtypes: $CD4^+$ T helper (Th) cells, $CD8^+$ cytotoxic T cells and memory T cells. Depending on the nature of the stimuli, naïve T cells differentiate either into Tregs or into effector T cells (e.g. Th1, Th2 and Th17 cells) each with different functions and patterns of released cytokines (Fig. 2) (Baumann 2015).

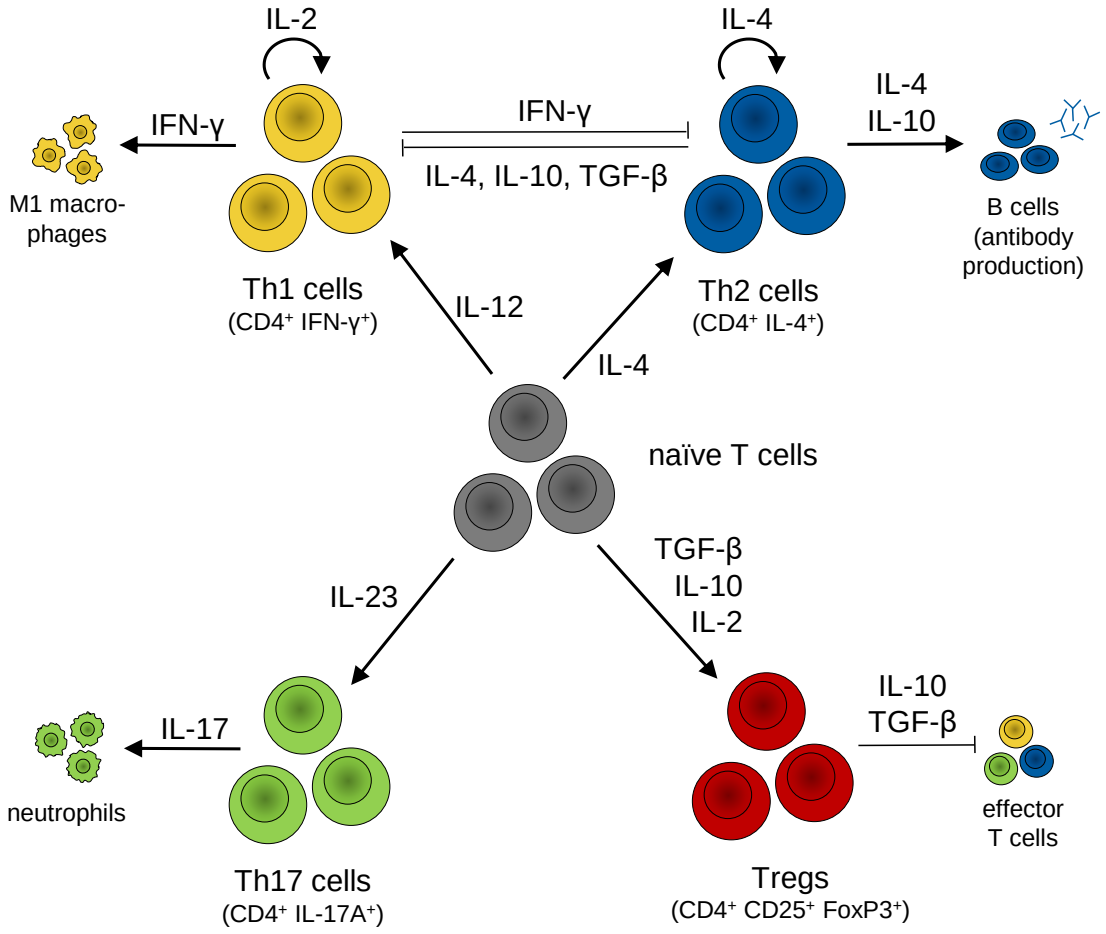

Figure 2: Differentiation of T cell subsets.
In hematopoiesis, naïve T cells develop from hematopoietic stem cells *via* lymphoid progenitor cells (not shown). Under the influence of certain cytokines naïve T cells differentiate into T helper (Th) 1, Th2, or Th17 cells, or into regulatory T cells (Tregs). Cytokines secreted by these cells subsequently activate or inhibit other immune cells. *FoxP3* forkhead box protein 3, *IFN* interferon, *IL* interleukin, *TGF* transforming growth factor, *TNF* tumor necrosis factor, *Tregs* regulatory T cells. Figure adapted from Graefe (2016).

1.2.2.1 Th1 cells

IL-12 stimulates the differentiation of naïve T cells into pro-inflammatory Th1 cells which then activate macrophages either by production of IFN-γ or in a cell-cell contact-dependent manner by an interaction of TCR/MHC-II and CD40L/CD40 (Baumann 2015, Graefe 2016). Macrophages then process the incorporated pathogen(s) and release ROS, NO, proteases and antimicrobial peptides (Baumann 2015). Th1 cells also support the differentiation of $CD8^+$ T cells into cytotoxic T cells, triggered by the release of IL-2 (Graefe 2016). Furthermore, proliferation of Th1 cells is increased by autocrine IL-2 stimulation while at the same time inhibiting Th2 cell proliferation by IFN-γ secretion (Baumann 2015, Graefe 2016). Therefore, activation of the Th1 immune response is associated with an inhibition of the production of antibodies by plasma cells (Walzog et al. 2018). Pro-inflammatory Th1 cells are involved in processes leading to allograft rejection (Liu et al. 2013). In general, Th1 cells are considered to act as pro-inflammatory actors that also contribute to the progression of autoimmune diseases. Due to their specific production of IFN-γ, Th1 cells are phenotypically characterized as $CD4^+$ IFN-γ^+ cells (Hirahara et al. 2016).

1.2.2.2 Th2 cells

IL-4 stimulates the differentiation of naïve T cells into anti-inflammatory Th2 cells, which induce naïve B cells to proliferate and become antibody-producing plasma cells in a similar cell-cell contact-dependent way described for the activation of macrophages by Th1 cells, or by generation of IL-4, IL-5 and IL-6 (Baumann 2015, Graefe 2016). Furthermore, the release of IL-4, IL-10 and TGF-β inhibits the co-activation of Th1 cells, thereby also impeding the stimulation of macrophages (Graefe 2016, Walzog et al. 2018). However, Th2 cell-expressed IL-4 induces (alternatively activated) M2 macrophages (Yang et al. 2016). By inhibiting Th1 cells, Th2 cells should promote prolongation of allograft survival, but on the other hand IL-4 and other Th2-expressed cytokines may also contribute to allograft rejection (Liu et al. 2013). IL-4 expression is considered as a specific feature of Th2 cells which are therefore defined by the marker combination $CD4^+$ IL-4^+ (Hirahara et al. 2016).

1.2.2.3 Th17 cells

Differentiated from naïve T cells after their stimulation with IL-23 or other cytokines, Th17 cells secrete IL-17 and thereby activate neutrophils attracting them to the site of inflammation (Baumann 2015, Bedoya et al. 2013). Th17 cells play a crucial role in the development of autoimmune diseases and – together with Th2 cells – of allergies and inflammatory conditions, e.g. asthma (Hirahara et al. 2016). In addition, Th17 cells were found to be involved in mechanisms leading to allograft rejection (Liu et al. 2013). Due to their secretion of IL-17, Th17 lymphocytes are defined as $CD4^+$ $IL\text{-}17A^+$ cells (Bedoya et al. 2013).

1.2.2.4 Tregs

Tregs, as well as MDSCs, are crucially involved in the maintenance of immune self-tolerance (Qiao et al. 2017). As modulators of the immune response, Tregs have mainly immunosuppressive functions. In detail, they attenuate T cell responses by inhibiting naïve T cell proliferation and differentiation into effector T cells (Sakaguchi et al. 2008). Among other mechanisms, Treg-expressed IL-10 and TGF-β play an important role in the suppression of effector T cell activation, proliferation and cytotoxicity (Baumann 2015, Budhwar et al. 2018). Tregs are generated in the thymus or can be converted from peripheral naïve T cells under the influence of TGF-ß, IL-10, retinoic acid and IL-2. The production of IL-2 by effector T cells ensures maintenance of sufficient numbers of Tregs, providing a negative feedback to the immune response (Sakaguchi et al. 2008). If this balance is disturbed, a dysregulated immune response might cause autoimmune diseases (Qiao et al. 2017). The transcription factor forkhead box P3 (FoxP3) is the most specific marker indicative of mature Tregs and it is therefore used in combination with CD25, the α-subunit of the IL-2 receptor, to define and measure Tregs as $CD4^+$ $CD25^+$ $FoxP3^+$ cells (Sakaguchi et al. 2008). In transplantation studies, Tregs were found to be capable of inducing tolerance toward the allograft thus preventing allograft rejection (Lopez-Hoyos et al. 2009, Pilat et al. 2019). Accordingly, higher numbers of Tregs were generated by patients after successful heart transplantations (Lee et al. 2020).

1.2.3 Macrophages

Traditionally, macrophages were seen as monocyte-derived cells of the innate immune system, which are responsible for phagocytosis and elimination of pathogens after their recognition of pathogen-associated molecular patterns (PAMPs) through interaction with TLRs (Baumann 2015). However, further scientific insights revealing their obvious heterogeneity required further classification to describe specialized subgroups of macrophages. There are now two main categories of classically activated M1 macrophages or alternatively activated M2 macrophages, also defined by their distinctive functions. M2-like or regulatory macrophages were added as third principal category to adequately describe the observed phenotypic complexity of these cells (Fig. 3) (Boorsma et al. 2013).

Macrophages are key effector cells in acute allograft rejection and indicators of an impaired outcome (Broichhausen et al. 2012, Jiang et al. 2014). Accumulation of pro-inflammatory macrophages directly correlates with the degree of tissue damage in acute allograft rejection (Jose et al. 2003). Infiltration of the allograft by macrophages is also known as a central process involved in chronic allograft rejection (Magil 2009). In contrast, the rather immunosuppressive regulatory macrophages were found to act in favor of allograft survival (Li et al. 2019, Riquelme et al. 2013).

1.2.3.1 M1 macrophages

Differentiation into cells of the subgroup named M1 macrophages is induced by lipopolysaccharides (LPS), IFN-γ and TNF-α. Macrophages of this type are crucially involved in the elimination of pathogens by producing NO and ROS as well as through secretion of pro-inflammatory cytokines like IL-1β, IL-6, IL-12, IL-23 and TNF-α to activate Th1 and Th17 cells (Boorsma et al. 2013, Mosser et al. 2008). This leads to the induction of the inflammatory immune response, but might also result in tissue damage (Sica et al. 2012). M1 macrophages are characterized by their expression of the surface markers F4/80 and CD11c (Cao et al. 2015).

1.2.3.2 M2 macrophages

Derived by differentiation of monocytes induced by IL-4 and IL-13, M2 or alternatively activated macrophages play a role in wound healing and defense against parasites (Sica et al. 2012). Thus, they also promote inflammation by secreting Arg-1, resistin-like molecule beta (RELM-β) and chitinase-3 like protein-3 (YM1, CHI3L3) (Boorsma et al. 2013, Sica et al. 2012). Similar to Th2 cells, M2 macrophages play a role in the development of allergic and inflammatory diseases like asthma (Sica et al. 2012). A characteristic feature of M2

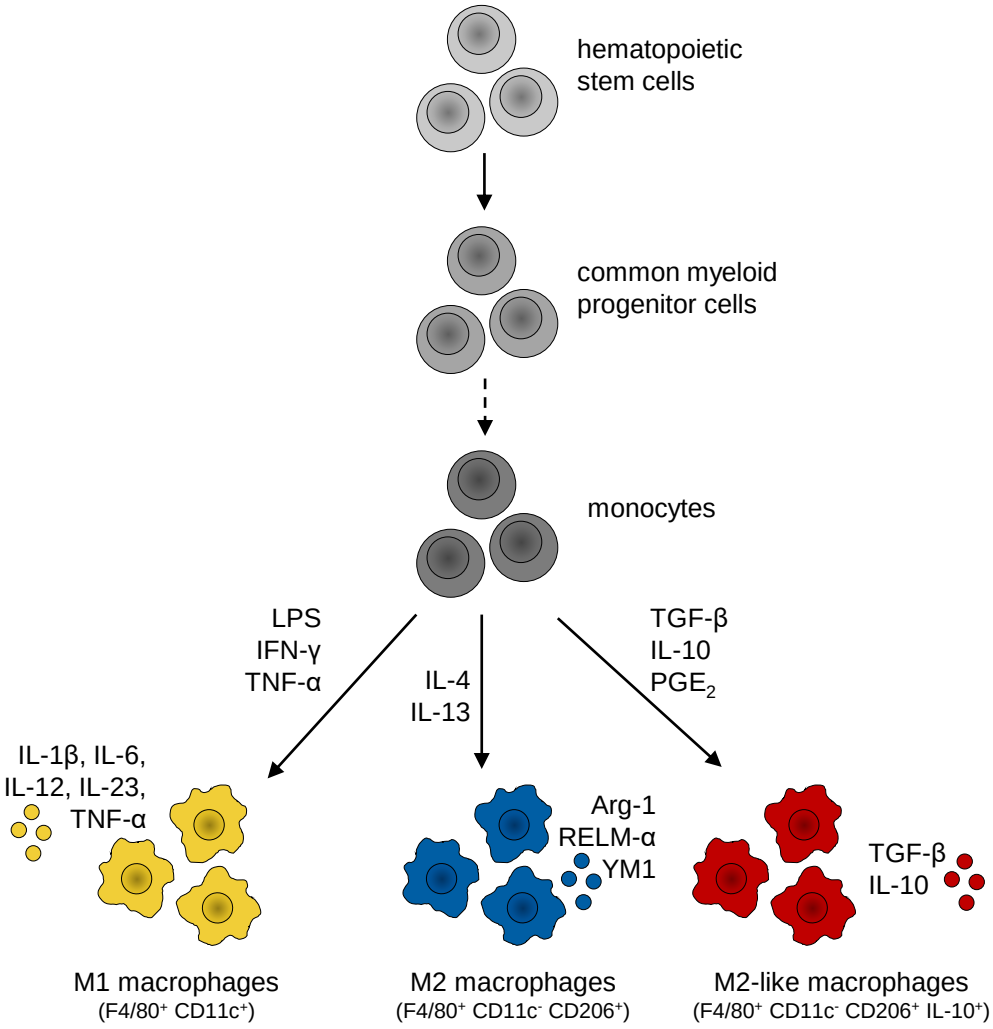

Figure 3: Differentiation into main macrophages subtypes.
In hematopoiesis, monocytes develop from hematopoietic stem cells *via* myeloid progenitor cells and other progenitor cells (dashed arrow, not shown). Exposed to certain cytokines, monocytes alternatively differentiate into M1, M2 or M2-like macrophages, each type producing specific cytokines to influence other immune cells. *Arg-1* arginase-1, *IFN* interferon, *IL* interleukin, *LPS* lipopolysaccharide, *RELM* resistin-like molecule, *TGF* transforming growth factor, *TNF* tumor necrosis factor, *YM1* chitinase-3 like protein-3. Figure adapted from Boorsma et al. (2013).

macrophages is the up-regulation of their mannose receptor (CD206) (Boorsma et al. 2013).

1.2.3.3 M2-like macrophages

M2-like or regulatory macrophages also up-regulate the mannose receptor (CD206), but in addition they secrete the anti-inflammatory cytokines IL-10 and TGF-β, which activate Th2 cells (Boorsma et al. 2013, Mosser et al. 2008). They are in turn stimulated by IL-10 secreted by Tregs or other immune cells, activating STAT3-mediated downstream signaling (Mosser et al. 2008). Thus, M2-like macrophages – induced by IL-10, TGF-β and PGE2 – are considered to regulate the immune response in concert with MDSCs and Tregs (Boorsma et al. 2013, Sica et al. 2012). The only marker allowing to distinguish M2-like from M2 macrophages is their expression of IL-10 (Boorsma et al. 2013).

1.3 Effect of obesity on the immune response

1.3.1 Obesity-related chronic inflammation

In general, obesity represents a state of chronic low-grade systemic inflammation caused by dysfunction of adipocytes resulting from massive storage of triglycerides (Maurizi et al. 2018).

An acute local inflammation – such as the reaction to pathogens or trauma – is characterized by local infiltration of neutrophils and monocytes/macrophages which then remove pathogens or endogenous cell debris. During systemic inflammation caused by cytokines like IL-1, IL-6 or TNF-α and typically accompanied by fever, acute phase proteins (e.g. C-reactive protein and ferritin) are secreted by hepatocytes (Walzog et al. 2018). In contrast, chronic inflammation is a long lasting condition often associated with infiltration of lymphocytes and macrophages at the affected sites and formation of new blood vessels and connective tissue (Ellulu et al. 2017).

Originally, fat and thereby energy storage was thought to be the only function of adipose tissue, but nowadays it is broadly accepted that this tissue is a complex organ composed of a number of different cell types such as adipocytes, fibroblasts, vascular endothelial cells, macrophages and other immune cells, which secrete pro- and anti-inflammatory mediators as well (Maurizi et al. 2018, Quante et al. 2015). In the adipose tissue of lean individuals more Th2-polarized immune cells, such as Th2 cells, Tregs or anti-inflammatory macrophages, are present and suppress Th1-dependent immune responses through secretion of IL-4 and IL-10 (Quante et al. 2015, Yang et al. 2016). In contrast, a steady Th1-driven immune response is characteristic of the obese state. This includes recruitment of other immune cells, mainly effector T cells and pro-inflammatory macrophages, and secretion of pro-inflammatory factors such as IL-6, TNF-α, CCL2 and IFN-γ, whose expression is up-regulated by autocrine IFN-γ/TNF-α stimulation, thereby meeting the criteria for a chronic systemic inflammation (Ellulu et al. 2017, Quante et al. 2015, Yang et al. 2016).

In adipose tissue of obese individuals, the number of macrophages is considerably higher and their phenotype has changed towards pro-inflammatory functions, e.g. expression of TNF-α, IL-1β, IL-6, PGE2 and CCL2 (Fantuzzi 2005, Pawelec et al. 2019, Saltiel et al. 2017). Adipose tissue growing by hypertrophy and hyperplasia releases pro-inflammatory mediators such as CCL2 (attracting monocytes and M1 macrophages), leptin, IL-1β, IL-6, TNF-α and PGE2, in response to cellular stress caused by hypoxia. Effects of these factors, accompanied by intra-adipocyte iron accumulation, subsequently lead to activation and recruitment of pro-inflammatory macrophages into the adipose tissue (Ellulu et al. 2017, Pawelec et al. 2019, Quante et al. 2015, Yang et al. 2016). There is evidence indicating that obesity and inflammation are also connected through other mechanisms. The impaired function of the barrier formed by intestinal epithelial cells allows LPS, generated by bacteria in the colon, to pass into the blood stream and stimulate the immune response by binding to the TLR-4 on adipocytes. In addition, fatty acids can directly bind to this receptor, leading to secretion of CCL2 and subsequently to an increased proliferation of pro-inflammatory M1 macrophages (Saltiel et al. 2017).

The main adipocytokines (cytokines released from adipose tissue) leptin and adiponectin also have significant effects regarding the immune system. In lean individuals, serum concentrations of leptin, which inhibits feelings of hunger and appetite, are proportional to the adipose tissue mass, whereas obese patients often have developed a partial or complete tolerance to leptin function (Gekle 2015). The concept that leptin supports a mainly Th1-driven immune response can be concluded from several of its effects: stimulation of IFN-γ secretion by T cells and of effector T cell proliferation, up-regulation of activation markers (e.g. CD25), activation of macrophages, neutrophils and natural killer cells, and suppression of memory T cell proliferation (Fantuzzi 2005, Heinbokel et al. 2013, Quante et al. 2015, Yang et al. 2016). For maintenance of the type 1 immune responses, IFN-γ and TNF-α are considered key factors (Yang et al. 2016). Furthermore, expression and secretion of leptin's counterpart, the anti-inflammatory adiponectin, is lower in obese individuals, which is probably due to higher levels of TNF-α associated with obesity-caused Th1-type immune responses (Ellulu et al. 2017, Fantuzzi 2005). Adiponectin inhibits secretion of TNF-α and IL-6, leading to a decrease of T cell proliferation, and restrains macrophage activation while at the same time promoting Th2-type immune responses and increasing the number of regulatory T cells by inducing secretion of IL-10 (Heinbokel et al. 2013, Quante et al. 2015). Adiponectin action in the context of a type 2 immune response also contributes to activation of anti-inflammatory macrophages (Yang et al. 2016). Additionally, a low-level but permanent activation of the innate immune system is considered as a consequence of obesity (Saltiel et al. 2017). The underlying mechanisms include activation of pro-inflammatory M1 macrophages by CCL2, IL-6 and TNF-α (Yang et al. 2016). All these factors contribute to the obesity-related activation of signaling processes in favor of further Th1 polarization of immune cells.

Taken together: In lean individuals adiponectin promotes a Th2-type immune response with dominating regulatory T cells and anti-inflammatory macrophages, and production of anti-inflammatory IL-10. In contrast, obesity is typically associated with a Th1-type immune response with dominating effector T cells, pro-inflammatory macrophages, and production of pro-inflammatory mediators

such as TNF-α, IL-6 and CCL2 (Quante et al. 2015, Saltiel et al. 2017). Such systemic inflammation not only results in an altered immune response but also in obesity-associated complications potentially leading to chronic pathological conditions.

1.3.2 Effect of obesity on an alloimmune response

Acute allograft rejections are type IV immune reactions of the delayed type, mediated by recipient T cells that recognize unknown extrinsic donor MHC molecules (Bartels et al. 2008, Baumann 2015). Such a host-versus-graft reaction is characterized by a Th1-type immune response including interstitial lymphocyte infiltration and subsequent inflammation (Gulbins et al. 2019, Yang et al. 2016). Therefore it can be hypothesized that allograft rejection might occur more frequently in obese individuals with an already established chronic inflammation driven by a Th1-type immune reaction. Results of several studies suggest that adipocytokines might be involved in the rejection process: Leptin shortage leads to prolonged allograft survival and increased numbers of Tregs and Th2 cells (Moraes-Vieira et al. 2013). In contrast, adiponectin deficiency aggravates acute allograft rejection and is associated with more effector T cells and stronger expression of pro-inflammatory cytokines (Okamoto et al. 2009). Taken together, although obese patients generally benefit from organ transplantation, they seem to have a substantially higher risk of severe complications and an impaired overall outcome compared to lean individuals (Heinbokel et al. 2013).

1.4 Post-transplantation immunosuppressive therapy with rapamycin

Despite of the detrimental effects of obesity on the immune system, its potential interference with immunosuppressive therapy following solid organ transplantation has not been explored so far. Both obesity and immunosuppressive therapy are known to increase the risk of developing certain types of cancer and of (perioperative) infections potentially leading to transplant

failure (Au et al. 2018, Friedenreich et al. 2020, Milner et al. 2012, Mueller 2008). This might call for a particular immunosuppressive regimen for obese allograft recipients beyond mere weight-adjusted dosing, which has not been established yet. In addition, results of studies based on suitable animal models or clinical trials focusing on safety and effectiveness of immunosuppressive drugs in the group of obese patients are not available.

1.4.1 Rapamycin's mechanisms of action

The macrolide rapamycin is widely used to prevent allograft rejection in patients after organ transplantation (Moes et al. 2015). Rapamycin suppresses T cell proliferation and activation by interfering with the IL-2 receptor signaling pathway (Bartels et al. 2008, Baumann 2015, Graefe 2016).

After transition through the plasma membrane, rapamycin binds to its intracellular cytosolic receptor, the macrolide FK506 (tacrolimus) binding protein 12 (FKBP12). This complex inhibits the mammalian target of rapamycin (mTOR), a serine/threonine protein kinase which is the catalytic subunit of two alternatively formed protein aggregates, the mTOR complexes 1 and 2 (mTORC1, mTORC2; Fig. 4). In addition to mTOR, the mTORC1 consists of several regulatory proteins: "regulatory protein associated with mTOR" (Raptor), "mammalian lethal with Sec13 protein 8" (mLST8), and the two inhibitory proteins "proline-rich Akt substrate of 40 kDa" (PRAS40) and "dishevelled Egl-10 and pleckstrin domain containing mTOR interacting protein" (DEPTOR). Beside DEPTOR and mLST8, the mTORC2 contains "rapamycin insensitive companion of mTOR" (Rictor), "mammalian SAPK interacting protein 1" (mSin1) and the "protein observed with Rictor 1/2" (Protor1/2). Short-term exposure to the macrolide only blocks mTORC1's activity due to direct binding of rapamycin-FKBP12 to mTOR in the complex, whereas similar interaction with mTOR in mTORC2 is not possible and inhibition only be achieved by long-term treatment over several weeks, likely because mTOR bound to rapamycin cannot be assembled into new protein complexes which are thereby deprived of mTOR. As a central component in an important signaling cascade, mTOR regulates metabolism, cell proliferation and

cell growth in response to fluctuations in environmental conditions. Hormones (e.g. insulin-like growth factor), energy excess in the form of adenosine triphosphate (ATP) and nutrients, and oxygen saturation activate mTORC1 and thereby different downstream signaling pathways. This results in an overall anabolic metabolism indicated by increased mRNA translation and synthesis of proteins, lipids and nucleotides, and eventually in cell proliferation, whereas typical catabolic processes like autophagy are inhibited. Interestingly, chronic mTORC1 activation was found to be associated with obesity (Blenis 2017, Saxton et al. 2017). Activity of mTORC2 counteracts mechanisms resulting in cell death and enhances cell proliferation and growth after stimulation with growth factors.

The rapamycin/FKBP12 complex suppresses T and B cell proliferation and differentiation by downregulating the p70S6 kinase – important for protein synthesis and cell cycle progression – as well as cyclin-dependent kinases and cyclins, thereby halting the cell cycle in the G1 phase (Moes et al. 2015). Mainly by inhibiting the key kinase mTOR of the IL-2 signaling pathway, rapamycin restrains T cell proliferation (Graefe 2016, Moes et al. 2015).

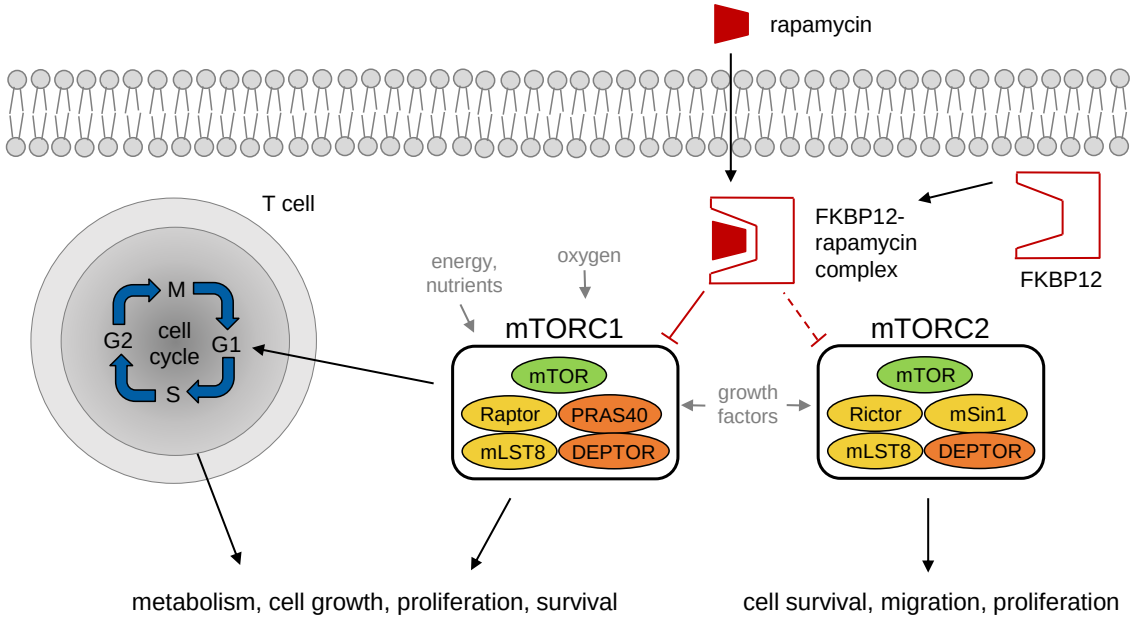

Figure 4: Mechanism of mTOR inhibition by rapamycin.
Rapamycin passes the cell membrane and binds to its receptor, the FK506 binding protein 12 (FKBP12). This complex inhibits the mammalian target of rapamycin (mTOR) complex (mTORC) 1 directly, whereas mTORC2 is only sensitive to long-term treatment depriving the complex of mTOR. Inhibitory factors within mTORC1 and 2 are marked orange while other regulatory proteins are highlighted yellow. mTORC1 and 2 are activated by various factors and regulate metabolism, cell growth and proliferation through different downstream signaling pathways (not shown) (Blenis 2017, Saxton et al 2017). *DEPTOR* dishevelled Egl-10 and pleckstrin domain containing mTOR interacting protein, *mLST8* mammalian lethal with Sec13 protein 8, *mSin1* mammalian SAPK interacting protein 1, *PRAS40* proline-rich Akt substrate of 40 kDa, *Raptor* regulatory protein associated with mTOR, *Rictor* rapamycin insensitive companion of mTOR.

1.5 Aim of the study and experimental approach

In view of the constantly increasing number of obese transplant candidates and allograft recipients it is of critical importance to better understand how adjuvant immunosuppressive therapy alters the immune response in obese versus lean allograft recipients. Aim of this project was to elucidate if rapamycin improves allograft survival particularly in obese mice and to reveal its effects on the activities of involved immune cells and their generation by proliferation and differentiation of precursor cells. To gain information on these processes, a full MHC-mismatched skin allograft transplantation was performed on obese and lean recipient mice to evaluate allograft survival and potential obesity-specific effects of rapamycin. At the day of rejection, the numbers of MDSCs, T cells and macrophages derived from spleens were determined. In addition, the immunosuppressive activities of M-MDSCs and PMN-MDSCs were assessed and expression levels of mRNAs coding for proteins involved in immunosuppression by MDSCs were measured, as well as the plasma concentrations of relevant cytokines and chemokines. The *in vitro* analyses were also conducted at defined time points during the pre-rejection period with cells from sacrificed animals to study the time course of processes involved in allograft rejection.

2. Materials and methods

2.1 Outline of the experimental approach

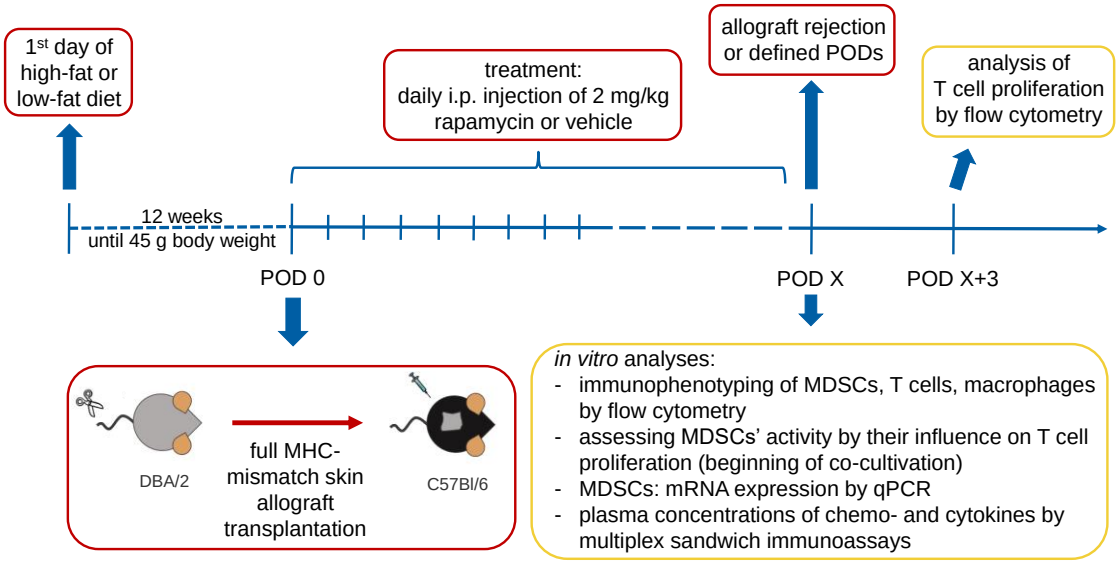

Figure 5: Schematic overall illustration of the experimental approach.
C57Bl/6 mice were fed a high-fat or a low-fat diet for 12 weeks resulting in obese and lean mice, respectively. Animals in both groups then underwent full major histocompatibility complex (MHC-) mismatched skin allograft transplantation and were treated intraperitoneally (i.p.) either with the vehicle alone or 2 mg/kg rapamycin i.p. daily. Animals were sacrificed at defined postoperative days (POD) or when allograft rejection was observed to perform *in vitro* analyses as indicated. *MDSCs* myeloid-derived suppressor cells, *qPCR* quantitative real-time polymerase chain reaction. Figure adapted from Deissler et al. (2021).

2.2 Animals

Male C57Bl/6J and male DBA/2N mice, all 6-8 weeks old, were purchased from Charles River Laboratories (Sulzfeld, Germany).

2.3 Materials

2.3.1 Reagents, enzymes and proteins

7-aminoactinomycin D (7-AAD)	BD Biosciences (Heidelberg, Germany)
dimethyl sulfoxide (DMSO)	AppliChem (Darmstadt, Germany)
Dulbecco's phosphate buffered saline (PBS) without calcium and magnesium	Gibco/ThermoFisher Scientific (Schwerte, Germany)

ethanol, absolute for analysis (> 99.9%)	Sigma-Aldrich/Merck (Darmstadt, Germany)
fixation buffer	BioLegend (Amsterdam, Netherlands)
intracellular staining permeabilization wash buffer (10X)	BioLegend
50 mM β-mercaptoethanol	Gibco/ThermoFisher Scientific
nuclease-free water	Qiagen (Hilden, Germany)
trypan blue	Gibco/ThermoFisher Scientific

2.3.2 Consumables

0.2 ml polymerase chain reaction (PCR) reaction tubes	Greiner Bio-One (Frickenhausen, Germany)
1.5 ml reaction tubes	Greiner Bio-One
26G Microlance™ 3 needle	BD Biosciences
40 µm nylon cell strainer	Corning (Amsterdam, Netherlands)
5-0 Ethicon prolene suture material	Johnson & Johnson Medical (Norderstedt, Germany)
96-well PCR microplate, full-skirt	Greiner Bio-One
96-well suspension culture plate, U-bottom	Greiner Bio-One
AMPLIseal adhesive sealer	Greiner Bio-One
Cellstar® polypropylene tubes (15 ml, 50 ml)	Greiner Bio-One
Falcon round-bottom polystyrene tubes (5 ml, FC tubes)	Corning
LS columns	Miltenyi Biotech (Bergisch Gladbach, Germany)
MS columns	Miltenyi Biotech
Nalgene™ Rapid-Flow™ sterile single use bottle top filters	Fisher Scientific/ThermoFisher Scientific (Schwerte, Germany)

2.3.3 Drugs and diets

carprofen	Zoetis (Berlin, Germany)
high fat diet (HFD; D12492)	Brogaarden/Research Diets (Gentofte, Denmark)
isoflurane 1 ml/ml	CP-Pharma (Burgdorf, Germany)
low fat diet (LFD; D12450B)	Brogaarden/Research Diets
rapamycin	LC Laboratories (Woburn, MA, USA)

2.3.4 Cell culture medium, supplements and buffers

fetal bovine serum (FBS)	Gibco/ThermoFisher Scientific
L-glutamine	Gibco/ThermoFisher Scientific
mouse IL-2	Miltenyi Biotech
penicillin	Gibco/ThermoFisher Scientific
Roswell Park Memorial Institute (RPMI) - 1640 medium without glutamine, 2-(4-hydroxyethyl)-1-piperazineethanesulfonic acid (HEPES), or phenol red	Gibco/ThermoFisher Scientific
streptomycin	Gibco/ThermoFisher Scientific

Cell culture medium was prepared by supplementing RPMI-1640 medium with 2 mM L-glutamine, 1% penicillin/streptomycin and 10 % FBS.

Below listed buffers were made immediately before start of the experiments by adding the other components to PBS or water. After complete dissolution of solid substances, homogeneous solutions were sterilized by filtration through a sterile bottle top filter. All standard chemicals used were purchased from Merck (Darmstadt, Germany) or Carl Roth (Karlsruhe, Germany).

Magnetic-activated cell sorting (MACS®) buffer

500 ml	PBS (without calcium and magnesium)
2.5 g	Bovine serum albumin (BSA)
3.26 ml	307.3 mM ethylendiaminetetraacetic acid (EDTA)

Red blood cell (RBC) lysis buffer

500 ml	ddH_2O
4.12 g	NH_4Cl
0.5 g	$KHCO_3$
100 µl	0.5 M EDTA

Flow cytometry (FC) buffer

500 ml	PBS (without calcium and magnesium)
5 g	BSA
0.1 g	NaN_3

2.3.5 Kits

$CD4^+$ T Cell Isolation Kit	Miltenyi Biotech
carboxyfluorescein succinimidyl ester (CFSE) Cell Division Tracker Kit	BioLegend
FoxP3 Fixation/Permeabilization Buffer Set	BioLegend
High Capacity complementary deoxyribonucleic acid (cDNA) Reverse Transcription Kit with RNAse Inhibitor	ThermoFisher Scientific
Magnetic Luminex® Assay (mouse premixed multi-analyte kit, 11-plex, order number: LXSAMSM-11)	R&D Systems/Bio-Techne (Wiesbaden, Germany)
Myeloid-Derived Suppressor Cell Isolation Kit	Miltenyi Biotech
RNeasy Micro Kit	Qiagen
RNeasy Mini Kit	Qiagen
SsoAdvanced Universal SYBR® Green Supermix	Bio-Rad (Feldkirchen, Germany)
T Cell Activation/Expansion Kit	Miltenyi Biotech

2.3.6 Antibodies used for flow cytometric analyses

Fluorescent dye-labelled antibodies used for flow cytometric analyses are listed in Table 2, their optimal working dilutions were determined prior to the experiments by titration.

Table 2: Monoclonal antibodies specific for mouse proteins.
APC allophycocyanin, *CD* cluster of differentiation, *FoxP3* forkhead box P3, *Cy7* cyanine 7, *FITC* fluorescein isothiocyanate, *IFN* interferon, *IL* interleukin, *PE* phycoerythrin, *PerCP* peridinin-chlorophyll-protein.

target	conjugated fluorochrome	working dilution	clone	source
CD11b	APC	1:3200	M1/70	BioLegend
CD11c	FITC	1:625	N418	
CD16/CD32 (Fc-blocking reagent)		1:20	93	
CD206	Pacific Blue	1:20	MR5D3	Bio-Rad
CD25	FITC	1:1200	3C7	BioLegend
CD4	APC	1:800	GK1.5	
F4/80	PE	1:320	BM8	
FoxP3	PE	1:40	150D	
IFN-γ	FITC	1:200	XMG1.2	
IL-10	APC	1:160	JES5-16E3	
IL-17A	PerCP	1:200	TC11-18H10.1	
IL-4	PE	1:500	11B11	
Ly-6C	PE/Cy7	1:3200	HK1.4	
Ly-6G	FITC	1:1600	1A8	

2.3.7 Primers for qPCR

All primers were purchased from biomers.net, Ulm, Germany and are listed in Table 3.

Table 3: Forward and reverse primers used to quantify transcripts by qPCR.
Arg-1 arginase-1, *COX-2* cyclooxygenase-2, *IDO* indoleamine-2,3-dioxygenase, *IL* interleukin, *iNOS* inducible nitric oxide synthase, *STAT3* signal transducer and activator of transcription 3, *TGF-β* transforming growth factor beta. Table from Deissler et al. (2021).

target sequence	encoded protein	primer sequence	
Actb	β-actin	forward:	5'-CGTGCGTGACATCAAAGAGAAG-3'
		reverse:	5'-CGTTGCCAATAGTGATGACCTG-3'
Arg1	Arg-1	forward:	5'-ATTATCGGAGCGCCTTTCTC-3'
		reverse:	5'-ACAGACCGTGGGTTCTTCAC-3'
COX2	COX-2	forward:	5'- CCTGGTGAACTACGACTGCT-3'
		reverse:	5'-GCCTGGGATGGCATCAGTT-3'
Nos2	iNOS	forward:	5'-CACCTTGGAAGAGGAGCAAC-3'
		reverse:	5'-AAGGCCAAACACAGCATACC-3'
Stat3	STAT3	forward:	5′-CCCGTACCTGAAGACCAAGT-3′
		reverse:	5′-ACACTCCGAGGTCAGATCCA-3′
Il10	IL-10	forward:	5′-GAGAGCTGCAGGGCCCTTTGC-3′
		reverse:	5′-CTCCCTGGTTTCTCTTCCCAAGACC-3′
Tgfb1	TGF-β	forward:	5′-TGTACGGCAGTGGCTGAACCA-3′
		reverse:	5′-TGTCACAAGAGCAGTGAGCGCT-3′
Ido1	IDO1	forward:	5'-TCTGGGAATAAAACACGAGG-3'
		reverse:	5'-GAAATGACAAACTCACGGAC-3'
Ido2	IDO2	forward:	5'-CACAAGTACAACCACACAGA-3'
		reverse:	5'-ATTTGGAAGGAGAAAGCCAT-3'

2.3.8 Laboratory equipment

BD FACSCanto II flow cytometer	BD Biosciences
C1000 Touch thermal cycler	Bio-Rad
Centrifuge 5810 R	Eppendorf (Hamburg, Germany)
HERA safe work bench	Thermo Scientific/Thermo Fisher Scientific (Langenselbold, Germany)
Heraeus Laminair work bench	Thermo Scientific/Thermo Fisher Scientific
Heraues Pico 17 centrifuge	Thermo Scientific/Thermo Fisher Scientific
Isoflurane vaporizer HNG6	H. Hölzel (Wörth, Germany)
LightCycler® 480 II	Roche Diagnostics (Basel, Switzerland)
Luminex® FLEXMAP 3D®	Luminex Corporation, Austin, TX, US
MACS® MultiStand	Miltenyi Biotech
MCO-18AIC CO_2 incubator	Sanyo (Moriguchi, Japan)
Microcentrifuge 5430R	Eppendorf
MidiMACS® Separator	Miltenyi Biotech
MiniMACS® Separator	Miltenyi Biotech
MR 3001 magnetic stirrer	Heidolph Instruments (Schwabach, Germany)
NanoPhotometer® N60 (microvolume spectrophotometer)	Implen, Munich, Germany
Primo Vert microscope	Carl Zeiss (Oberkochen, Germany)

2.3.9 Software

BD FACSDiva™	BD Biosciences
FlowJo™ v10	BD Biosciences
GraphPad Prism v5	GraphPad Software (San Diego, CA, USA)
LightCycler® 480 software	Roche
MasterPlex ReaderFit v5	MiraiBio/Hitachi (San Francisco, CA, USA)

2.4 Methods

2.4.1 Surveying of allograft survival in obese recipients treated with rapamycin

2.4.1.1 Mouse model of diet-induced obesity

Animal experimentation was approved by the Regierungspräsidium Tübingen, Germany (Tierversuchsvorhaben C2/17) and all procedures were conducted according to the German legal provisions to protect animal life. Six to eight weeks old male C57Bl/6J mice were kept in groups of two to five animals at 22°C ± 2°C in an environment with a 12 h-light/12 h-dark cycle. They received either a commercial HFD or LFD; for compositions of diets see Table 4) *ad libitum* for at least 12 weeks (Leontieva et al. 2013). Under these conditions, all HFD-fed mice reached a weight of more than 45 g. Two days prior to the transplantation, the mice were separated and subsequently kept in individual cages.

Table 4: Basic compositions of high fat diet (HFD) and low fat diet (LFD).

	HFD	LFD
protein	20%	20%
fat	60%	10%
carbohydrates	20%	70%
energy density	5.21 kcal/g	3.82 kcal/g

2.4.1.2 Skin allograft transplantation

Full MHC-mismatched skin allograft transplantation was performed as described previously (Quante et al. 2018). The full-thickness skin allografts (0.5 cm x 0.5 cm) were prepared from the tail skin of a CO_2-euthanized donor DBA/2N mouse as follows: The skin was cut around the tail root, an incision made along the full length of the tail, and the complete tail skin was detached by pulling it off with a needle holder (Fig. 6 A). The skin was cut into four to six squares and these allografts were kept in 0.9% NaCl at 4°C until transplantation (Fig. 6 B). Obese or lean C57Bl/6J recipient mice were weighed before 5 mg/kg carprofen was administered by subcutaneous injection for analgesia. Subsequently, mice were

anesthetized by exposure to isoflurane vapor generated in a vaporizer. A skin area of the allograft's size was removed from the shaved dorsolateral thoracic wall (Fig. 6 C) and the skin allograft fixated onto the subcutaneous layer with one stich at each corner using a 5-0 prolene suture (Fig. 6 D). Bandages were applied after transplantation and removed on postoperative day (POD) 7 (Fig. 6 E). The transplanted mice were monitored by daily examinations of their weight, general health, spontaneous behavior and the condition of the skin graft using a score sheet (see appendix).

Allograft loss was indicated by a brownish decoloration of the allograft or its complete dryness, compared to a pinkish viable and blood-supplied allograft. As assessed accordingly, allografts with less than 50% remaining viability were considered rejected and animals euthanized.

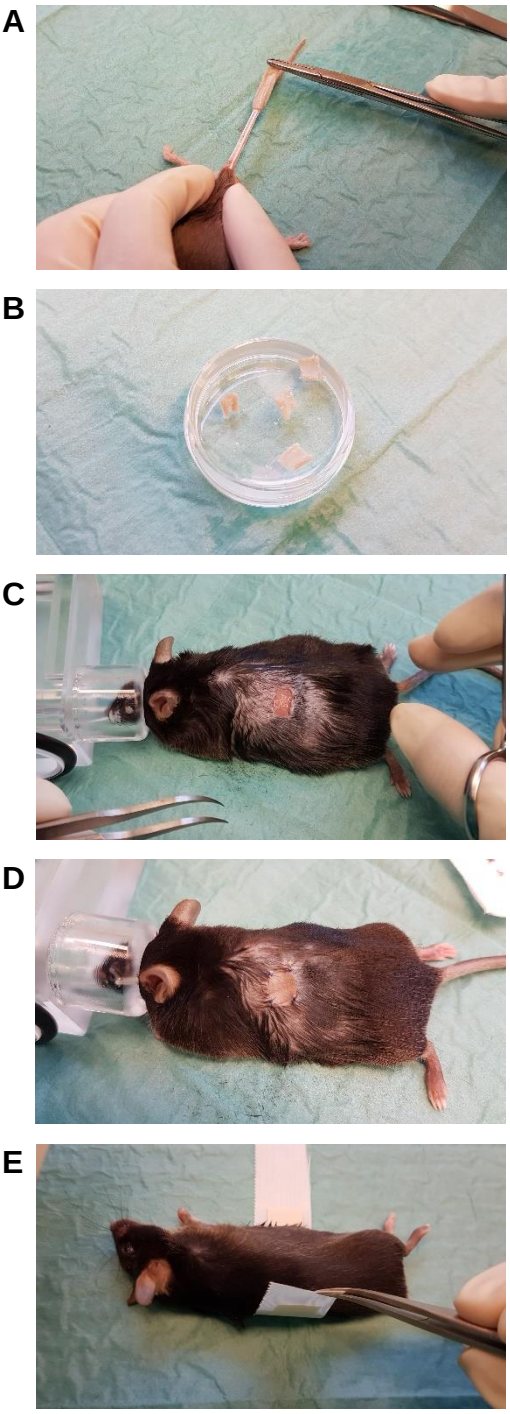

Figure 6: Skin allograft transplantation.
(**A**) Removal of donor tail skin. (**B**) Storage of skin allografts. (**C**) Subcutaneous transplantation area. (**D**) Transplanted skin allograft. (**E**) Bandage application.

2.4.1.3 Administration of rapamycin

Rapamycin dissolved in DMSO at a concentration of 50 mg/ml was further diluted in the same solvent to 10 mg/ml and stored in aliquots at -20°C. Prior to the injection, thawed aliquots were further diluted 1:10 with sterile H_2O, resulting in a final concentration of 1 mg/ml rapamycin in 10% DMSO (Sato et al. 2012).

Starting on the day of transplantation, 2 mg/kg body weight rapamycin were administered daily by intraperitoneal injection to the mice subsequently referred to as rapamycin-treated (Rapa) group. In detail, each mouse was restrained and the drug was injected into the left lower quadrant of the abdomen through a 26 G needle connected to a 1 ml syringe. For example, an obese mouse weighting 50 g received 100 µl of 1 mg/ml rapamycin in 10% DMSO. To enable injection of the same volume into lean mice with weights of around 25 g, this solution was further diluted to 0.5 mg/ml with 10% DMSO in sterile water. Obese and lean mice in the untreated (vehicle, VHC) group received 100 µl 10% DMSO in sterile water daily.

2.4.1.4 Collection of tissue and blood samples

On the day of allograft rejection or pre-defined PODs, mice were euthanized by isoflurane-overdose followed by cervical dislocation. For this purpose, the head of a mouse was fixated towards the neck between two fingers and the tail strongly pulled away to remove the skull bone from the spine with the skin still being intact. After disinfection, the skin and thoracic cavity was opened with surgical forceps and scissors to allow blood collection: The left atrium of the heart was punctured and as much blood as possible was aspirated through a 26 G needle attached to a 1 ml syringe containing 50 µl 305 mM EDTA to avoid clotting. The collected blood was transferred to a 1.5 ml reaction tube and 50 µl 305 mM EDTA were added for every 200 µl blood to further prevent clotting. Then, the incision was extended to open the abdomen. The ligament of the spleen was cut and the organ removed to be weighed and stored in PBS in a 1.5 ml tube on ice. Mouse carcasses were disposed according to German legal provisions.

2.4.2 In vitro analyses of immune cells

All steps including processing of cells were performed under sterile conditions. Unless indicated otherwise, centrifugations of cell suspensions were carried out at 500 x g for 5 min at 4°C; and samples were always kept at 4°C on ice. The subsequently used term “washing” means adding a certain amount of liquid, followed by centrifugation and removal of the supernatant.

2.4.2.1 Determination of cell numbers

To determine the number of living cells, dead cells were stained by adding a sufficient amount of 8 mM trypan blue solution (in PBS) appropriately to the expected cell number – for example 1:10. The suspension of stained cells was analyzed with a Neubauer hemocytometer containing 16 small squares within four large squares covering a volume of 0.1 µl. Cells were examined by microscopy and unstained cells were counted, allowing calculation of their concentration:

$$\frac{number\ of\ cells\ counted}{number\ of\ \ large\ squares\ covered} * dilution\ factor * 10^4 = cell\ number/ml$$

2.4.2.2 Preparation of single cell suspensions from spleen and blood

All subsequent procedures (i.e. flow cytometry, cell isolation) required single cell suspensions of splenocytes or peripheral blood mononuclear cells (PBMCs), respectively; therefore other tissue components and red blood cells had to be removed.

Single splenocyte suspension

A mouse spleen was gently squeezed through a cell strainer (pore size: 40 µm) with the plunger of a 5 ml syringe. Cells were flushed out with a sufficient amount of PBS and collected in a 50 ml tube. By repeating this step with another fresh cell strainer, adhesive tissue was most efficiently removed to yield high numbers of cells. After centrifugation, the supernatant was aspirated and discarded. For erythrolysis, the cell pellet was re-suspended in 3 ml RBC lysis buffer and kept

for 3 min on ice, followed by washing the cells with PBS. To lyse still remaining erythrocytes – visible as a small red staining on top of the cell pellet - another ml RBC lysis buffer was added for 1 min before the cells were washed again with PBS. Next, the cells were transferred to a 15 ml tube, thereby washed with PBS to remove all traces of the RBC lysis buffer, and re-suspended in 1 ml PBS. After counting the cells, their suspension was diluted with PBS to a concentration of 2 x 10^7/ml. For immunophenotyping, two 50 µl portions of the suspension (10^6 cells each) per parameter to be analyzed were transferred into wells of a U-bottom 96-well plate, which was stored at 4°C until cells were stained and analyzed by flow cytometry. The remaining cells were centrifuged and re-suspended in MACS® buffer to enable subsequent isolation of M-MDSCs, PMN-MDSCs or $CD4^+$ T cells.

Single PBMC suspension

After centrifugation of the blood/EDTA-mixture (see 2.4.1.4) at 500 x g for 10 min at 4°C, the plasma-containing supernatant was collected and stored in a 1.5 ml tube at -80°C. For erythrolysis, the remaining cell pellet was re-suspended in 5 ml RBC lysis buffer in a 15 ml tube and incubated on ice for 5 min. Next, the cells were washed with PBS, the supernatant aspirated and discarded. If necessary, 1 ml RBC lysis buffer was added repeatedly for 1 min until a red staining on the cell pellet was no longer visible. Finally, the PBMCs were washed again with PBS, quantified and prepared for immunophenotyping as described above (see “single splenocyte suspension”).

2.4.2.3 Phenotyping of immune cells by flow cytometry

Flow cytometry

Target cell types present in the cell suspensions derived from spleen and blood were identified and quantified by flow cytometry. This method is based on analyzing optical characteristics and fluorescence of single cells passing a laser beam. Depending on different cell characteristics (e.g. size, structure, granularity etc.) or staining patterns of molecules typical or even specific for a certain cell type which are targeted with fluorochrome-labeled antibodies, different cell types can be identified and quantified. Based on the measurement of light emission

after excitation of different antibody-bound fluorochromes with laser light of corresponding wave lengths, the method allows parallel assessment of several marker molecules. After injection of the sufficiently diluted suspensions into the buffer sheath flow, the hydrodynamically focused single cells pass the laser beam separately (Cossarizza et al. 2017). Fluorochromes are excited by light of a particular wave length and emit light of another distinct wave length which is measured by fluorescence detectors. In addition, forward and side scattered light (FSC and SSC) can be determined as measures of cell size and granularity, respectively. Since overlapping of excitation and emission spectra might impede with the clear identification of the signal's source, preliminary compensation measurements are mandatory when using a combination of such fluorochromes.

Protein targets used as single markers or in combinations to identify distinct cell types are listed in Table 5.

Table 5: Markers used for immunophenotyping of distinct cell types.
CD cluster of differentiation, *FoxP3* forkhead box P3, *IFN* interferon, *IL* interleukin, *MDSCs* myeloid-derived suppressor cells, *Tregs* regulatory T cells.

	MDSCs	T cells	Tregs	macrophages
cell surface molecules	CD11b Ly-6C Ly-6G	CD4	CD4 CD25	F4/80 CD11c CD206
intracellular targets		IFN-γ IL-4 IL-17A	FoxP3	IL-10

Immunostaining of cell surface molecules

Working solutions of antibodies (for dilutions see Table 2) as specified in Table 5 for the analyzed cell types, Fc-blocking reagent (dilution 1:20) and 7-AAD (dilution 1:40) were all prepared in FC Buffer. The 96-well plate containing the single splenocyte or PBMC suspension (see 2.4.2.2) was centrifuged and the supernatant was removed by turning the plate upside down onto an absorbent paper and tapping it gently to remove residual fluid. To prevent unspecific binding of the Fc termini of detection antibodies, Fc receptors were blocked by incubation

with 50 µl CD16/CD32-specific antibodies per well for 10 min. Subsequently, cells were incubated with 50 µl of the appropriate fluorochrome-labeled anti-mouse antibody or antibody mix for additional 20 min. After washing the cells with 150 µl PBS, 100 µl 7-AAD solution were added to the wells in which MDSCs were stained, before the cell suspension was transferred to FC tubes, incubated for 10 min and then diluted with 200 µl PBS. The fluorescent dye 7-AAD stains DNA by intercalation and is used to exclude dead cells with permeable plasma membranes from flow cytometry analyses (Schmid et al. 1992).

Samples stained to determine MDSCs were measured within 1 hour after addition of 7-AAD to avoid a potential effect of this agent on cell viability. In the remaining samples (for determinations of T cells and macrophages), staining of cell surface markers was followed by staining of intracellular cell type-specific molecules.

Immunostaining of intracellular molecules

The intracellular staining permeabilization wash buffer (PW buffer) and the FoxP3 permeabilization buffer were diluted 1:10 in ddH_2O or PBS, respectively; the FoxP3 fixation/permeabilization buffer 1:4 in PBS. For staining of T cells or macrophages, antibodies or mixtures thereof (see Table 5) were diluted in PW buffer, the Tregs-specific anti-FoxP3 antibody was prepared in an optimized FoxP3 permeabilization buffer. The cells were re-suspended in 100 µl of either fixation buffer (for measuring T cells and macrophages) or FoxP3 fixation/permeabilization buffer (for measuring Tregs) and incubated for 20 min in the dark. After centrifugation and discarding the supernatant, the cells were washed either twice with 200 µl PW buffer, or successively with 200 µl FC buffer and 200 µl FoxP3 permeabilization wash buffer. Next, the cells were re-suspended in 200 µl PW buffer or 200 µl FoxP3 permeabilization wash buffer, respectively, and incubated for 15 min. After centrifugation and addition of the appropriate antibody (mix), the cells were further incubated for 30 min. Cells were then washed twice with PW buffer (staining of T cells and macrophages) or FC buffer (detection of Tregs) before they were re-suspended in 150 µl FC Buffer and transferred to FC tubes for subsequent measurement. As permeabilization of the cells is required to allow uptake of antibodies, differentiation between dead and vital cells based on membrane transition of DNA-intercalating fluorescent

dyes like 7-AAD is not possible. Furthermore, 7-AAD was not compatible with the only available fluorochrome-labeled antibodies specific for T cells and macrophages because of their overlapping fluorochrome emission spectra.

Flow cytometric analyses

The samples containing the stained cells - kept in the dark at 4°C prior to further processing - were analyzed with the FACSCanto™ II cytometer controlled by the FACSDiva™ software. First the appropriate signal compensation for each staining approach was established based on data from the samples in preliminary experiments and applied to all subsequent measurements of the same type. Per sample, data from about 500,000 analyzed individual events were acquired after staining of cell surface molecules (e.g. analysis of MDSCs), but only about 300,000 events when intracellular molecules were assessed as cells had been lost during the additional washing steps. In addition to the fluorescence signals originating from the labeled antibodies used to identify the relevant cell types, FSC and SSC of individual cells were measured.

Data analyses

Raw data obtained by flow cytometric measurements were analyzed with the FlowJo software. The following gating strategies were used to analyze the amounts of target cells in the sample:

The first two gates were used to exclude doublets and cell debris based on their different FSC and SSC signals (Fig. 7 A). 7-AAD-positive dead cells were excluded from the analyses of MDSCs (Fig. 7 B). Then, $CD11b^+$ cells and the distinct subpopulations of Ly-$6G^-$ Ly-$6C^{high}$ M-MDSCs and Ly-$6G^{high}$ Ly-$6C^{low}$ PMN-MDSCs were selected (Fig. 7 B). The fractions of gated M- and PMN-MDSCs were calculated in relation to the number of vital, i.e. 7-AAD-negative cells.

$CD4^+$ cells were selected and cells also positive for IFN-γ were considered to be Th1 cells, those also positive for IL-4 Th2 cells, the IL17A-positive subgroup as Th17 cells, and those also positive for FoxP3 and CD25 Tregs (Fig. 7 C). The fractions of Tregs, Th1, Th2 and Th17 cells were calculated in relation to $CD4^+$ cells. Additionally, ratios between the fractions of T cells were determined.

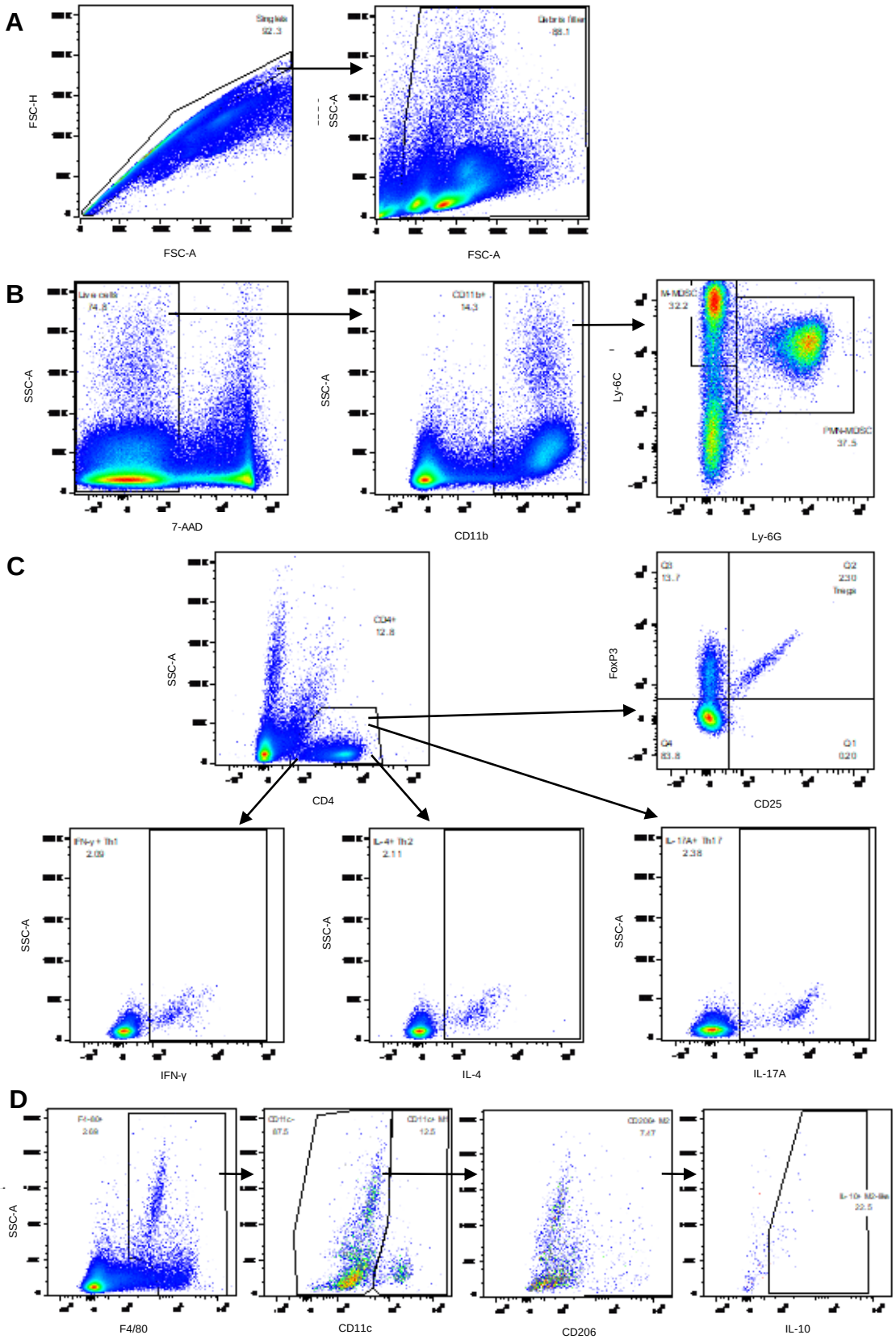

Figure 7: Gating strategies for flow cytometry data.
(**A**) Gates based on forward scatter (FSC-) height (H) and area (A) as well as sideward scatter area (SSC-A) to exclude doublets and cell debris. (**B**) Gating strategy for M-MDSCs and PMN-MDSCs. (**C**) Gating strategy for Tregs, Th1, Th2 and Th17 cells. (**D**) Gating strategy for M1, M2 and M2-like macrophages. Figure adapted from Deissler et al. (2021).

To determine the numbers of distinct macrophage subtypes, first F4/80$^+$ macrophages were selected (Fig. 7 D). Next, CD11c$^+$ M1 macrophages were separated from CD11c$^-$ cells which were subdivided into CD206$^+$ M2 macrophages and a CD206$^-$ population. The CD206$^+$ IL-10$^+$ cells were considered to be M2-like macrophages. The portions of M1, M2 and M2-like macrophages were calculated in relation to F4/80$^+$ cells. Ratios between the fractions of macrophage subsets were also calculated.

2.4.2.4 Cell isolation from single cell suspensions by magnetic-activated cell sorting

Magnetic-activated cell sorting (MACS®)

To assess a characteristic function of M- and PMN-MDSCs, their effect on CD4$^+$ T cell proliferation was measured. For MACS®, cells labeled with magnetic beads are separated in a magnetic field from non-labeled cells (Miltenyi et al. 1990). The method is based on binding of biotinylated primary antibodies targeting cell type-specific molecules to an anti-biotin antibody or streptavidin coupled to magnetic microbeads. The cell suspension then passes through a column placed in a magnetic field, in which labelled but not unlabeled cells are retained. Target cells labeled with magnetic beads can then be eluted from the column. In contrast to this process of positive selection, unlabeled cells, not expressing the marker molecules, can be collected directly after unhindered passage through the column (negative selection).

Isolation of CD4$^+$ T cells

Single cell suspension was prepared from the spleens of naïve C57Bl/6J mice which did not undergo allograft transplantation. Negative selection of CD4$^+$ T cells was performed with the CD4$^+$ T Cell Isolation Kit according to the manufacturer's instructions. In detail, the cells were re-suspended in 40 µl MACS® buffer per 10^7 cells and the suspension was incubated for 5 min with 10 µl biotin-antibody cocktail per 10^7 cells which contains antibodies against antigens expressed by non-target cells. Subsequently, 30 µl MACS® buffer and 20 µl anti-biotin microbeads per 10^7 cells were added. After incubation for 10 min, the suspension

of labelled and unlabeled cells (minimum volume of 500 µl; supplemented with MACS® buffer if necessary) was applied onto a LS column placed in the magnetic field of the MACS® Separator that had been rinsed with 3 ml MACS® buffer. Additional 3 ml MACS® buffer was allowed to flow through the column and the unlabeled $CD4^+$ T cells thereby flushed out were collected in a 15 ml tube and kept on ice until performing the CFSE proliferation assay.

Isolation of MDSCs

MDSC isolation was performed with the Myeloid-Derived Suppressor Cell Isolation Kit according to the manufacturer's instructions with adaptation of the volumes of the reagents used. The MDSC isolation consisted of two successive positive selections of Gr-1^{high}Ly-$6G^+$ PMN-MDSCs and Gr-1^{dim}Ly-$6G^-$ M-MDSCs. Splenocytes were re-suspended in 100 µl MACS® buffer and incubated with 25 µl Fc receptor blocking reagent for 10 min to avoid unspecific binding of antibodies. For isolation of PMN-MDSC, the suspension was further incubated with 30 µl anti-Ly-6G-biotin for 10 min before the cells were washed with PBS. After re-suspension in 300 µl MACS® buffer and addition of 50 µl anti-biotin microbeads, cells were then incubated for 15 min and washed again with PBS. Subsequently, the cell suspension, adjusted to a final volume of 500 µl with MACS® Buffer, was applied onto a LS column that had been rinsed with 3 ml MACS® buffer and exposed to the magnetic field of the MACS® Separator. Three portions of MACS® buffer (3 ml each) were allowed to flow through the column and the not bound unlabeled cells were collected in a 15 ml tube to be further used to isolate the M-MDSCs. The Ly-$6G^+$ PMN-MDSCs, detached outside the magnetic field, were eluted with 5 ml MACS® buffer.

After centrifugation of the M-MDSC-containing flow-through from the first separation step, PMN-MDSC-depleted cells were re-suspended in 200 µl MACS® buffer and 30 µl anti-Gr-1-biotin were added. Cells were incubated with this antibody for 10 min and, after washing with PBS, then with 50 µl streptavidin microbeads in 350 µl MACS® buffer for 15 min. Following another washing step with PBS, the re-suspended cells (in 500 µl MACS® buffer) were applied onto a MS column pre-rinsed with 500 µl MACS® buffer and placed in the magnetic field of the MACS® Separator. The column was washed with three 500 µl portions of

MACS® buffer, before the M-MDSCs were eluted from the column outside the magnetic field with 1 ml MACS® buffer.

After centrifugation of the respective eluates, PMN-MDSCs and M-MDSCs were re-suspended in supplemented RPMI-1640 medium and their numbers were determined. The isolated sub-fractions of MDSCs were kept on ice until performing the CFSE proliferation assay or isolation of ribonucleic acid (RNA).

2.4.2.5 Assessing the immunosuppressive activity of MDSCs

CFSE proliferation assay

MDSCs and T cells were co-cultivated in different ratios of M- or PMN-MDSCs to naïve T cells to assess inhibition of the T cell proliferation induced by MDSCs in the presence of the fluorescent dye CFSE which can be measured by flow cytometry. During cell division, intracellular CFSE is passed along to both daughter cells in equal amounts (Lyons et al. 1994). The mean fluorescence intensity of the measured cells, which divides in halves with every population doubling, inversely correlates with the number of cell divisions and is therefore a direct measure of proliferation.

Co-cultivation of $CD4^+$ T cells and MDSCs

$CD4^+$ T cells isolated from a spleen of a naïve C57Bl/6J mouse by MACS® were incubated in 1 ml PBS/5% FBS containing 1 µM CFSE for 15 min, before 15 ml supplemented RPMI-1640 medium were added. After further incubation for 10 min, the cells were washed with PBS. The CFSE-stained $CD4^+$ T cells were then re-suspended in supplemented RPMI-1640 medium and their number was determined. Mixtures of $CD4^+$ T cells and MDSCs in a total medium volume of 100 µl were plated in duplicates in wells of a U-bottom 96-well plate; the ratios and numbers of the cells per well are listed in Table 6.

Table 6: Carboxyfluorescein succinimidyl ester (CFSE) proliferation assay: Numbers per well and ratios of myeloid-derived suppressor cells (MDSCs) and $CD4^+$ T cells.

MDSC / $CD4^+$ T cell ratio	number of MDSCs	number of $CD4^+$ T cells
1:1	100,000	100,000
1:2	50,000	100,000
1:4	25,000	100,000
1:8	12,500	100,000

To stimulate $CD4^+$ T cell proliferation, 10 µl activation beads coupled to biotinylated antibodies against CD3ε- and CD28 (10^5 beads/µl) were added to 10^6 of these cells. The mixture was supplemented with IL-2 (final concentration: 250 U/ml) to further support T cell proliferation, and 1 µl/ml 50 mM β-mercaptoethanol as an antioxidant. Stimulated $CD4^+$ T cells without MDSCs and unstimulated $CD4^+$ T cells without CD3ε-/CD28-beads were used as controls. Cells were cultivated for 72 hours at 37°C in an atmosphere containing 5% V/V CO_2.

Staining of cells and flow cytometric analyses

Cells were washed with PBS at room temperature and then stained with 50 µl allophycocyanin (APC) -conjugated anti-CD4 antibody (diluted 1:800 in FC buffer) for 20 min at 4°C. After washing with PBS, the cells were re-suspended in 150 µl FC buffer and transferred to FC tubes for flow cytometric measurement. Data from about 100,000 events at the laser window of the flow cytometer were acquired per sample, including FSC, SSC and the emissions of APC and CFSE.

Data analyses

Assessment of $CD4^+$ T cell proliferation was based on measured amounts of CFSE in APC-labeled CD4+ cells, determined with the following gating strategy, also illustrated in Fig. 8 for stimulated $CD4^+$ T control cells.

After setting a gate on singlets (Fig. 8), $CD4^+$ and $CFSE^+$ T cells were selected from this population. Unstimulated, non-proliferative $CD4^+$ T cells served as control to set the gate for the determination of proliferating T cells. The fractions of proliferating $CD4^+$ T cells in their total population, cultivated together with the

different amounts of M- or PMN-MDSCs, were normalized in relation to the control containing only stimulated $CD4^+$ T cells to compare independent experiments.

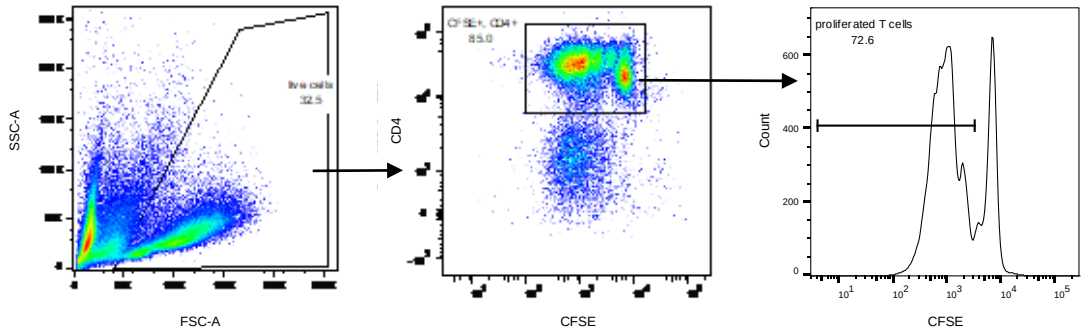

Figure 8: Gating strategy to measure proliferation with the carboxyfluorescein succinimidyl ester (CFSE) assay.
The label "proliferated T cells" refers to the cells that underwent at least one division. *FSC-A* forward scatter area, *SSC-A* sideward scatter area. Figure adapted from Deissler et al. (2021).

2.4.2.6 Analyses of MDSCs' relative expression of specific messenger RNAs by quantitative real-time PCR

Quantitative real-time PCR (qPCR)

The impact of obesity and rapamycin treatment on relative expression of specific messenger RNAs (mRNAs) encoding relevant proteins by M- and PMN-MDSCs was also investigated, covering the period between POD 3 and POD 11. For this, total RNA was isolated from MDSCs and transcribed with reverse transcriptase into cDNA for subsequent analysis by qPCR, a method first described by Heid et al. (1996).

The used variant of qPCR allows quantification of RNA molecules transcribed into cDNA and amplified by PCR based on intercalation of a present fluorescence dye into the increasing amount of newly formed double-stranded DNA (dsDNA). The intercalation is associated with a characteristic fluorescence that can be recorded during the amplification process. The target sequences are amplified from cDNA templates by a thermostable polymerase with primers specific for the sequence of interest and deoxyribose nucleoside triphosphates (dNTPs) in the presence of a fluorescent dye, e.g. SYBR® Green. Exponential amplification of the target sequence is achieved by repeating cycles of (three) temperatures the sample is exposed to, which are appropriate to allow denaturation of dsDNA,

annealing of the primers, and synthesis of the PCR products. As the emission wavelength of SYBR® Green I depends on its binding to dsDNA, the changed signal can be measured and used to determine the amount of the formed PCR product (Lekanne Deprez et al. 2002). The threshold cycle (C_T) is defined as cycle number at which the amount of amplified target or the corresponding fluorescence signal reaches a fixed threshold value (Livak et al. 2001). The threshold value needs to be set at the point where the fluorescence signal exceeds the background signal and the amplification is still in the phase of almost linear product increase. After completion of the final step, a melting curve typically showing a single characteristic peak is generated to confirm authenticity of the PCR product and high specificity of the amplification process (Lekanne Deprez et al. 2002). An inter-run calibration with total cDNA from naïve mouse bone marrow cells as a reference sample allowed direct comparison of C_T-values from different experiments.

Isolation of RNA

Purification of total RNA from isolated M- and PMN-MDSCs was performed according to the manufacturer's protocol with the RNeasy micro and mini kit, respectively, chosen according to cell numbers obtained. In detail, the cells were lysed and homogenized with 350 µl RLT buffer containing guanidine thiocyanate to inactivate RNases and β-mercaptoethanol (1% V/V). Then 350 µl 70% ethanol was added to improve RNA binding to the silica membrane in a micro spin-column on which the sample was applied. After centrifugation (8000 x g for 20 s) the RNA was bound to the silica membrane and the flow-through was discarded. Washing steps were performed by successive centrifugations of solutions through the membrane at 8000 x g for 20 s: 350 µl (M-MDSCs) or 700 µl (PMN-MDSCs) RW1 buffer to remove non-specifically bound molecules from the membrane, 500 µl RPE buffer for removal of traces of salt. Followed by the addition of 500 µl 80% ethanol (M-MDSCs) or only 500 µl RPE buffer (PMN-MDSCs) and centrifugation at 8000 x g for 2 min (M-MDSCs) or 20 s (PMN-MDSCs), the RNA was eventually eluted by pipetting 14 µl (M-MDSCs) or 30 µl (PMN-MDSCs) RNase-free water on top of the membrane and centrifugation for 1 min at 8000 x g. The absorptions of the RNA solution at 260 nm and 280 nm were measured by spectrophotometry

with the NanoPhotometer® to assess purity (A_{260}/A_{280} ratio affected by DNA or protein contamination) and to determine the concentration (proportional to A_{260}) of the RNA. Immediately after isolation, the RNA was converted to cDNA by reverse transcription.

Reverse transcription (RT)

RT from RNA to single-stranded cDNA was performed with the High Capacity cDNA Reverse Transcription Kit according to the manufacturer's protocol. Briefly, 10 µl RT master mix per reaction was prepared by mixing 2 µl RT buffer, 2 µl random primers, 0.8 µl dNTP mix, 1 µl reverse transcriptase, 1 µl RNase inhibitor and 3.2 µl RNase-free H_2O. Next, 10 µl RT master mix and 10 µl containing up to 2 µg total RNA were combined in a 0.2 ml PCR reaction tube which was placed in a thermal cycler. The conditions for reverse transcription were as follows: 25°C for 10 min, 37°C for 120 min, 85°C for 5 min and 4°C on hold until the reaction tube was removed. Aliquots of the cDNA were stored at -20°C until their analyses by qPCR were carried out.

qPCR analyses

cDNA samples and primers were diluted to concentrations of 2 ng/µl and 10 pmol/µl, respectively. For each PCR reaction to be carried out, 7.5 µl qPCR master mix, consisting of 1.7 µl nuclease-free water, 0.4 µl forward primer, 0.4 µl reverse primer and 5 µl SYBR® green master mix (SYBR® Green I dye, SSo7d fusion polymerase, dNTPs and $MgCl_2$), were placed in a well of a qPCR plate.

Then, 2.5 µl cDNA sample, inter-run calibration sample, or nuclease-free water was added to result in a total volume of 10 µl per well. The plate was sealed firmly with an adhesive sealer and centrifuged at 300 x g for 2 min at 4°C to spin down liquid potentially adhering to the walls of the wells. To perform the qPCR analyses, the plate was inserted in a LightCycler® 480 II controlled by LightCylcler® 480 software and processed as listed in Table 7.

On one plate, three cDNA samples, the inter-run calibration sample and nuclease-free water as no-template control (NTC) were analyzed with primer sets for 9 target sequences: *Actb*, *Arg1*, *COX2*, *Nos2*, *Stat3*, *Il10*, *Ido1*, *Ido2* and *Tgfb*.

Table 7: Quantitative real-time polymerase chain reaction (qPCR) conditions.
DNA deoxyribonucleic acid.

step		number of cycles	temperature	time
pre-incubation	initial denaturation, polymerase activation		95°C	5 min
amplification	DNA denaturation	45	95°C	10 s
	primer annealing		55°C	10 s
	primer extension		72°C	20 s
melting curve			95°C	5 s
			65°C	1 min
			97°C	until 97°C
cooling			40°C	30 s

Data analyses

qPCR raw data were analyzed with the LightCylcler® 480 software. The relative expression of a target RNA was calculated with the $\Delta\Delta C_T$ method as described previously (Hellemans et al. 2007, Livak et al. 2001) with β-actin encoding mRNA/cDNA as a reference. The ΔC_T values were normalized in relation to the inter-run calibration sample, and $\Delta\Delta C_T$ values of the different treatment groups were normalized in relation to either the untreated lean group (lean VHC) or the treated lean group (lean Rapa).

$$\Delta C_T = C_T(\beta - actin) - C_T(target\ of\ interest)$$

$$\Delta\Delta C_T = \Delta C_T(target\ of\ interest) - \Delta C_T(inter - run\ calibration)$$

$$normalized\ 2^{\Delta\Delta C_T} = \frac{2^{\Delta\Delta C_T}(other\ treatment\ groups)}{\bar{X}(2^{\Delta\Delta C_T}(lean\ VHC\ or\ lean\ Rapa))}$$

2.4.2.7 Measuring the concentrations of cytokines and chemokines in plasma

Multiplex sandwich immunoassay

To determine the potentially changed expression profile of cytokines, chemokines and growth factors involved in MDSC and Treg activation and expansion, a multiplex sandwich immunoassay was performed. The used Luminex® xMAP® (multi-analyte profiling) technology allowed parallel analyses of various biomarkers in small samples. Analyte-specific capture antibodies are coupled to magnetic polystyrene microparticles stained with different combinations of fluorochromes. Distinction between beads with antibodies of different specificities is possible because of their particular color, defined by the ratio of incorporated fluorochromes. Parallel to measuring the analyte-specific signal, the color of a bead is recognized after laser excitation (Elshal et al. 2006). The analyte of interest binds to the capture antibody - coupled to a fluorochrome-labelled bead - and to a second (detection) antibody also coupled to a fluorescent dye, e.g. phycoerythrin (PE). During flow of the microspheres through the analyzer the fluorochromes inside every bead are excited by a laser to identify the color of the bead and thereby the associated analyte. Another laser, emitting light of a different wave length, excites the fluorochrome of the detection antibody (e.g. PE) and the intensity of its fluorescence is recorded as a measure of the amount of analyte. By means of a standard curve, the concentration of a specific analyte in the sample can be calculated.

Preparation of analyte-binding microspheres and determination of cytokine/chemokine concentrations

The concentrations of CCL2, CXCL1, CXCL2, CXCL12, GM-CSF, IFN-γ, IL-1β, IL-6, IL-10, IL-17, and TNF-α in plasma samples were measured with the Magnetic 11-plex Luminex® Assay according to the manufacturer's instructions. In detail, an 8-fold dilution row in calibrator diluent RD6-52 was prepared from the included standard cocktail and plasma samples were diluted 2-fold in RD6-52. Microparticles and biotin-antibody cocktails were diluted 1:10 in assay diluent RD1W prior to use. Immediately before adding the streptavidin-PE conjugate to the beads, it was diluted 1:25 in wash buffer. Each standard or sample (50 µl) was mixed with 50 µl of the diluted microparticles in a well of a 96-well flat-bottom

microplate. The sealed plate was incubated for 2 hours on a microplate shaker at 800 rpm and room temperature. A magnet was then placed under the microplate to keep the magnetic beads at the bottom of the wells. After 1 min, the supernatant was discarded and the plate was put on an absorbent paper and tapped to completely remove residual liquid. The magnet was then removed and the beads in each well were re-suspended in 150 µl wash buffer. The magnet was again placed under the plate, and after 1 min the wash buffer was removed from the beads as described above. This washing step was repeated twice, before the beads in each well were re-suspended in 50 µl of the diluted biotin-antibody solution and the plate was incubated for 1 hour on the shaker at 800 rpm. After the beads had been washed three times, 50 µl of the streptavidin-PE conjugate was added and the plate was incubated for 30 min. Subsequently, the beads were again washed three times and re-suspended in 100 µl wash buffer to be measured in the Luminex® FLEXMAP 3D® analyzer shortly thereafter.

For each of the analytes assessed in the multiplex assay, data from 50 microparticles were acquired and the median fluorescence intensity (MFI) was recorded.

Data analyses

Standard curves based on the MFIs resulting from standard samples containing known concentrations of the proteins were calculated (after subtracting the blank value from measured values) by a five parameter logistic curve-fit using MasterPlex ReaderFit software. This allowed the concentrations of the analytes in each sample to be determined, taking the initial dilution of the samples into account. In addition, correlation analyses of cytokine and chemokine concentrations with cell numbers were performed.

2.4.3 Statistical analyses

All statistical analyses were performed with GraphPad Prism. The data were presented as mean ± standard deviation (SD) and p-values <0.05 were considered statistically significant. The Kaplan-Meier curves for allograft survival were compared with the log-rank test. Comparisons of means between four groups were conducted by one-way analysis of variance (ANOVA) including a Bonferroni post-hoc test, means of two groups were compared with the unpaired Student's t-test.

3. Results

The results presented here have been published elsewhere (Deissler et al. 2021).

3.1 Skin allograft survival was prolonged by rapamycin treatment particularly favoring obese recipients

Rapamycin treatment had a significant effect on survival of skin allografts received by both obese and lean mice (Fig. 9). While allograft survival was not different between the untreated groups of lean (mean 8.4 days) and obese (8.7 days) recipient mice, treatment with rapamycin significantly prolonged allograft survival in both lean (10.7 days vs. 8.4 days; p = 0.02) and obese (14.5 days vs. 8.7 days; p = 0.0001) recipients compared to their untreated counterparts. Notably, the rapamycin-induced prolongation of allograft survival was considerably longer (mean survival of 14.5 days vs. 10.7 days, p = 0.005) in the group of obese recipient mice.

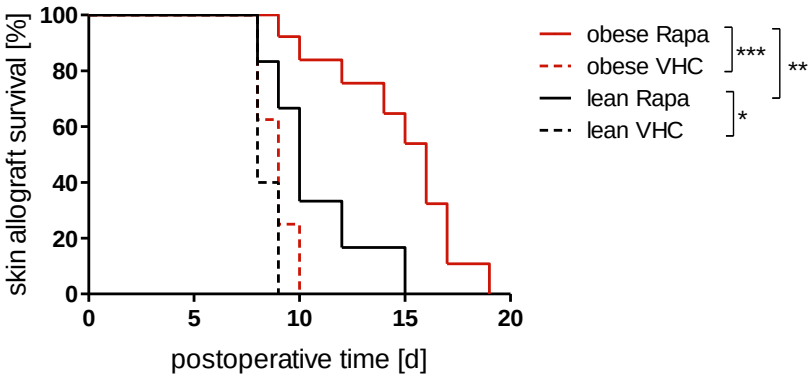

Figure 9: Rapamycin-induced extension of skin allograft survival was more pronounced in obese recipients.
Obese and lean mice underwent full-MHC-mismatched skin allograft transplantations and were treated either with the vehicle DMSO (VHC) or 2 mg/kg rapamycin (Rapa) i.p. daily (see 2.4.1). Allografts were evaluated on each POD until allograft rejection, defined as < 50% allograft viability. Kaplan-Meier curves of graft survival are shown. * $p < 0.05$, ** $p < 0.01$, *** $p < 0.001$; lean VHC: n = 5, lean Rapa: n = 6, obese VHC: n = 7, obese Rapa: n = 10. Figure adapted from Deissler et al. (2021).

3.2 Number of splenic M-MDSCs and their relative abundance was increased by rapamycin in obese allograft recipients

The fractions of M-MDSCs and PMN-MDSCs in the isolated splenocytes were determined by flow cytometry at the day of rejection or at defined PODs. At POD

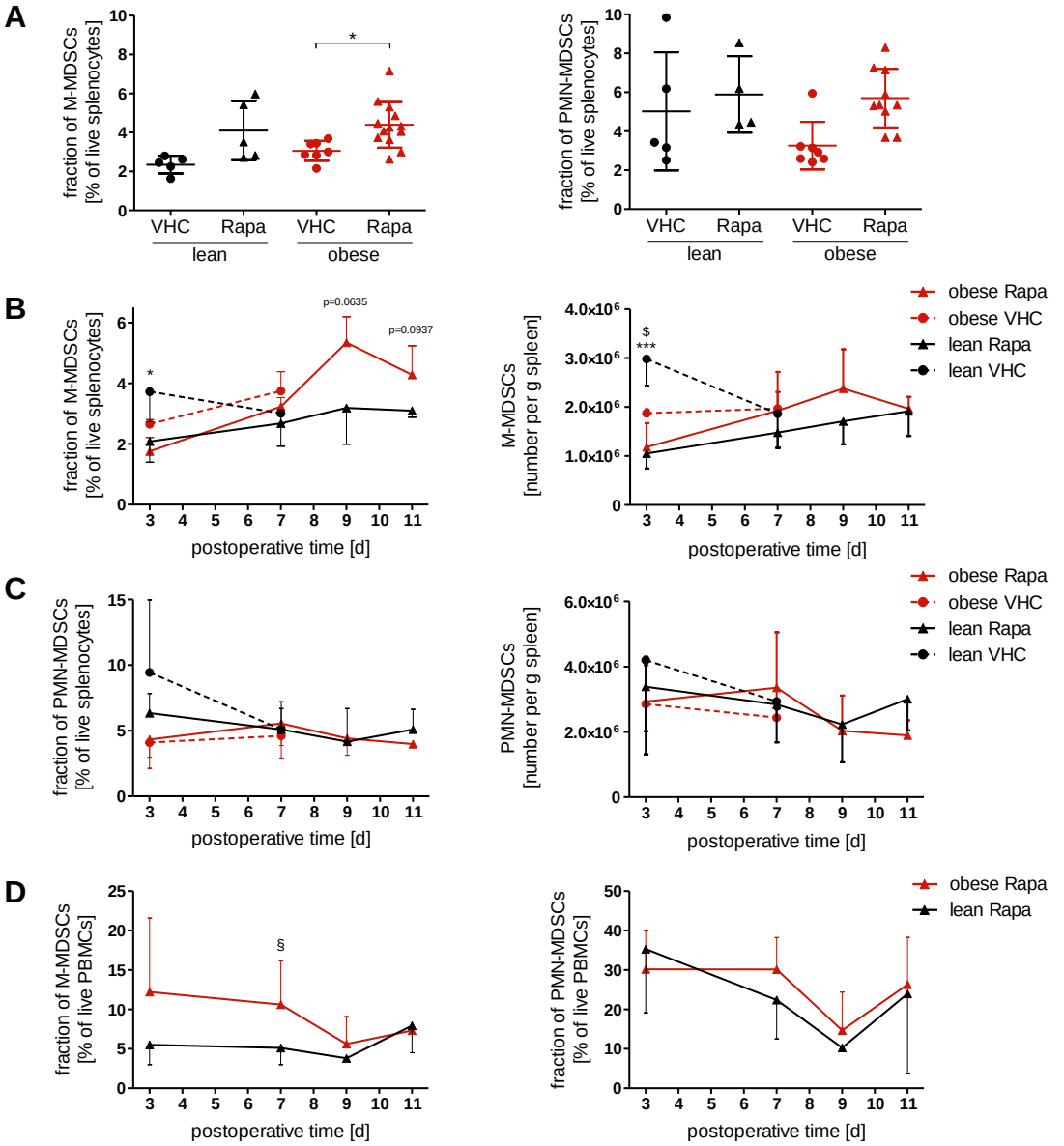

Figure 10: Number of splenic monocytic (M-) myeloid-derived suppressor cells (MDSCs) from obese mice increased during rapamycin treatment.

Obese and lean mice underwent full-MHC-mismatched skin allograft transplantation and were treated either with the vehicle DMSO (VHC) or 2 mg/kg rapamycin (Rapa) i.p. daily (see 2.4.1). On the day of rejection, animals were sacrificed and spleens collected to prepare single splenocyte suspensions. Expression of the markers CD11b, Ly-6C and Ly-6G by the cells was analyzed by flow cytometry and the numbers of $CD11b^{+}$ $Ly\text{-}6G^{-}$ $Ly\text{-}6C^{high}$ M-MDSCs and $CD11b^{+}$ $Ly\text{-}6G^{high}$ $Ly\text{-}6C^{low}$ polymorphonuclear (PMN-) MDSCs, respectively, were determined.

(**A**) Fractions of M- and PMN-MDSCs in spleen-derived cells at the day of allograft rejection. Data are presented as mean ± SD; * $p < 0.05$, comparisons of indicated groups; lean VHC: n = 5, lean Rapa: n = 4-5, obese VHC: n = 7, obese Rapa: n = 10-13.

(**B, C**) The time course of absolute numbers and relative abundance of M-MDSCs (**B**) and PMN-MDSCs (**C**) in spleen-derived cells isolated at PODs 3, 7, 9 and 11 was analyzed. Data are presented as mean ± SD; * $p < 0.05$, *** $p < 0.001$ for lean Rapa compared to lean VHC; $ $p < 0.05$ for obese VHC compared to lean VHC; lean VHC: n = 3, lean Rapa: n = 6, obese VHC: n = 3, obese Rapa: n = 6. P-values slightly above the significance threshold are provided as exact numbers.

(**D**) Blood was taken from mice on POD 3, 7, 9 and 11, and fractions of M- and PMN-MDSCs in peripheral blood mononuclear cells (PBMCs) were determined. Data are presented as mean ± SD; § $p < 0.05$ for obese Rapa compared to lean Rapa; lean VHC: n = 3, lean Rapa: n = 6, obese VHC: n = 3, obese Rapa: n = 6.

Figure adapted from Deissler et al. (2021).

3, the number of M-MDSCs was slightly higher in untreated lean mice (Fig. 10 B, C), but from POD 7 until the day of rejection, fractions of both M-MDSCs and PMN-MDSCs isolated from untreated lean or obese mice were of comparable sizes (Fig. 10 A). However, rapamycin treatment significantly increased the number of M-MDSCs in spleens obtained at the day of allograft rejection from obese mice. Similar trends, though not statistically significant, were also observed for PMN-MDSCs from obese recipients and M-MDSCs from lean mice (Fig. 10 A). Accordingly, more M-MDSCs were detected in spleens isolated from obese rapamycin-treated mice still having vital allografts between POD 3 and POD 11 – reaching a maximum on POD 9 – and these cells also represented a larger fraction of the total cell population (Fig. 10 B). The portion of PMN-MDSCs remained rather constant over time with a pronounced peak only observed at POD 7 (Fig. 10 C). In line with these tissue-based results, peripheral blood obtained from obese mice treated with rapamycin contained a larger fraction of M-MDSCs compared to blood from their lean counterparts, even though the differences were only significant at POD 7 (Fig. 10 D).

3.3 The immunosuppressive activity of M-MDSCs was enhanced by rapamycin in obese allograft recipients

To assess the immunosuppressive capacities of isolated MDSCs, their effect on proliferation of CFSE-stained $CD4^+$ T cells was measured. Representative histograms of $CD4^+$ T cells that had been allowed to proliferate in co-cultivation experiments with M-MDSCs and PMN-MDSCs at MDSC/T cell ratios of 1:1, 1:2, 1:4 and 1:8 are shown in Fig. 11 and 12. Distinct generations of T cells having undergone one or more cell divisions are identifiable as (small) peaks (red arrows) beside the most prominent peak (black arrow) in each histogram representing the generation of parental $CD4^+$ T cells containing the highest amounts of CFSE. At a ratio of 1:1, the $CD4^+$ T cell proliferation was almost completely blocked by M- or PMN-MDSCs with the only exception being splenic MDSCs isolated from obese, untreated mice. A smaller fraction of MDSCs in the co-cultivation experiments resulted in an increased $CD4^+$ T cell proliferation, confirming the MDSC-dependent inhibition of $CD4^+$ T cell proliferation.

M-MDSCs isolated at the day of rejection from lean animals strongly inhibited CD4$^+$ T cell proliferation irrespective of the animals' treatment (Fig. 13 A). However, CD4$^+$ T cell proliferation was only weakly inhibited by splenic M-MDSCs isolated from untreated obese recipients at the day of rejection. In strong contrast, M-MDSCs originating from rapamycin-treated obese recipients blocked CD4$^+$ T cell proliferation similarly efficient as those from lean recipients. PMN-MDSCs

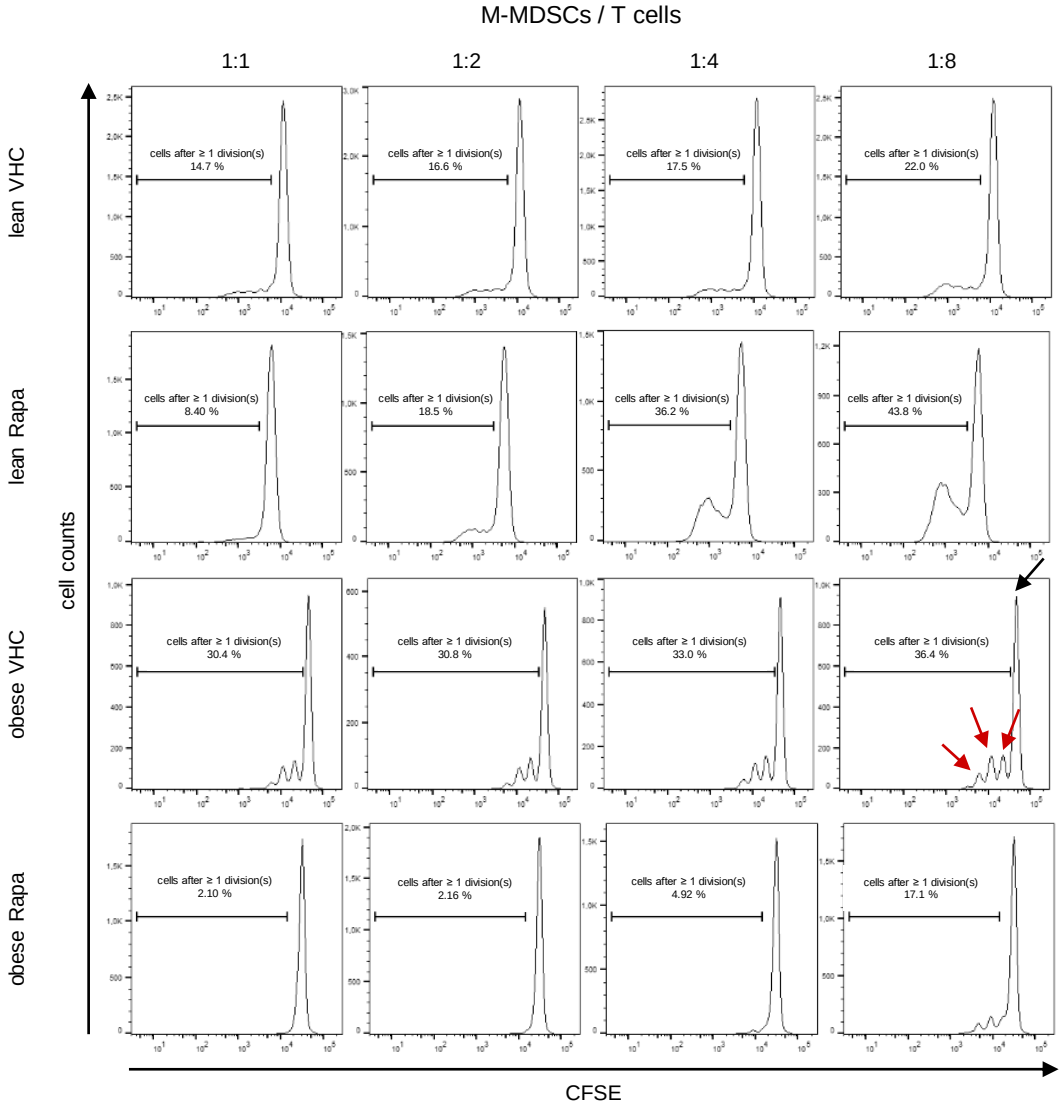

Figure 11: Representative histograms of carboxyfluorescein succinimidyl ester (CFSE) -stained CD4$^+$ T cells co-cultivated with monocytic myeloid-derived suppressor cells (M-MDSCs).
Obese and lean mice underwent full-MHC-mismatched skin allograft transplantation and were treated with rapamycin as described or assigned to the respective untreated control group (see 2.4.1). On the day of rejection, spleens were removed to prepare single splenocyte suspensions. M-MDSCs were isolated and co-cultivated for 72 hours with CFSE-stained CD4$^+$ T cells from naïve mice in M-MDSC/CD4$^+$ T cell ratios of 1:1, 1:2, 1:4 and 1:8. Proliferation of CD4$^+$ T cells was determined by flow cytometric measuring of CFSE levels of CD4$^+$ cells depending on the number of divisions after labeling. Indicated gates are covering the fraction of CD4$^+$ T cells having undergone at least one division. Exemplarily, the black arrow shows the peak of the unproliferative CD4$^+$ T cells, whereas the red arrows point to daughter cell populations after one, two or three divisions. Every row represents an experiment with M-MDSCs derived from one mouse of the respective group. Figure adapted from Deissler et al. (2021).

isolated from obese and lean recipients at the day of rejection also substantially inhibited CD4$^+$ T cell proliferation irrespective of rapamycin treatment, although at a 1:1 ratio, the effect of PMN-MDSCs from rapamycin-treated obese mice was more pronounced compared to these cells from untreated obese animals. Interestingly, inhibition of CD4$^+$ T cells by PMN-MDSCs from rapamycin-treated lean animals was less pronounced than that of cells of this type from untreated

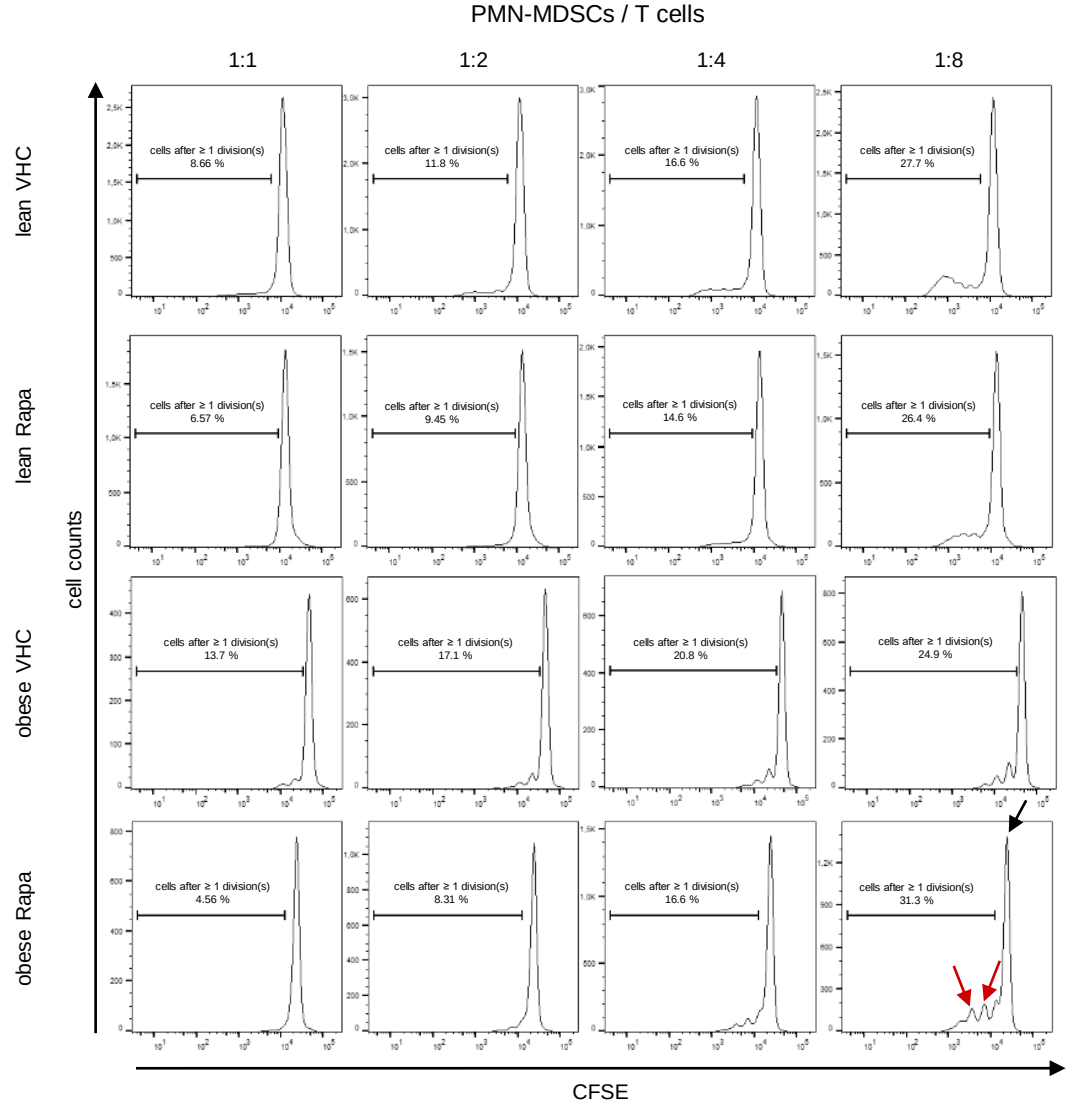

Figure 12: Representative histograms of carboxyfluorescein succinimidyl ester (CFSE) -labeled CD4$^+$ T cells co-cultivated with polymorphonuclear myeloid-derived suppressor cells (PMN-MDSCs).

Obese and lean mice underwent full-MHC-mismatched skin allograft transplantation and were treated with rapamycin as described or assigned to the respective untreated control group (see 2.4.1). On the day of rejection, spleens were removed to prepare single splenocyte suspensions. PMN-MDSCs were isolated and co-cultivated for 72 hours with CFSE-stained CD4$^+$ T cells from naïve mice in PMN-MDSC/CD4$^+$ T cell ratios of 1/1, 1/2, 1/4 and 1/8. Proliferation of CD4$^+$ T cells was determined by flow cytometric measuring of CFSE levels of CD4-positive cells depending on the number of divisions after labeling. Indicated gates are covering the fraction of CD4$^+$ T cells having undergone at least one division. Exemplarily, the black arrow shows the peak of the unproliferative CD4$^+$ T cells, whereas the red arrows point to daughter cell populations after one, two or three divisions. Every row represents an experiment with PMN-MDSCs derived from one mouse of the respective group. Figure adapted from Deissler et al. (2021).

lean recipients at lower ratios in the co-cultivation experiments, reflected by a statistically significant difference at a ratio of 1:8 (Fig. 13 A). Taken together, these in vitro experiments indicate that the impaired immunosuppressive activity of M-MDSCs (and PMN-MDSCs) in obese mice could be restored by rapamycin whereas such treatment had no effect or even counteracted MDSC-mediated immunosuppression in lean mice at the day of rejection.

Notably, when equal numbers (ratio of 1:1) of the different cell types were co-cultivated, the capacity of M-MDSCs (but not of PMN-MDSCs) from rapamycin-treated obese mice to lower CD4$^+$ T cell proliferation increased from POD 3 to POD 11, reaching maximum inhibition at POD 9 (Fig. 13 B). M-MDSCs and PMN-

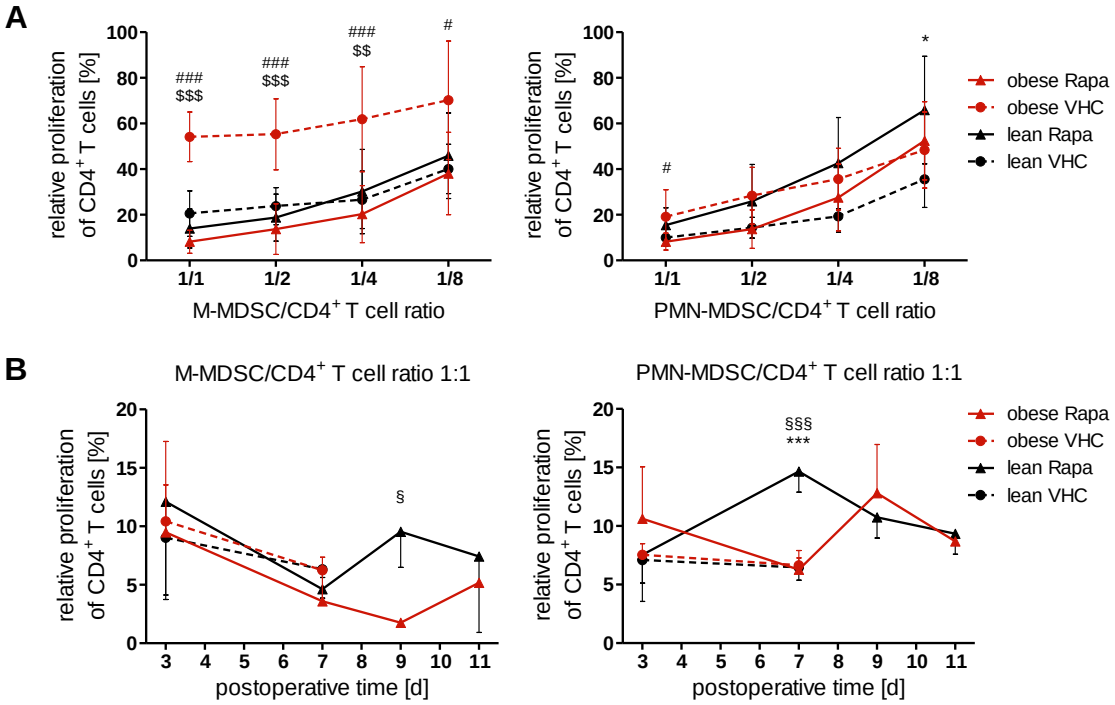

Figure 13: Rapamycin increased the suppressive effect of monocytic (M-) myeloid-derived suppressor cells (MDSCs) on T cell proliferation.
Skin allograft transplantation and rapamycin treatment of obese and lean mice were performed as described (see 2.4.1). On the day of rejection (**A**) or on defined postoperative days (**B**), M- and PMN-MDSCs were isolated from splenocyte suspensions, co-cultivated with carboxyfluorescein succinimidyl ester (CFSE) –stained CD4+ T cells from naïve mice for 72 hours, and proliferation of CD4$^+$ T cells was assessed as described above (see Figs. 11, 12). The fraction of proliferative CD4$^+$ T cells was set in relation to that of the control containing only stimulated CD4$^+$ T cells.
(**A**) Proliferation of CD4$^+$ T cells co-cultivated with M- or polymorphonuclear (PMN-) MDSCs isolated at the day of allograft rejection. Data are presented as mean ± SD; means were compared for every MDSC/CD4$^+$ T cell ratio; * $p < 0.05$, lean VHC compared to lean Rapa; # $p < 0.05$, ### $p < 0.001$, obese VHC compared to obese Rapa; $$ $p < 0.01$, $$$ $p < 0.001$, lean VHC compared to obese VHC; lean VHC: n = 4-5, lean Rapa: n = 5, obese VHC: n = 7, obese Rapa: n = 8-9.
(**B**) Representative time courses of inhibition of CD4$^+$ T cell proliferation by M- and PMN-MDSCs at a ratio of 1:1 in the co-cultivation experiments. Data are presented as mean ± SD; means were compared for every MDSC/CD4$^+$ T cell ratio; * $p < 0.05$, *** $p < 0.001$, lean VHC compared to lean Rapa; ## $p < 0.01$, obese VHC compared to obese Rapa; § $p < 0.05$, §§ $p < 0.01$, §§§ $p < 0.001$, lean Rapa compared to obese Rapa; lean VHC: n = 3, lean Rapa: n = 6, obese VHC: n = 3, obese Rapa: n = 6.
Figure adapted from Deissler et al. (2021).

MDSCs isolated at PODs 3, 7, 9 or 11 all strongly inhibited CD4$^+$ T cell proliferation at all ratios tested and irrespective of treatment, although subtle

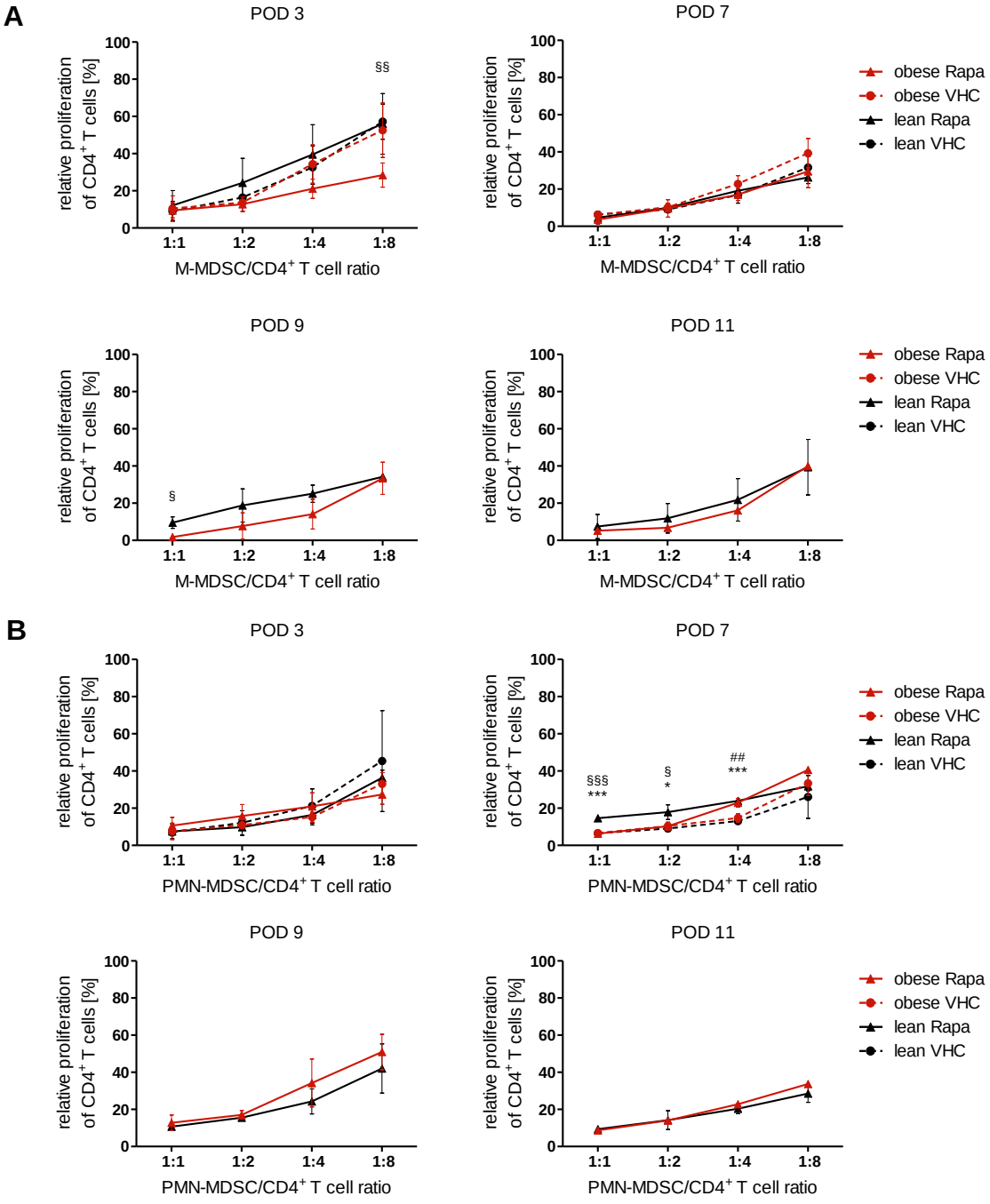

Figure 14: From postoperative day (POD) 3 until POD 11, rapamycin only slightly altered the effects of monocytic (M-) and polymorphonuclear (PMN-) myeloid-derived suppressor cells (MDSCs) on T cell proliferation.

Skin allograft transplantation and rapamycin treatment of obese and lean mice were performed as described (see 2.4.1). On defined PODs, M- and PMN-MDSCs were isolated from splenocyte suspensions, co-cultivated for 72 hours with carboxyfluorescein succinimidyl ester (CFSE) –stained CD4$^+$ T cells from naïve mice, and proliferation of CD4$^+$ T cells was assessed as described above. The portion of proliferative CD4$^+$ T cells was set in relation to that of the control containing only stimulated CD4$^+$ T cells. Values of relative proliferation of CD4$^+$ T cells co-cultivated with (**A**) M- and (**B**) PMN-MDSCs isolated on PODs 3, 7, 9 or 11 are shown. Data are presented as mean ± SD; means were compared for every MDSC/CD4$^+$ T cell ratio; * $p < 0.05$, *** $p < 0.001$, lean VHC compared to lean Rapa; ## $p < 0.01$, obese VHC compared to obese Rapa; § $p < 0.05$, §§ $p < 0.01$, §§§ $p < 0.001$, lean Rapa compared to obese Rapa; lean VHC: n = 3, lean Rapa: n = 6, obese VHC: n = 3, obese Rapa: n = 6. Figure adapted from Deissler et al. (2021).

differences were observed: M-MDSCs isolated at PODs 3 or 9 from obese rapamycin-treated mice inhibited proliferation of $CD4^+$ T cells stronger compared to those obtained from treated lean mice, which was obvious only at certain MDSC/$CD4^+$ T cell ratios (Fig. 14 A). Interestingly, the anti-proliferative effect on $CD4^+$ T cells of PMN-MDSCs derived from rapamycin-treated lean mice obtained on POD 7 was lower than that of PMN-MDSCs from untreated lean or treated obese mice, but PMN-MDSCs from rapamycin-treated obese mice inhibited $CD4^+$ T cell proliferation stronger compared to those from untreated obese mice when cultivated at a ratio of 1:4 (Fig. 14 B).

3.4 Rapamycin treatment changed expression of mRNAs encoding relevant proteins by M-MDSCs and PMN-MDSCs from obese mice

To gain insight into the mechanism of immunosuppression by MDSCs, their expression of potentially relevant mRNAs (i.e. *Arg1, Ido1, Ido2, Il10, Tgfb1, Stat3, and COX2*) from POD 3 to POD 11 was analyzed by qPCR. In general, the levels of these transcripts were found to be similar in M-MDSCs obtained from untreated lean and obese animals on POD 3 and POD 7 with the exceptions of *Tgfb1*-, *Nos2*- and *Ido1*-mRNAs which were less expressed by cells from obese mice (Fig. 15 A, B). Treatment of obese or lean mice with rapamycin resulted in changes of mRNA expression only early after transplantation: M-MDSCs isolated from treated obese mice expressed more *Il10*-, *Ido1*-, *Ido2*-, *Tgfb-1*- and *Nos2*-mRNAs, those from lean mice less *Stat3-,* and *Tgfb1*-mRNAs compared to the respective untreated animals (Fig. 15 A, B). Interestingly, expression of *COX2*-mRNA by M-MDSCs from treated lean animals was lower on POD3 and higher on POD 7. Late after transplantation, expression levels of all transcripts investigated did not differ between lean or obese animals and their counterparts under medication with rapamycin. Increased expressions of *Ido1*, *Ido2*, *Tgfb1*, *Stat3*, *and COX2* were measured in rapamycin-treated obese mice compared to treated lean mice.

Levels of investigated mRNAs expressed by PMN-MDSCs from untreated lean and obese mice were similar (Fig. 16 A, B). Rapamycin treatment resulted in higher levels of expression of *Arg1*, *Nos2*, *Stat3* and *Ido1* by PMN-MDSCs from lean mice early after transplantation. A similar trend was observed for PMN-MDSCs from obese animals although these differences were not above the

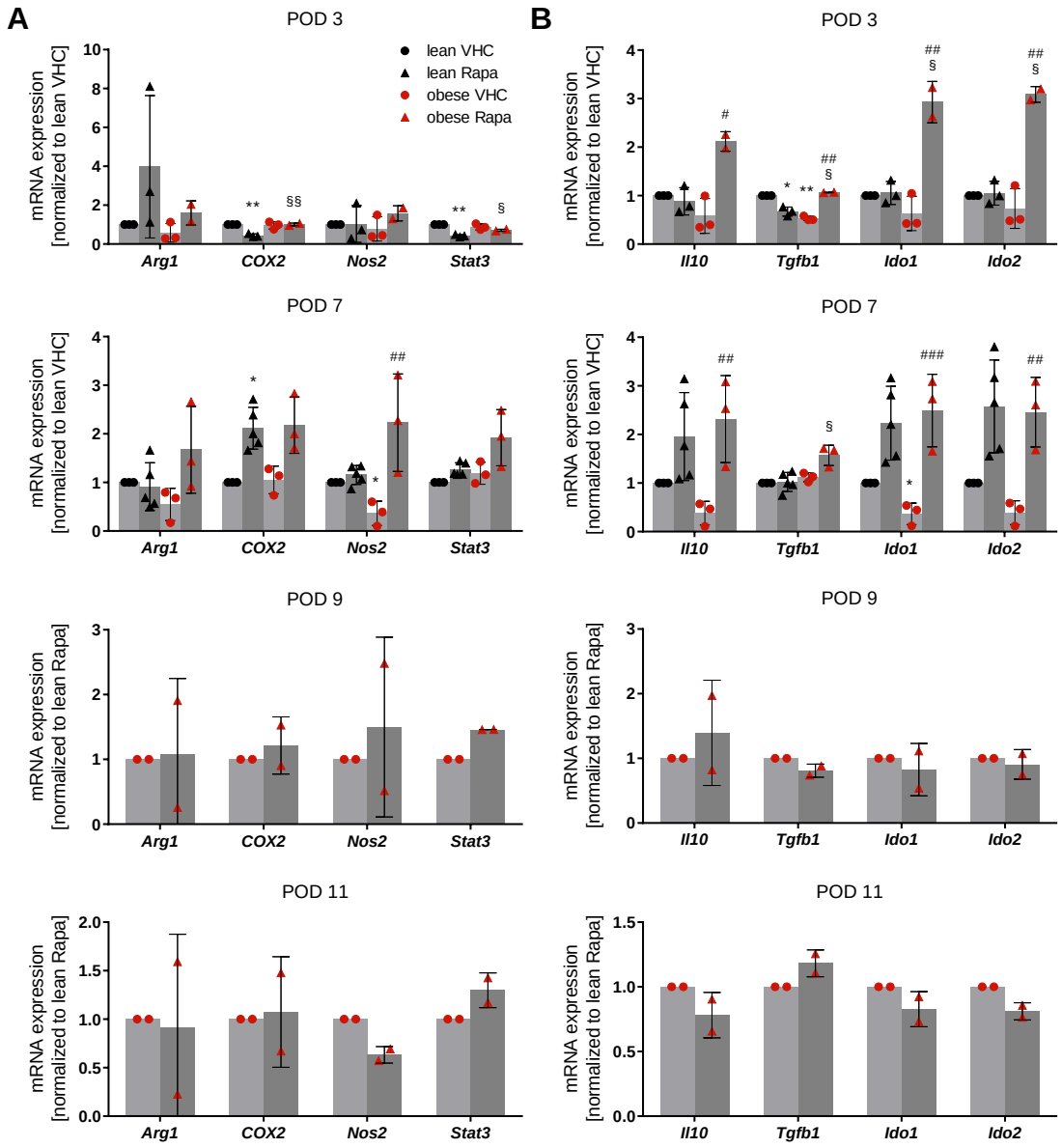

Figure 15: Rapamycin treatment induced monocytic myeloid-derived suppressor cells (M-MDSCs) to differently express mRNAs relevant to their function.
On different postoperative days (PODs), mRNA expression of (**A**) arginase-1 (*Arg1*), cyclooxygenase-2 (*COX2*), inducible nitric oxide synthase (*Nos2*), signal transducer and activator of transcription (*Stat3*) and (**B**) interleukin-10 (*Il10*), transforming growth factor beta (*Tgfb1*), indoleamine 2,3-dioxygenase (*Ido1* and *Ido2*) by M-MDSCs isolated from spleens of lean or obese allograft recipients treated with rapamycin or the vehicle DMSO (VHC) was analyzed by qPCR. For the sake of better visualization, signals were normalized after statistical analysis as described (see 2.4.2.6). Data are presented as mean ± SD; * $p < 0.05$, ** $p < 0.01$, compared to lean VHC; # $p < 0.05$, ## $p < 0.01$, ### $p < 0.001$, compared to obese VHC; § $p < 0.05$, §§ $p < 0.01$, compared to lean Rapa; lean VHC: n = 3, lean Rapa: n = 6, obese VHC: n = 3, lean Rapa: n = 6. Figure adapted from Deissler et al. (2021).

threshold of significance. On POD 9, PMN-MDSCs from obese treated animals expressed more *Nos2*-mRNA; expressions of all other studied transcripts by PMN-MDSCs from treated obese or lean mice did not differ. Taken together, rapamycin treatment of obese allograft recipients changed expression of certain mRNAs, relevant to the regulation of the immune response, by M-MDSCs and PMN-MDSCs.

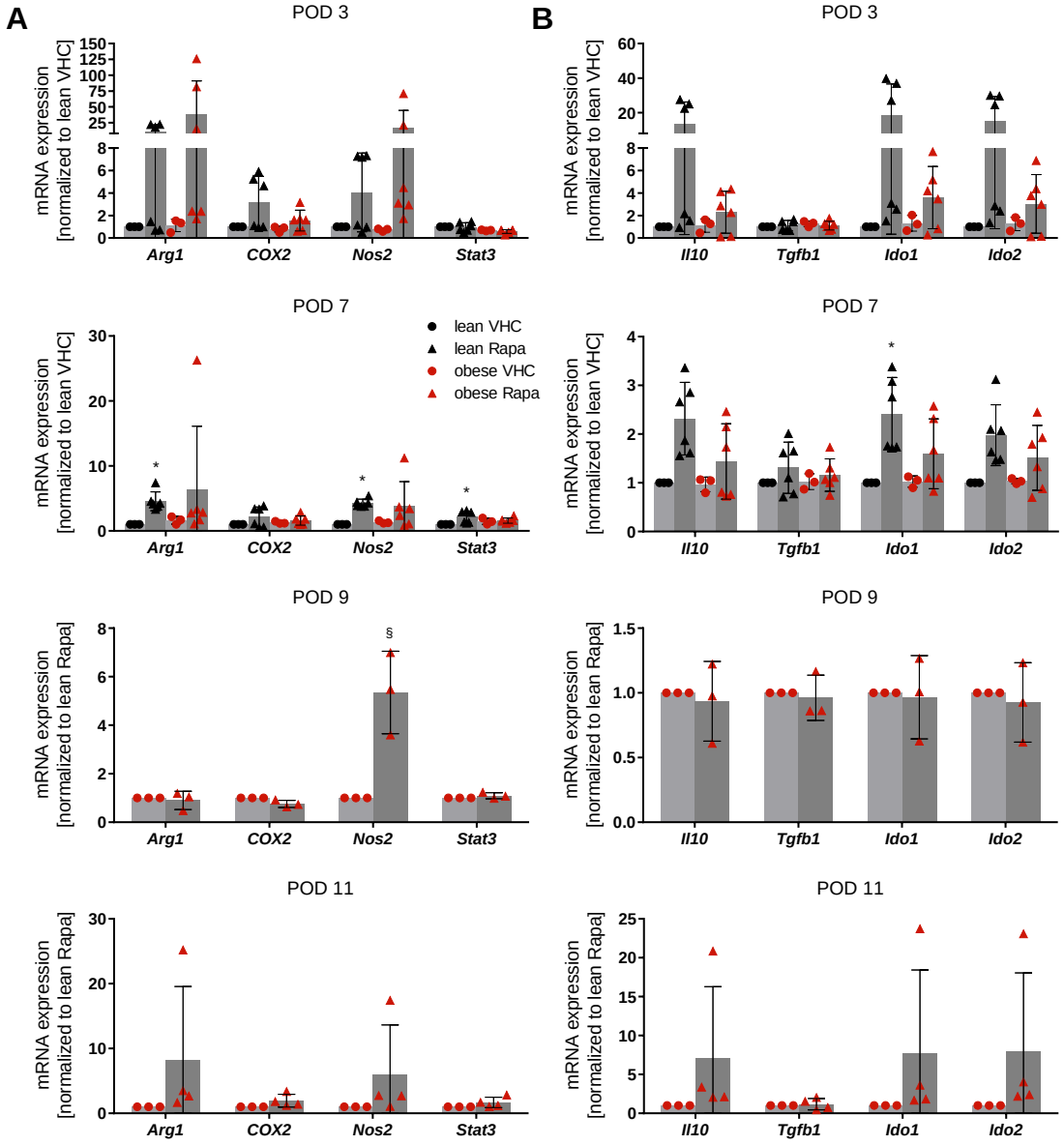

Figure 16: Rapamycin treatment induced polymorphonuclear myeloid-derived suppressor cells (PMN-MDSCs) to differently express mRNAs relevant to their function.
On different postoperative days (PODs), mRNA expression of (**A**) arginase-1 (*Arg1*), cyclooxygenase-2 (*COX2*), inducible nitric oxide synthase (*Nos2*), signal transducer and activator of transcription (*Stat3*) and (**B**) interleukin-10 (*Il10*), transforming growth factor beta (*Tgfb1*), indoleamine 2,3-dioxygenase (*Ido1* and *Ido2*) by PMN-MDSCs isolated from spleens of lean or obese allograft recipients treated with rapamycin or the vehicle DMSO (VHC) was analyzed by qPCR. For the sake of better visualization, signals were normalized after statistical analysis as described (see 2.4.2.6). Data are presented as mean ± SD; * $p < 0.05$, compared to lean VHC; § $p < 0.05$, compared to lean Rapa; lean VHC: n = 3, lean Rapa: n = 6, obese VHC: n = 3, lean Rapa: n = 6. Figure adapted from Deissler et al. (2021).

3.5 Rapamycin treatment enlarged the Treg population in obese mice

The fractions of Tregs, Th1, Th2 and Th17 cells in the total splenocyte population on the day of rejection or on defined PODs were determined by flow cytometry. Numbers of these cell types were not different in splenocytes from untreated obese and lean mice prepared at the day of allograft rejection (Fig. 17). In contrast, rapamycin treatment significantly increased the amount of pro-inflammatory Th1 cells in both lean and obese mice and that of Th17 cells only in lean mice, whereas the level of Th2 cells remained stable under all conditions tested. However, compared to untreated obese or treated lean mice, rapamycin treatment of obese mice resulted in a significantly higher number of Tregs, also reflected by significantly raised ratios of Tregs to Th1, Th2 and Th17 cells (Fig. 18). The ratios of Th1 to Th2 or Th17 cells were also higher in the rapamycin-treated obese animals.

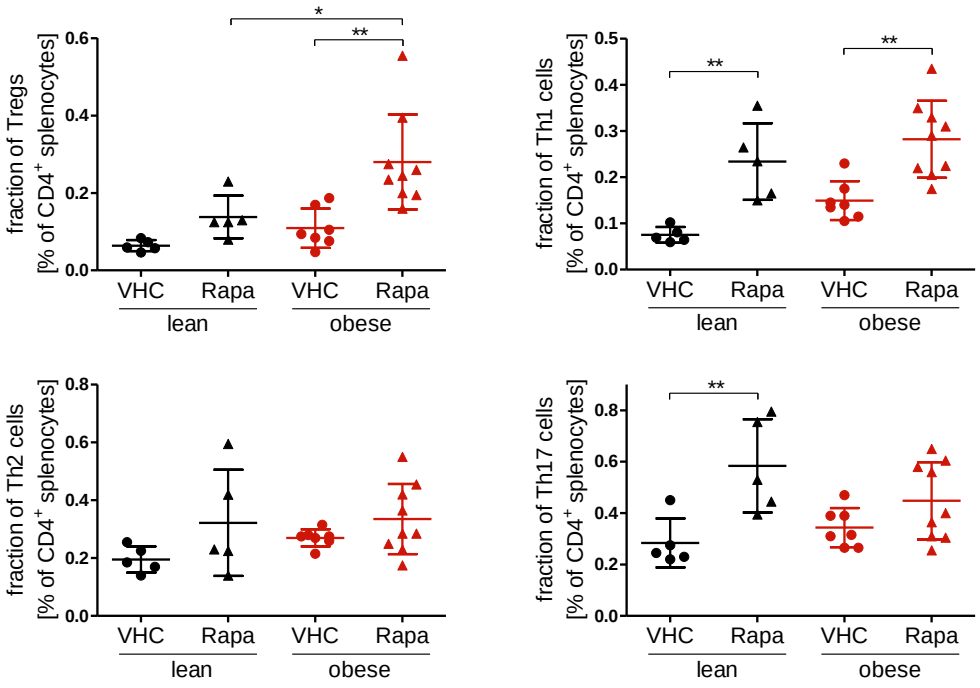

Figure 17: Rapamycin treatment increased the abundance of regulatory T cells (Tregs) in obese mice.

Obese and lean mice underwent full-MHC-mismatched skin allograft transplantation followed by rapamycin treatment as described (see 2.4.1). At the day of rejection, single splenocyte suspensions were prepared. The cells were immunostained with antibodies specific for CD4, CD25, FoxP3, IFN-γ, IL-4 and IL-17A and the numbers of $CD4^+$ $CD25^+$ $FoxP3^+$ Tregs, $CD4^+$ IFN-γ^+ T helper (Th) 1 cells, $CD4^+$ $IL\text{-}4^+$ Th2 cells and $CD4^+$ $IL\text{-}17A^+$ Th17 cells were determined by flow cytometry. Fractions of Tregs, Th1, Th2 and Th17 cells in the total splenocyte population at the day of allograft rejection are shown. Data are presented as mean ± SD; * $p < 0.05$, ** $p < 0.01$, compared between indicated groups; lean VHC: n = 5, lean Rapa: n = 5, obese VHC: n = 7, obese Rapa: n = 9. Figure adapted from Deissler et al. (2021).

The number of Tregs as well as their fraction in relation to all $CD4^+$ T cells significantly increased from POD 3 to POD 11 in lean or obese mice undergoing rapamycin treatment, which was similarly observed for Th1, Th2 and Th17 cells (Fig. 19 A – D). The fraction of Th2 cells from untreated lean mice conspicuously decreased from peaking at POD 3 to POD 7 (Fig. 19 C).

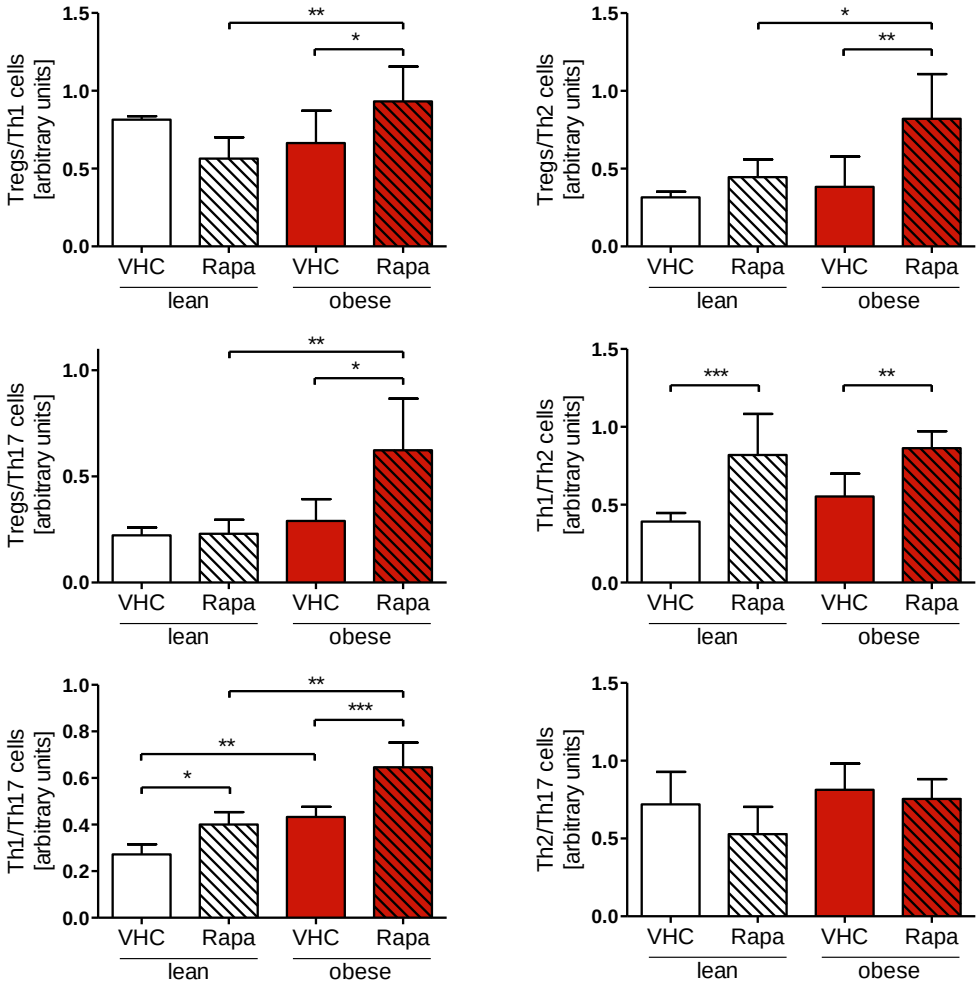

Figure 18: Rapamycin treatment shifted the T cell population in obese mice towards expansion of regulatory T cells (Tregs).
Obese and lean mice underwent full-MHC-mismatched skin allograft transplantation followed by rapamycin treatment as described (see 2.4.1). At the day of rejection, single splenocyte suspensions were prepared. The cells were immunostained with antibodies specific for CD4, CD25, FOXP3, IFN-γ, IL-4 and IL-17A and the numbers of $CD4^+$ $CD25^+$ $FOXP3^+$ Tregs, $CD4^+$ IFN-γ^+ T helper (Th) 1 cells, $CD4^+$ IL-4^+ Th2 cells and $CD4^+$ IL-$17A^+$ Th17 cells were determined by flow cytometry. Calculated ratios of the relative abundancies of splenic T cell subsets at the day of allograft rejection are shown. Data are presented as mean ± SD; * $p < 0.05$, ** $p < 0.01$, *** $p < 0.001$ for comparisons of indicated groups; lean VHC: n = 5, lean Rapa: n = 5, obese VHC; n = 7, obese Rapa: n = 9. Figure adapted from Deissler et al. (2021).

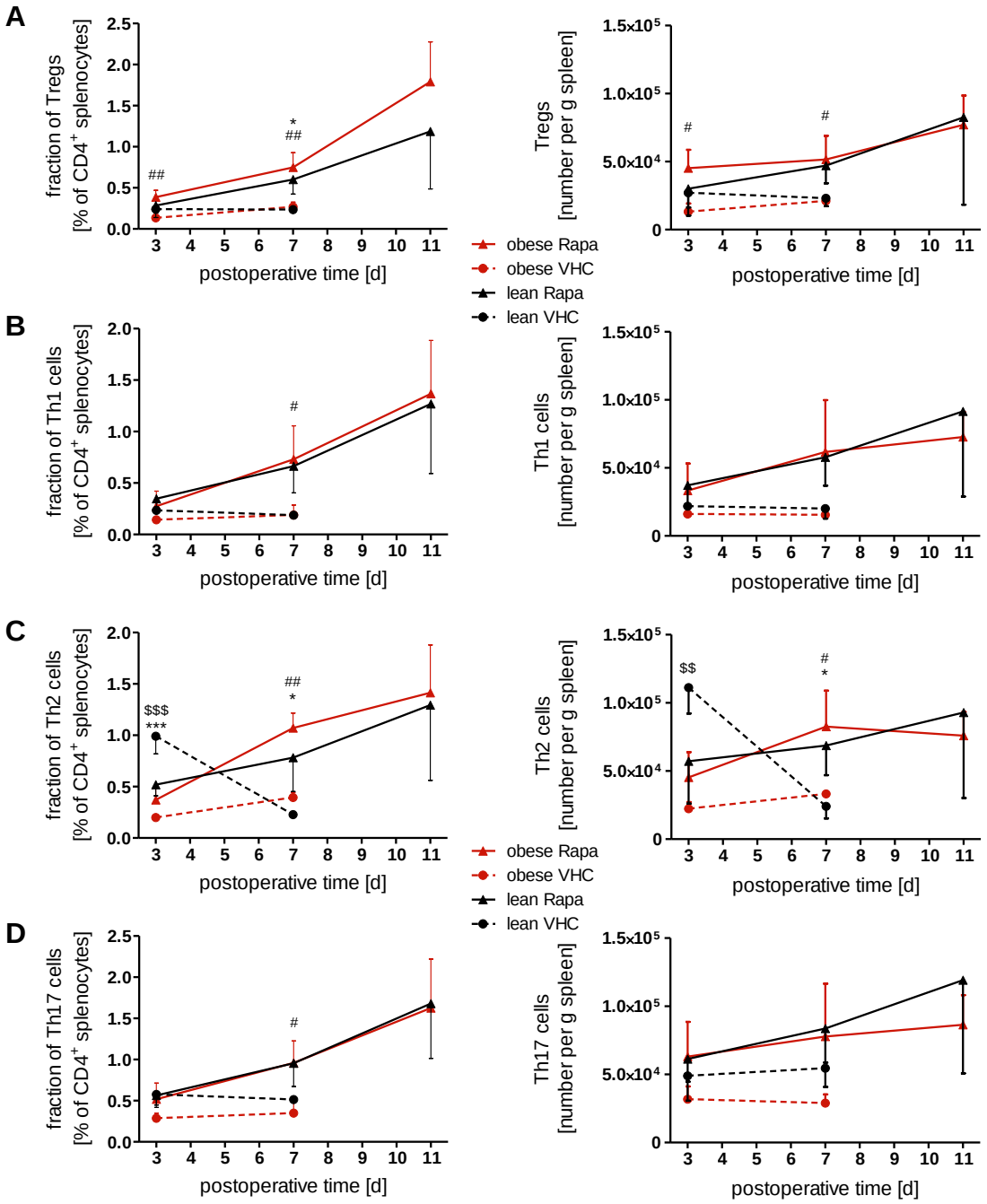

Figure 19: Rapamycin treatment increased the number of regulatory T cells (Tregs) in obese mice between postoperative day (POD) 3 and POD 11.

Single splenocyte suspensions were prepared from spleens removed at defined PODs from lean or obese allograft recipients that had (Rapa) or had not been treated (VHC) with rapamycin (see 2.4.1). The cells were immunostained with antibodies specific for CD4, CD25, FOXP3, IFN-γ, IL-4 and IL-17A and the numbers of $CD4^+$ $CD25^+$ $FOXP3^+$ Tregs, $CD4^+$ IFN-γ^+ T helper (Th) 1 cells, $CD4^+$ IL-4^+ Th2 cells and $CD4^+$ IL-$17A^+$ Th17 cells were determined by flow cytometry. Fractions and absolute numbers of (**A**) Tregs, (**B**) Th1, (**C**) Th2 and (**D**) Th17 cells in the total splenocyte population were determined at PODs 3, 7, 9 and 11, and time courses of these values are displayed. Data are presented as mean ± SD; * $p < 0.05$, *** $p < 0.001$ for lean Rapa compared to lean VHC; # $p < 0.05$, ## $p < 0.01$ for obese Rapa compared to obese VHC; $$ $p < 0.01$, $$$ $p < 0.001$ for obese VHC compared to lean VHC; lean VHC: n = 3, lean Rapa: n = 6, obese VHC: n = 3, obese Rapa: n = 6. Figure adapted from Deissler et al. (2021).

3.6 Numbers of pro-inflammatory M1 macrophages remained constant during rapamycin treatment

The numbers of M1, M2 and M2-like macrophages were determined by flow cytometry at the day of rejection or at defined PODs. Fractions of M1 and M2 macrophages did not differ between the treatment groups at the day of rejection, but that of M2-like macrophages was higher in splenocyte preparations from rapamycin-treated lean and obese mice in comparison to their lean untreated counterparts, although the observed differences were only significant for the lean animals (Fig. 20). Results regarding M2 and M2-like macrophages in the control group of obese mice at the day of rejection have to be evaluated with caution as only samples from two of these animals could be gathered.

Summarizing, the numbers of M1, M2 and M2-like macrophages and, accordingly, their fractions in relation to the total splenocyte population only

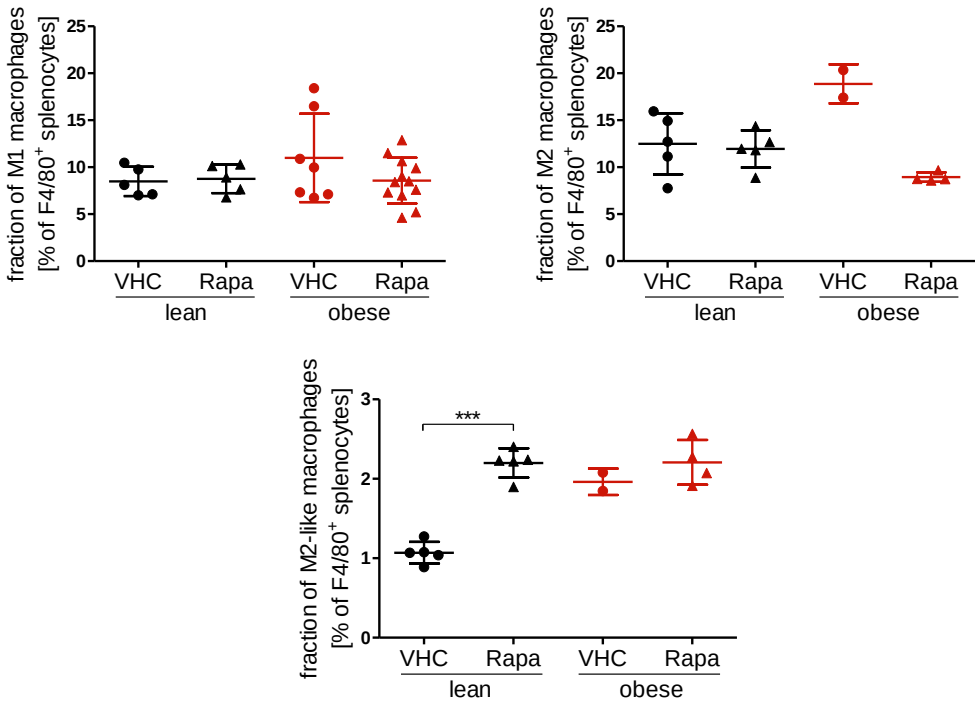

Figure 20: The splenocyte subpopulation of M2-like macrophages was increased by rapamycin treatment of lean allograft recipients.
Obese and lean mice underwent full-MHC-mismatched skin allograft transplantation and were treated either with the vehicle DMSO (VHC) or rapamycin (Rapa) as described (see 2.4.1). At the day of rejection, splenocyte suspensions obtained from the allograft recipients were immunostained with antibodies specific for F4/80, CD11c, CD206 and IL-10, and the numbers of F4/80$^+$ CD11c$^+$ M1 macrophages, F4/80$^+$ CD11c$^-$ CD206$^+$ M2 macrophages and F4/80$^+$ CD11c$^-$ CD206$^+$ IL-10$^+$ M2-like macrophages were determined by flow cytometry. Fractions of M1, M2 and M2-like macrophages in the total splenocyte population at the day of allograft rejection are shown. Data are presented as mean ± SD; * $p < 0.05$, ** $p < 0.01$, *** $p < 0.001$ for comparisons between groups as indicated; lean VHC: n = 5, lean Rapa: n = 5, obese VHC: n = 2-7, obese Rapa: n = 4-12. Figure adapted from Deissler et al. (2021).

changed marginally between POD 3 and POD 11 in all groups of transplant-receiving mice (Fig. 21 A – C).

A significantly higher ratio of M2-like to M2 macrophages was observed when cells were obtained from lean treated mice compared to their untreated counterparts (Fig. 22), and a similar trend was also seen between the groups of obese mice, although only few animals were analyzed. In addition, the ratios of pro-inflammatory M1 macrophages to immunosuppressive M- and PMN-MDSCs, and of M1 macrophages to Tregs were lower in splenocytes gained from obese mice treated with rapamycin (Fig. 22).

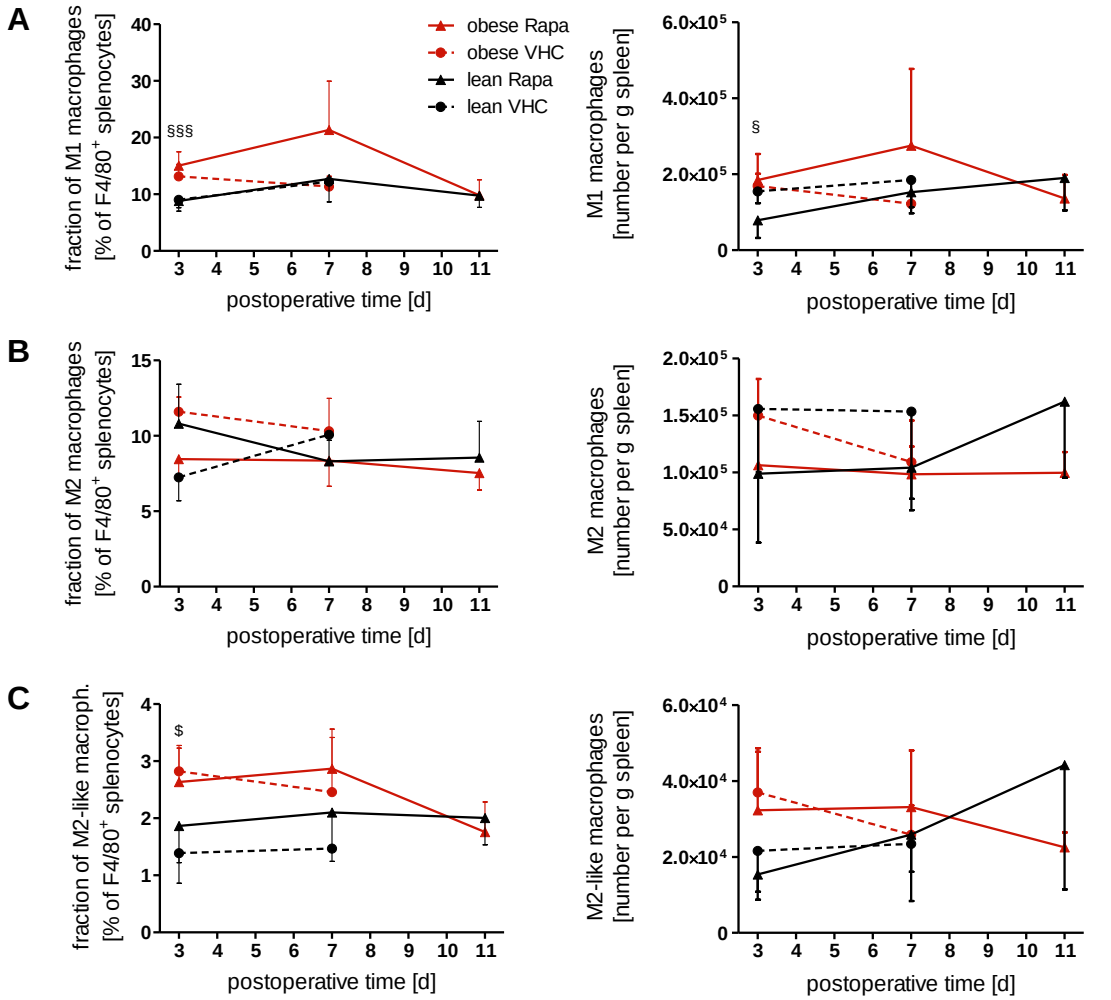

Figure 21: Rapamycin only slightly altered numbers of macrophages assessed in the period from postoperative day (POD) 3 to POD 11.
Obese and lean mice underwent full-MHC-mismatched skin allograft transplantation and were treated either with the vehicle DMSO (VHC) or rapamycin (Rapa) as described (see 2.4.1). At the day of rejection, splenocyte suspensions obtained from the allograft recipients were immunostained with antibodies specific for F4/80, CD11c, CD206 and IL-10, and the numbers of F4/80$^+$ CD11c$^+$ M1 macrophages, F4/80$^+$ CD11c$^-$ CD206$^+$ M2 macrophages and F4/80$^+$ CD11c$^-$ CD206$^+$ IL-10$^+$ M2-like macrophages were determined by flow cytometry. Fractions and absolute numbers of (**A**) M1, (**B**) M2 and (**C**) M2-like macrophages in the total splenocyte population at postoperative days (PODs) 3, 7, 9 and 11 are displayed. Data are presented as mean ± SD; $ $p < 0.05$ for obese VHC compared to lean VHC; § $p < 0.05$, §§§ $p < 0.001$ for obese Rapa compared to lean Rapa; lean VHC: n = 3, lean Rapa: n = 6, obese VHC: n = 3, obese Rapa: n = 6. Figure adapted from Deissler et al. (2021).

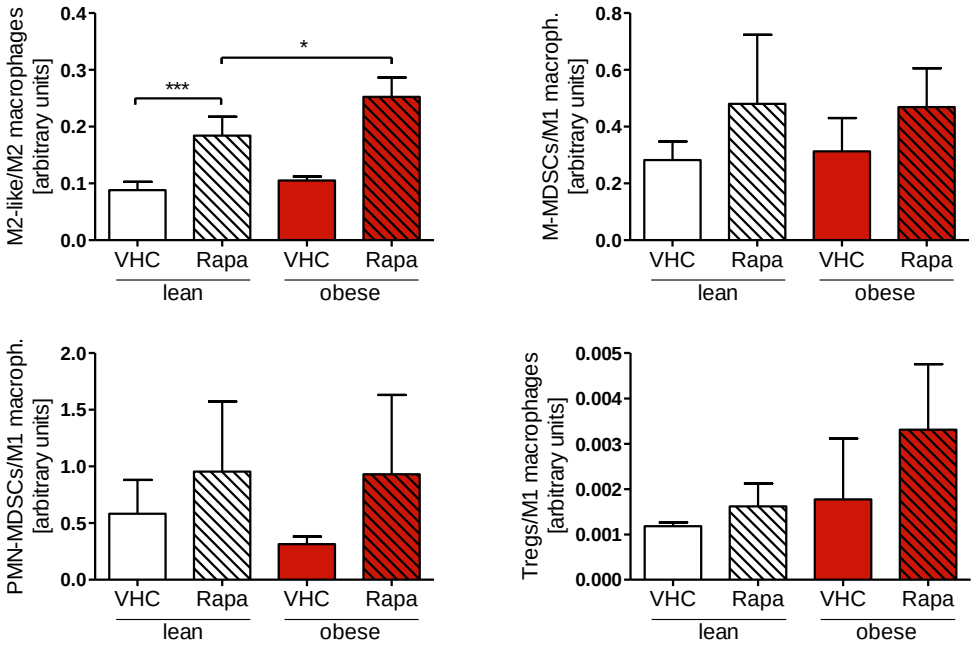

Figure 22: Rapamycin treatment resulted in a lower relative abundance of pro-inflammatory M1 and M2 macrophages in favor of anti-inflammatory M2-like macrophages, monocytic (M-) myeloid-derived suppressor cells (MDSCs), polymorphonuclear (PMN-) MDSCs and regulatory T cells (Tregs).

Spleen cells obtained at the day of rejection from allograft recipients previously treated as described (see 2.4.1) were immunostained with antibodies specific for CD11b, Ly-6C, Ly-6G, CD4, CD25, FoxP3, F4/80, CD11c, CD206, IL-10, and the numbers of $CD11b^+$ $Ly\text{-}6G^-$ $Ly\text{-}6C^{high}$ M-MDSCs, $CD11b^+$ $Ly\text{-}6G^{high}$ $Ly\text{-}6C^{low}$ PMN-MDSCs, $CD4^+$ $CD25^+$ $FOXP3^+$ Tregs, $F4/80^+$ $CD11c^+$ M1 macrophages, $F4/80^+$ $CD11c^-$ $CD206^+$ M2 macrophages, and $F4/80^+$ $CD11c^-$ $CD206^+$ $IL\text{-}10^+$ M2-like macrophages were determined by flow cytometry. Ratios of the determined numbers of cells of other types specified above to the number of M1 and M2 macrophages were calculated and displayed. Data are presented as mean ± SD; * $p < 0.05$, ** $p < 0.01$ for comparisons between indicated groups; lean VHC: n = 5, lean Rapa: n = 5, obese VHC: n = 7, obese Rapa: n = 4-12. Figure adapted from Deissler et al. (2021).

3.7 The CXCL2 concentration in blood of obese mice was increased by rapamycin treatment

At the day of allograft rejection and on PODs 3, 7, 9 and 11 peripheral blood was collected and plasma concentrations of various chemokines and cytokines were measured by a multiplex sandwich immunoassay. Concentrations of CCL2, CXCL12, GM-CSF, IFN-γ, IL-1β, IL-10, IL-17 and TNF-α were below the limit of detection and those of CXCL1 and IL-6 were similar in the different experimental groups (Fig. 23 A). However, rapamycin treatment significantly increased the plasma concentration of CXCL2 in obese mice and the measured values were also substantially higher than those of treated lean animals (Fig. 23 A). The plasma concentrations of IL-6 in all treatment groups did not change from POD 3 to POD 11 whereas that of CXCL1 declined slightly (Fig. 23 B). In contrast, the plasma concentration of CXCL2 in rapamycin-treated obese recipients remained

higher from POD 3 until POD 11 compared to treated lean mice, even though statistical significance was only reached for the comparison of data from POD 3. Interesting correlations of cytokine/chemokine plasma levels and data on MDSC abundance in treated obese mice could be recognized: The plasma concentration of IL-6 clearly correlated with numbers of PMN-MDSCs determined in spleen and blood, and that of CXCL1 with PMN-MDSCs in peripheral blood (Fig. 24).

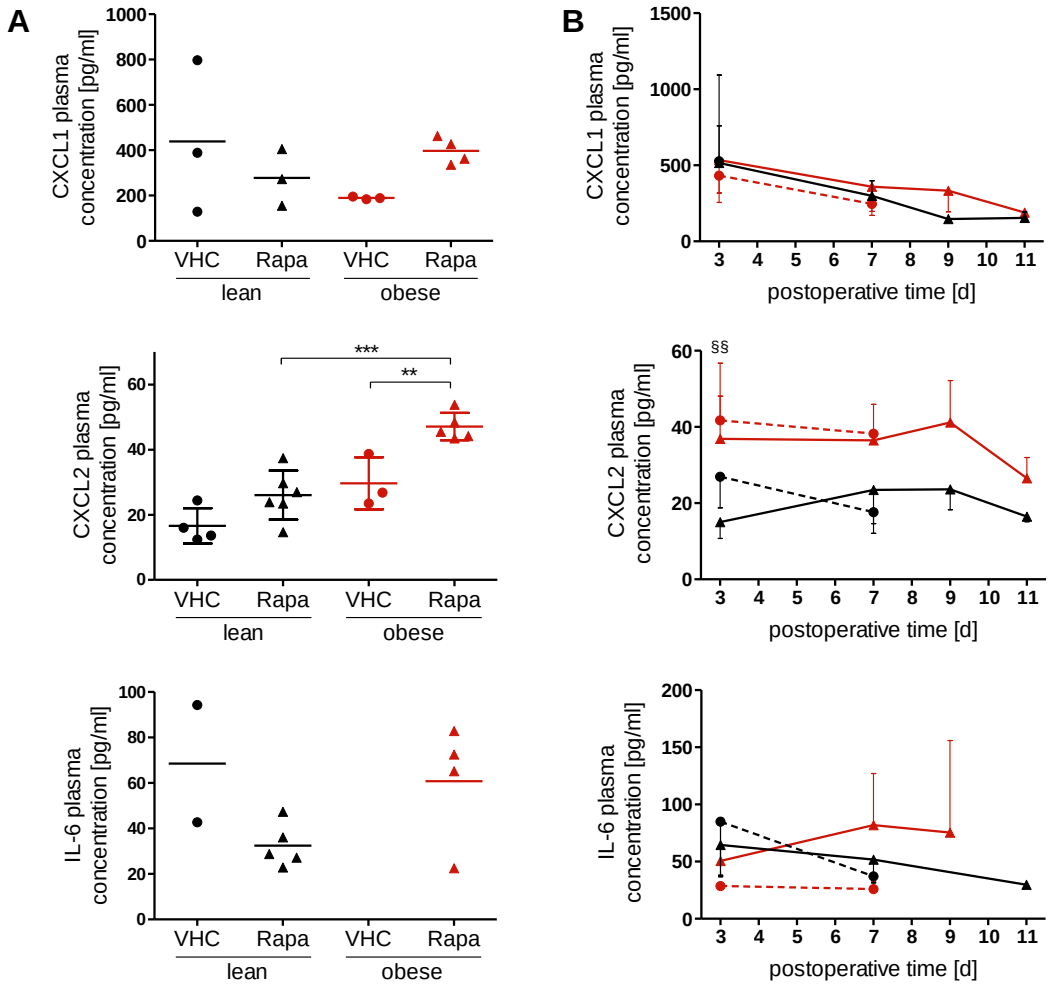

Figure 23: Rapamycin treatment of obese mice increased their plasma concentration of chemokine (C-X-C motif) ligand (CXCL) 2.
Peripheral blood was collected at the day of rejection or at defined PODs from allograft recipients treated as described above, and therein the plasma concentrations of CCL2, CXCL1, CXCL2, CXCL12, GM-CSF, IFN-γ, interleukin (IL-) 1β, IL-6, IL-10, IL-17 and TNF-α were determined by a multiplex sandwich immunoassay. (**A**) Plasma concentrations of CXCL1, CXCL2 and IL-6 at the day of allograft rejection are compared. Data are presented as mean ± SD; ** $p < 0.01$, *** $p < 0.001$ for comparisons between indicated groups; lean VHC: n = 5, lean Rapa: n = 6, obese VHC: n = 4, obese Rapa: n = 8. (**B**) Diagrams were based on the plasma concentrations of CXCL1, CXCL2 and IL-6 at PODs 3, 7, 9 and 11. Data are presented as mean ± SD; lean VHC: n = 6, lean Rapa: n = 17, obese VHC: n = 6, obese Rapa: n = 16. Figure adapted from Deissler et al. (2021).

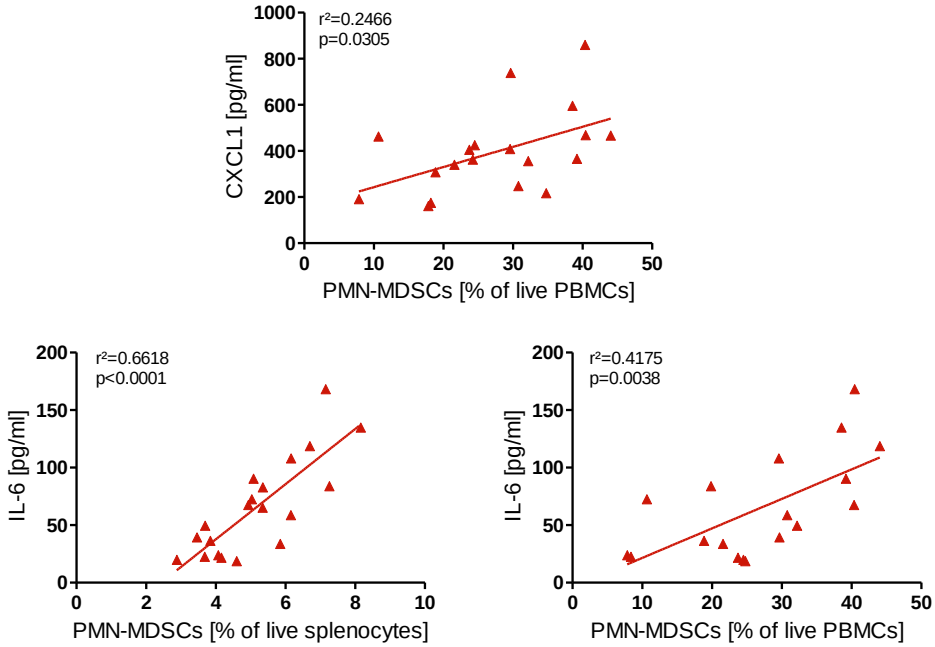

Figure 24: Chemokine (C-X-C motif) ligand (CXCL) 1 and interleukin (IL-) 6 plasma concentrations were positively correlated with polymorphonuclear myeloid-derived suppressor cell (PMN-MDSC) numbers.

Peripheral blood was collected at the day of rejection or at defined PODs from allograft recipients treated as described above, and therein the plasma concentrations of CCL2, CXCL1, CXCL2, CXCL12, GM-CSF, IFN-γ, IL-1β, IL-6, IL-10, IL-17 and TNF-α were determined by a multiplex sandwich immunoassay. Data on plasma concentrations of CXCL1, CXCL2, IL-6 and numbers of PMN-MDSCs in spleen and peripheral blood of rapamycin-treated obese animals obtained on the day of rejection and PODs 3, 7, 9 and 11 were pooled to calculate their correlations; n = 18-20. *PBMCs* peripheral blood mononuclear cells. Figure adapted from Deissler et al. (2021).

4. Discussion

4.1 Suitability of the murine model used to study obesity and allograft transplantation

In the vast majority of cases obesity is a consequence of prolonged overnutrition with all other reasons accounting only for 10% (Herold 2017). Therefore, HFD-fed mice were preferred over genetically modified mice to mimic human obesity and to maximize the likelihood of achieving transferable results. The induction of obesity in C57Bl/6 mice by means of a diet is a reliable and widely used animal model. In detail, the HFD-induced obesity of C57Bl/6 mice is characterized by abdominal fat accumulation, insulin resistance, hyperinsulinemia, hyperglycemia and hypertension, thereby better resembling the metabolic syndrome in humans than other mouse strains. Another important similarity is, that C57Bl/6 mice fed with a normal diet remain lean and do not develop metabolic disorders (Collins et al. 2004). Therefore, C57Bl/6J mice were used as transplant recipients, and of these only male animals to reduce further experimental complexity in view of potential sex-related differences. Experimental studies indeed revealed significant sex differences regarding the immune response, likely due to the effects of sex hormones on their receptors expressed on immune cells (Faas et al. 2011), including alterations of the relative abundances of certain types of immune cells (Dibbern et al. 2017, Erickson et al. 2018, Hensel et al. 2019, Kay et al. 2015). In detail, fewer T cells were found in spleens of male mice compared to their female counterparts, but more Tregs and Th1 cells in subgroup analysis (Elderman et al. 2016). Results of another study suggested a more efficient immune response to an acute infection or injury by female mice having a leukocyte composition different from that of the male animals (Scotland et al. 2011). In view of these differences, it seemed reasonable to include only mice of one sex in this pilot study to clearly attribute observed differences to obesity irrespective of sex. Of course, the results will need to be confirmed in further experimental settings including female mice, but this was beyond the scope of the current study.

Full MHC-mismatched skin allograft transplantation is an established and easily implementable model of allograft transplantation. It allows convenient monitoring

of allograft survival and, due to the small surgical intervention compared to heart or kidney transplantation, the procedure is usually well tolerated by the animals with a low risk of perioperative complications which are mainly associated with anesthesia (Cheng et al. 2017). In the human transplantation setting, extreme care is taken to ensure that the MHC tissue characteristics match as closely as possible, but nevertheless, in clinical practice complete MHC matching is not achieved, with transfers among identical twins being the only exceptions (Ayala Garcia et al. 2012). Therefore, the model of a full MHC-mismatched transplantation not fully resembles therapeutic transfer of human organs, but it is close enough to reveal mechanisms and initiate further investigations of their potential clinical relevance. These include processes that might contribute to allograft rejection and therefore this model allows the observation of a clear allograft rejection within a limited period of time, which was preferred over the induction of permanent tolerance towards the allograft. In addition, only a sub-therapeutical dose of rapamycin (2 mg/kg/d) was administered to reach the experimental end point of allograft rejection in combination with the strong alloimmune response provoked by full MHC-mismatched allogeneic skin transplantation. In this way, possible obesity-specific effects on allograft survival and the underlying immune response in rapamycin-treated recipients should become more apparent. In subsequent experiments based on the results of this study, an increase of the rapamycin dose and minor MHC-mismatched transplantation might be taken into consideration as further adjustments to foster the translational relevance towards human clinical transplantation. In this pilot study to reveal potential obesity-related effects, however, despite some limitations the chosen model of diet-induced obesity and allogeneic transplantation was sufficient to initially explore this field of research.

4.2 Allograft survival

Obesity induced by a HFD leads to an enhanced alloimmune T cell response consequently resulting in an earlier allograft rejection as demonstrated by a number of experiments based on different *in vitro* and *in vivo* model systems (Molinero et al. 2016). In support of this perception, leptin deficiency was found

to be associated with lower alloreactivity and improved allograft survival (Moraes-Vieira et al. 2013) and adiponectin also seems to ameliorate complications due to allograft rejection (Okamoto et al. 2009). In this study, however, different allograft survival between untreated lean and obese mice was not observed, suggesting that the effect of obesity alone on the rejection kinetics is not significant in this model. This is in accordance with observations by Molinero et al. (2016) who implemented a minor MHC-mismatched heart transplantation model to evaluate allograft survival in obese mice after they were not able to reveal any differences in experiments based on a full MHC-mismatched allograft transplantation setting. The authors provide the likely explanation that the rejection by lean animals occurs so fast in full MHC-mismatched settings that further acceleration due to obesity would not result in detectable differences (Molinero et al. 2016). In accordance, it seems plausible to assume that in the model of full MHC-mismatched skin allograft transplantation in the present study, the similarity of allograft survival only reflects the very fast rejection by both lean and obese animals.

As hypothesized and in accordance with several previous experimental studies (Koehl et al. 2004, Nakamura et al. 2015, Wei et al. 2018), we observed that rapamycin treatment prolonged skin allograft survival in both obese and lean mice. Remarkably, the positive effect of rapamycin on skin allograft survival was strongly pronounced in obese animals which carried the transplanted skin about 66% longer than their lean counterparts. This confirms and emphasizes the beneficial obesity-specific effects of rapamycin in the context of preventing allograft rejection.

4.3 Immune cells and proteins involved in the alloimmune response

4.3.1 Effect of obesity

The composition of immune cells in obese individuals is well studied: Low-grade chronic inflammation leads to an accumulation of MDSCs as a direct consequence of fatty acid-mediated processes *via* a pro-inflammatory condition

similar to a cancer microenvironment that might also increase the risk of developing malignant diseases (Budhwar et al. 2018, Clements et al. 2018, Ostrand-Rosenberg 2018, Pawelec et al. 2019). In accordance with the observation that human obesity is associated with more M-MDSCs (Bao et al. 2015, Iglesias-Escudero et al. 2020), murine models of obesity are characterized by higher numbers and activities of both M-MDSCs and PMN-MDSCs, resulting from increased levels of leptin (Clements et al. 2018, Ostrand-Rosenberg 2018, Pawelec et al. 2019). The MDSCs counteract inflammation and metabolic dysfunctions typically associated with obesity, e.g. insulin resistance (Clements et al. 2018). In the present study, such effect of obesity alone was not that obvious and comparison of untreated lean and obese recipients only showed a trend in favor of M-MDSCs on the day of rejection. On POD 3, lean mice even had more M-MDSCs than the obese animals. This might be a consequence of statistical uncertainty due to the limited animal number, just not sufficient to demonstrate a significant increase of M-MDSCs at the day of rejection.

Strikingly, the immunosuppressive capacity of M-MDSCs from obese mice was considerably lower, as concluded from weaker inhibition of T cells in a proliferation assay. In consistence with this result, M-MDSCs obtained from obese mice also showed lower expression of mRNAs encoding TGF-β, IDO1 or iNOS, suggesting an impaired Treg induction, and inhibition of effector T cells caused by secretion of lower amounts of these factors. This indicates that obesity leads to a significant impairment of M-MDSC activity, obvious at the time of allograft rejection, although the number of these immune cells was not found to be altered. While these effects were clearly visible at the time of allograft rejection, the same effects could not be observed earlier (PODs 3 and 7) which might be due to the limited number of animals in the time course experiments and high interindividual variability. Since an effect of obesity on the amount or immunosuppressive activity of PMN-MDSCs was not seen, M-MDSCs appear to play a more important or even exclusive role among the MDSC subtypes in mediating obesity-induced immune impairment. This assumption is in line with findings suggesting a similar human immune reaction (Bao et al. 2015, Iglesias-Escudero et al. 2020).

Molinero et al. (2016) observed a stronger allospecific T cell response to additional immunization with donor splenocytes leading to accelerated rejection of heart allografts in diet-induced obese mice. In addition, mice with HFD-induced obesity showed a pro-inflammatory immune cell pattern in adipose tissue with increased numbers of Th1 and Th17 cells, whereas Tregs were not affected. Results of the study also suggest that functions of Th2 cells and Tregs might protect against the development of metabolic disorders (Winer et al. 2009). Furthermore, macrophages in obese adipose tissue are mostly of the pro-inflammatory M1 subtype, although anti-inflammatory M2-like macrophages rather occur in adipose tissue gained from lean individuals (Saltiel et al. 2017, Sica et al. 2012).

In the present study, the fractions of Th1, Th2, Th17 cells and M1 macrophages, determined at the day of allograft rejection, were similar in obese and lean animals. Only the ratio of Th1 to Th17 cells was higher in obese mice and these animals had also generated more M2 macrophages. Besides the number of Th17 cells, their capacity to secrete IL-17 is an interesting parameter as this interleukin was found to accelerate allograft rejection in mice with hyperlipidemia (Yuan et al. 2015). It was, however, not possible to draw any conclusions regarding IL-17, because the sensitivity of the only available assay to measure its concentration in plasma was not high enough.

Results of another study also point to decreased numbers of Tregs in HFD-fed mice as well as in leptin-deficient obese mice. This, however, was only demonstrated for abdominal adipose tissue but was not similarly observed in the spleen (Feuerer et al. 2009). In line with this finding, this investigation confirmed that the population of Tregs among the spleen-derived $CD4^+$ T cells was not affected by obesity. Another interesting result was the up-regulation of anti-inflammatory IL-10-secreting M2-like macrophages on POD 3 and on the day of rejection, also reflected by a significant shift of the ratio of M2-like to M2 macrophages in favor or the M2-like subtype. However, the significance of these effects on M2 and M2-like macrophages will have to be confirmed by follow-up experiments more focused on this particular aspect and with higher numbers of individual samples.

In general, it cannot be ruled out that some of the effects on allograft survival or the studied immune cell populations were caused by the transplantation procedure itself rather than by the subsequent alloimmune reaction. This, however, seems not likely and only an unfeasible extension of the experimental concept by including additional control groups receiving no or syngeneic skin allografts would have yielded information relevant to this question.

In summary of the results regarding untreated animals, a remarkable reduction of immunosuppressive activity of M-MDSCs was seen at the day of allograft rejection in obese mice compared to their lean counterparts. In contrast to some previous reports, obesity did not influence pro-inflammatory Th1 or Th17 cells or M1 macrophages, but results suggested a potential expansion of anti-inflammatory and immunosuppressive M2-like macrophages as a consequence. Allograft survival was not different between groups of lean and obese mice in accordance with the assumption that an effect due to a reduced immunosuppression by M-MDSCs is too weak to be recognized in the process of fast and strong rejection process in a full MHC-mismatched experimental set-up (see also 4.2). Nevertheless, the observations made are a hint to an accelerated M-MDSC-mediated rejection that might be relevant to obese recipients of minor MHC-mismatched transplants.

4.3.2 Impact of mTOR inhibition by rapamycin on immune response and allograft survival

Nakamura et al. (2015) described prolonged heart allograft survival under rapamycin treatment associated with recruitment of MDSCs at the allograft site and induction of T cell-suppressing activity, exerted particularly by M-MDSCs. Notably, strong evidence indicated that activity of MDSCs was indeed the cause of improved allograft survival: Depletion of MDSCs with an anti-Gr-1 antibody abolished the effect, whereas prolonged survival was also achieved by adoptive transfer of MDSCs from rapamycin-treated recipients to untreated mice (Nakamura et al. 2015). Wei et al. (2018) demonstrated prolonged corneal allograft survival in mice treated with eye drops containing rapamycin nano-

micelles. This was also accompanied by higher numbers of MDSCs and their pivotal role was again confirmed by MDSC depletion with an anti-Gr-1 antibody, resulting in accelerated rejection. In addition to their higher abundance, MDSCs isolated from rapamycin-treated mice showed an enhanced immunosuppressive activity (Wei et al. 2018). The MDSC-inducing effect of rapamycin beneficial for patients suffering from inflammatory diseases has been demonstrated for graft-versus-host disease (GvHD) (Scheurer et al. 2020), heart failure (Zhou et al. 2018), acute kidney injury (AKI) (Zhang et al. 2017) and immunological hepatic injury (Zhang et al. 2014). However, the underlying mechanisms how mTOR inhibition by rapamycin leads to an accumulation and stimulation of MDSCs is not fully understood yet. Results of a recent study even suggested that rapamycin treatment might impair M-MDSC-mediated immunosuppression: Rapamycin increased the number of M-MDSCs generated *in vitro* from human whole blood, but surprisingly the ability of these cells to suppress T cells and their IDO expression were lower (Iglesias-Escudero et al. 2020). Of particular relevance to this work is the study by Makki et al. (2014) focusing on the effects of rapamycin on metabolism and immune cells in a similar mouse model of HFD-induced obesity. In brief, the authors found that rapamycin treatment resulted in an improved metabolic profile linked to weight loss and protection against insulin resistance as well as increased numbers of immunosuppressive MDSCs and Tregs (Makki et al. 2014).

In line with these findings, rapamycin treatment resulted in higher numbers of M-MDSCs in obese but not lean mice, as determined on the day of allograft rejection in the present study. In the time course experiment, M-MDSCs in obese rapamycin-treated mice increased until POD 11 with a peak on POD 9 when untreated mice had already rejected their allograft, providing a possible explanation for the prolonged allograft survival in these animals. That the splenic M-MDSC count reached a peak on POD 9 when their corresponding numbers in peripheral blood samples were lowered invites the speculation that a temporary spleen-directed homing process might play a role.

Rapamycin treatment did not affect the immunosuppressive activities of M-MDSCs or PMN-MDSCs obtained from lean allograft recipients on the day of

allograft rejection. In these mice, rapamycin treatment might even lead to a weaker inhibition of T cell proliferation by MDSCs, as observed only on POD 7. In contrast, the T cell-suppressing activity of M-MDSCs compromised by obesity was completely restored in mice of this group treated with rapamycin. Obviously, rapamycin cannot further enhance the normal M-MDSC-mediated immunosuppression maintained in lean mice, but normalizes this function in obese mice. The significantly increased immunosuppressive activity of M-MDSCs along with prolonged skin allograft survival in rapamycin-treated obese mice points out to an important role of these cells in the related immune response. Time course analyses also revealed enhanced immunosuppression by M-MDSCs on several PODs in combination with higher M-MDSC/$CD4^+$ T cell ratios in obese compared to lean mice when both were treated with rapamycin. This strongly supports the observation of beneficial obesity-specific effects of rapamycin. Interestingly, M-MDSCs from obese rapamycin-treated graft recipients showed the strongest immunosuppressive activity on POD 9, when untreated obese and lean mice had already rejected their allograft.

In addition to their induction of Tregs, MDSCs inhibit T cell proliferation through regulation of extracellular signal transmitters. Thereby, immunosuppression by M-MDSCs mainly depends on functions of Arg-1, iNOS and IL-10, whereas PMN-MDSCs rather use Arg-1 and ROS (Budhwar et al. 2018, Raber et al. 2014, Yang et al. 2019, Youn et al. 2008, Yu et al. 2013, Zhang et al. 2016). In various experimental settings including *in vitro* and *in vivo* transplantation models, rapamycin was found to increase iNOS and Arg-1 expression by M-MDSCs and PMN-MDSCs, respectively (Nakamura et al. 2015, Wei et al. 2018, Zhang et al. 2017). In accordance, the amounts of *Arg1* and Nos2 mRNAs expressed by PMN-MDSCs from rapamycin-treated lean and obese mice were higher compared to their untreated counterparts. The increase of mRNA expression of *Ido1*, *Ido2*, *Il10*, *Tgfb1* and *Nos2* by M-MDSCs from obese allograft recipients under rapamycin treatment is particularly relevant to the induction of Tregs and therefore discussed below in this context. The measured mRNA expression profiles did not reveal steady trends over the complete observation period which might be explained by the interindividual variability in the small groups of animals.

However, data on mRNA expression can only provide hints and their relevance will have to be confirmed by analyses of the encoded proteins and their functions in subsequent studies (Bustin et al. 2009).

MDSCs, expressing the respective receptors, are attracted in response to various different chemokines: CCL2 and CCL5 recruit M-MDSCs whereas PMN-MDSCs are attracted by CXCL1, CXCL5, CXCL6, CXCL8 and CXCL12 (Kang et al. 2016, Kumar et al. 2016, Wang et al. 2017).

Up-regulation of CXCL1, CXCL2 and their receptor CXCR2 in kidney tissue of rapamycin-treated mice with AKI provides evidence that these factors are crucially involved in recruitment of protective MDSCs (Zhang et al. 2017). In accordance, measured numbers of PMN-MDSCs clearly correlated with CXCL1 concentrations in peripheral blood of rapamycin-treated obese allograft recipients. CXCL1 and CXCL2 were found to promote generation of M-MDSCs (Shi et al. 2018) and these factors might also contribute to the immune response by obese rapamycin-treated mice, which showed higher CXCL2 plasma concentrations than their lean counterparts. This study also supported that IL-6 enhances MDSC proliferation and their T cell-suppressing activity (Jiang et al. 2017) because its plasma concentration correlated with the relative abundances of PMN-MDSCs both in spleens and peripheral blood samples from rapamycin-treated obese allograft recipients. In summary of these partial results, this pilot study further supported the assumption of positive effects of CXCL1 and CXCL2 on recruitment and of IL-6 on the generation of MDSCs.

All results combined indicate that obesity per se affects immunosuppression by M-MDSCs which can be restored by treatment with rapamycin, which in contrast had only a minimal effect on M-MDSCs from lean mice or on PMN-MDSCs. The M-MDSCs from rapamycin-treated animals also appeared to be stronger immunosuppressive than the respective PMN-MDSCs, at least regarding T cell proliferation. This clearly supports the hypothesis that of two main MDSC subtypes, M-MDSCs seem to play a more important role in post-transplant immunosuppressive therapy of obese recipients.

Despite improved graft survival in rapamycin-treated obese (versus lean) mice, determined numbers of MDSCs at the time of allograft rejection were not different. However, there is increasing evidence indicating that M-MDSCs are more immunosuppressive and, in addition, that other regulatory immune cells like Tregs may also play an important role in processes supporting allograft viability. In the experimental study by Nakamura et al. (2015) the depletion of MDSCs with anti-Gr-1 antibody shortened heart allograft survival dramatically when recipients were treated with rapamycin (21 days vs. 67 days), but notably, untreated mice rejected their cardiac allograft already after 7 days. This clearly points to a considerable contribution of other immune cells to the mechanisms underlying the rapamycin-caused prolongation of allograft survival.

Here, Tregs are prime candidates since it has been reported that rapamycin is capable of inducing immunosuppressive Tregs (Thomson et al. 2009). Battaglia et al. (2005) showed that rapamycin boosts the accumulation of immunosuppressive Tregs *in vitro* and demonstrated that these cells have the potential to prolong pancreatic islet allograft survival *in vivo* (Battaglia et al. 2005). Increased numbers of Tregs were also found in rapamycin-treated rats which underwent liver transplantation (Lu et al. 2010). In mTOR-deficient mice, the differentiation of precursor cells to Tregs was enhanced. In addition, the crucial role of mTOR in the differentiation processes leading to Th1, Th2 and Th17 cells was confirmed by down-regulation of these effector T cells as a consequence of the mTOR deficiency (Delgoffe et al. 2009). In line with these findings, interference with mTOR signaling by rapamycin treatment in the present study resulted in significantly more Tregs generated in obese skin allograft recipients, also reflected by a higher relative abundance among all T cells. Interestingly, this strong effect of rapamycin was not similarly observed in lean mice, although in both groups the numbers of Tregs increased over the observed period. Thus, the rapamycin-induced Treg accumulation is a mechanism that seems to be of particular relevance to obese individuals.

MDSCs are considered important regulators of Treg activities as they are capable of inducing Tregs through IDO, IL-10, TGF-β or programmed death-ligand 1 (Nakamura et al. 2018, Yu et al. 2013). Nakamura et al. (2016) also demonstrated

that adoptively transferred murine MDSCs originating from rapamycin-treated heart allograft recipients lead to a more substantial recruitment of Tregs in the cardiac allograft than MDSCs from untreated animals (Nakamura et al. 2016). This suggests an enhancement of the Treg-attracting activity of MDSCs by rapamycin. In the experiments described here, rapamycin increased the number and activity of immunosuppressive M-MDSCs as well as the number of Tregs in obese mice, and caused a shift from pro-inflammatory T cell subsets to immunosuppressive Tregs. M-MDSCs from these mice also expressed higher amounts of *Ido1*, *Ido2*, *Il10* and *Tgfb1* mRNAs. This suggests that, besides its direct effect on Treg activity, rapamycin's induction of MDSCs might lead to further Treg expansion mediated by IDO1, IDO2, IL-10 and TGF-β. Additional analyses of mTOR expression by MDSCs and Tregs might help to distinguish between these alternative mechanistic routes in follow-up investigations.

Notably, rapamycin treatment also increased numbers of Th1 and Th17 cells and thereby favored Th1 cells in relation to Th2 and Th17 populations. This is a consequence of the steady increase of pro-inflammatory Th1 and Th17 cells in rapamycin-treated lean and obese mice from POD 3 until POD 11 in contrast to a constant fraction of Th2 cells. In accordance with several other studies, the ratio of Tregs to Th17 cells was also significantly increased by rapamycin treatment of obese mice (Gu et al. 2016, Jing et al. 2017, Kopf et al. 2007).

Based on theoretical considerations, rapamycin might have resulted in reduced numbers of pro-inflammatory T cells by inhibiting mTOR (Delgoffe et al. 2009, Thomson et al. 2009). However, proliferation of T cells, with the exception of the Th2 subtype, generally appeared to be stimulated over the period observed in the experiments despite treatment with rapamycin. Potential stimuli of T cell proliferation may include postoperative inflammation and wound healing, pain or stress caused by the daily injections of DMSO or rapamycin, and stress due to wearing the bandage. However, since the T cell increase, observed on PODs 3 and 7 and the day of allograft rejection, was more pronounced in rapamycin-treated mice it seems likely that the effect is at least partly due to the administered rapamycin. Experimental studies showed that rapamycin does not or only slightly inhibit the proliferation of Th1 cells under Th1-polarzing conditions, but

significantly reduces their cytokine production as an important function of these cells (Amarnath et al. 2010, Jung et al. 2006). Thus, assuming that the aforementioned experimental conditions are associated with Th1 polarization the expansion of pro-inflammatory T cell populations due to rapamycin treatment is consistent with the results of these studies. In the used animal model, a potential Th1 polarization would likely had been triggered by other factors than IFN-γ, of which plasma concentrations generally were below the detection limit of the method. Interestingly, a recent study found that rapamycin treatment as effective GvHD prophylaxis does not alter the composition of T cell subsets in any way, but clearly increases the immunosuppressive activity of MDSCs, associated with elevated levels of IDO and iNOS (Scheurer et al. 2020).

In summary of rapamycin's effects, the treatment mainly led to a shift in in the composition of the T cell population towards immunosuppressive Tregs, although it also increased the number of pro-inflammatory Th1 and Th17 cells. Clearly, the impact of anti-inflammatory Tregs and MDSCs turned out to be stronger than the effects of pro-inflammatory Th1 and Th17 cells, resulting in an extension of skin allograft survival in rapamycin-treated animals. T cell numbers were not different between rapamycin treated obese and lean allograft recipients with the only exception being the enrichment of Tregs in the total T cell population. In contrast to MDSCs, Tregs are generated more slowly and contribute therefore mainly to the immune tolerance in a later phase of the immune response, whereas MDSCs are considered to be more effective at earlier stages (Nakamura et al. 2018). This is consistent with the fact that increased numbers of Tregs were observed only on the day of allograft rejection, while during the course of the experiments Treg abundance in obese and lean treated mice was not different. Overall, the results of this study clearly indicate that both Tregs and M-MDSCs play important roles in rapamycin-induced processes leading to prolongation of skin allograft survival in obese animals.

In *in vitro* and *in vivo* investigations rapamycin has been demonstrated to interfere with the balance of human macrophage sub-populations in favor of pro-inflammatory M1 macrophages (Mercalli et al. 2013). Furthermore, rapamycin induces the secretion of pro-inflammatory IL-12 by macrophages while reducing

that of anti-inflammatory IL-10 (Rojas Marquez et al. 2018). In contrast, numbers of M1 macrophages in lean and obese skin allograft recipients determined in this study on the day of rejection were not significantly affected by rapamycin treatment. However, early after transplantation (POD 3), rapamycin-treated obese mice had more M1 macrophages than their lean counterparts, suggesting a differential but temporary effect. In obese mice, the decrease of the relative abundance of M2 macrophages during rapamycin treatment is in line with the result of Mercalli et al. (2013) who observed rapamycin-induced apoptosis of M2 macrophages polarized by LPS and IL-4.

It is surprising that to date, no data on the influence of rapamycin on M2-like macrophages have been published. Therefore, it is an interesting result of this study that rapamycin treatment of lean mice resulted in a higher portion of anti-inflammatory M2-like macrophages, although obese allograft recipients were not similarly affected. As a clear trend, rapamycin treatment appears to change the overall composition of immune cells by increasing anti-inflammatory M2-like macrophages, M-MDSCs and Tregs, in parallel to reducing pro-inflammatory (M1 and M2) macrophages. However, particularly the results concerning M2 and M2-like macrophages would need to be confirmed in follow-up experiments to confirm statistical and translational significance especially for M2-like macrophages which are only a small subset of M2 macrophages.

Taken together, rapamycin treatment of obese mice resulted in an increase of M-MDSCs and restoration of their immunosuppressive capacity, associated with effects on T cell and macrophage populations in favor of anti-inflammatory Tregs and M2-like macrophages. Even though obesity itself did not significantly alter the composition of immune cells and thereby the immune response to skin allograft transplantation, the impact of rapamycin differed significantly between lean and obese mice. The stronger effects in obese allograft recipients were also reflected by substantially prolonged allograft survival. Of course, results of these experiments, yielding data on cell numbers, immunosuppressive activity and mRNA expression, cannot be considered as a proof of a causal involvement of

MDSCs, Tregs and M2-like macrophages in immunoregulatory processes leading to allograft survival, but they might serve as a first step towards subsequent experimental studies to confirm their roles in the alloimmune response and the process of allograft rejection. Here, future experiments may focus on adoptive transfer of the identified regulatory cells generated *in vitro* or on *in vivo* depletion of immunosuppressive cells by specific antibodies or drugs. Further analyses of the potentially involved IDO1, IDO2 and TGF-β signaling pathways in model systems of transplantation, e.g. by specific targeting of key components, might also be helpful to reveal mechanistic links between activities of MDSCs and Tregs and allograft survival.

4.4 Clinical relevance and outlook

Rapamycin was found to counteract the development of nutrition-induced obesity in mice. It was clearly demonstrated in two studies that weekly injections of low doses of rapamycin (2 mg/kg/week) generally improved the metabolic profile of HFD-fed obese mice, including an increased energy expenditure, slower weight gain, reduction of adipose tissue, decreased leptin blood levels and enhanced insulin sensitivity (Chang et al. 2009, Makki et al. 2014). Results by Fang et al. (2013) indicated that an improved metabolic profile only develops during long-term therapy with rapamycin, whereas shorter treatment at first even has detrimental metabolic effects, e.g. on insulin sensitivity and triglyceride blood levels. An important general side effect of an immunosuppressive therapy is the increased risk of getting infectious or malignant diseases (Au et al. 2018, Mueller 2008). Obesity itself is considered a risk factor for postoperative infections and the development of cancer as a consequence of affected MDSCs and M2 macrophages (Clements et al. 2018, Friedenreich et al. 2020, Milner et al. 2012, Okwan-Duodu et al. 2013). Thus, the surplus risks related to immunosuppressive therapy might be of particular relevance to obese individuals. Particularly in view of such adverse effects of immunosuppressive therapy, rapamycin appears to be an interesting drug as anti-cancer effects of rapamycin were demonstrated even in an animal model of transplantation: Rapamycin not only prevented heart allograft rejection but also inhibited tumor growth after subcutaneous injection of

carcinoma cells (Koehl et al. 2004). These result of animal experimentation point to superior properties of rapamycin in immunosuppressive therapy, from which in particular obese allograft recipients might benefit. However, results of animal studies with rodents can only provide hints and their relevance to human diseases and therapies needs to be evaluated carefully. In two clinical studies, increased numbers of Tregs in renal allograft recipients treated with rapamycin were demonstrated (Li et al. 2015, Noris et al. 2007), but the effects of rapamycin on MDSCs and macrophages in humans undergoing transplantations still need to be investigated. Numbers of M-MDSCs were, however, described to increase in human renal allograft recipients during treatment with tacrolimus and prednisolone (Luan et al. 2013). Thus, the promising effects of rapamycin in initial studies will have to be confirmed by further research with special attention to obese human allograft recipients.

In this study, an advantage of the well-established immunosuppressive drug rapamycin in the treatment of obese murine skin allograft recipients was clearly demonstrated. Prior to clinical trials based on these results, follow-up studies of minor MHC-mismatched transplantations and heart or kidney allografts will have to be conducted and dose-dependent effects of rapamycin evaluated. Then it seems possible to establish rapamycin in a specifically adapted immunosuppressive therapy of human obese allograft recipients. In addition to therapeutic and potential side effects, pharmacokinetic properties of the lipophilic rapamycin molecule have to be considered. Rapamycin could accumulate in adipose tissue and take effect over a longer period of time in obese compared to lean individuals through constant release from this depot. Based on the analyses of such effects, different dosing schemes might be established for obese and lean patients receiving immunosuppressive rapamycin. Nevertheless, this experimental study provides initial data in support of a promising adapted strategy of immunosuppressive therapy particularly beneficial to the steadily increasing number of obese allograft recipients. Furthermore, it was the first investigation of the effect of obesity on the immunosuppressive therapy following allograft transplantation. Based on the results obtained with rapamycin, it seems reasonable to assume different effects also of other immunosuppressive drugs

such as other mTOR inhibitors (everolimus, temsirolimus), calcineurin inhibitors (tacrolimus, cyclosporine A) or checkpoint inhibitors (CTLA4-Ig) on immune cells of obese individuals. Future comparative studies are therefore needed to find the best treatment options for this group of transplantation patients. An alternative novel therapeutic approach to induce immune tolerance towards an allograft is the yet to be established cell-based therapy, e.g. with immunosuppressive MDSCs and Tregs. Initial animal experiments to provide proof of this concept were promising (Cai et al. 2020).

4.5 Conclusion

In conclusion, obesity turned out to be beneficial to rapamycin-treated recipients of skin allografts as indicated by later rejection. An increased number and immunosuppressive activity of M-MDSCs as well as the expansion of Tregs and the shift towards immunosuppressive T cell and macrophage subsets contributed to the overall effect of prolonged skin allograft survival in obese mice. Thus, this study provides insight into obesity-specific effects of immunosuppressive therapy with rapamycin and points to advantages that obese allograft recipients might have.

5. Abstracts

5.1 English abstract

Obesity has emerged into a substantial problem in transplantation medicine with steadily increasing numbers of obese graft donors and recipients. Despite this development and high impact on the transplantation outcome, research addressing the question how the effectiveness of immunosuppressive drugs might be modulated by obesity is still in its initial phase. In this study, the effect of the widely used immunosuppressive drug rapamycin on immune cells and skin allograft survival was investigated in a murine model of diet-induced obesity.

After having received a high-fat diet, obese mice underwent full major histocompatibility complex (MHC-) mismatched skin allograft transplantation. Starting at the day of transplantation, allograft recipients were treated daily with 2 mg/kg rapamycin. Allograft survival was monitored and at defined postoperative days and the day of allograft rejection, pro- and anti-inflammatory cells, such as MDSCs, T cells and macrophages, were quantified by flow cytometry with cell type-specific antibodies. As a measure of the immunosuppressive activity of MDSCs, suppression of proliferation of co-cultivated T cells was determined with the carboxyfluorescein succinimidyl ester (CFSE) proliferation assay. To get hints on mechanisms underlying the observations on the cellular level, expression of potentially relevant mRNAs by MDSCs was analyzed by qPCR, and plasma concentrations of selected chemokines and cytokines were measured.

Strikingly, rapamycin treatment prolonged skin allograft survival and this effect was significantly more pronounced in obese recipients compared to their lean counterparts. In obese mice rapamycin increased the percentage of M-MDSCs and even more importantly enhanced their capacity to suppress T cell proliferation. In addition, obese mice treated with rapamycin had more immunosuppressive regulatory T cells than corresponding lean animals. Rapamycin-treated obese allograft recipients also showed altered compositions of T cell and macrophage populations with a shift towards anti-inflammatory cell subsets. Expression of certain mRNAs encoding proteins involved in

immunoregulation of MDSCs changed between allograft transplantation and rejection, and as a consequence of rapamycin treatment and obesity.

Taken together, generation and activation of immunosuppressive M-MDSCs in rapamycin-treated obese allograft recipients is accompanied by an increase of Tregs and anti-inflammatory M2-like macrophages which may additionally support allograft survival. These results provide first evidence of obesity-dependent positive effects of immunosuppressive drugs that might pave the way towards more tailored protocols for obese graft recipients.

5.2 German abstract / deutsche Zusammenfassung

Adipositas hat sich aufgrund einer stetig zunehmenden Zahl adipöser Transplantationskandidaten und -empfängern zu einem erheblichen Problem in der Transplantationsmedizin entwickelt. Trotz der hohen Relevanz für den Transplantationserfolg befindet sich die Forschung zu der Frage, wie die Wirkung von Immunsuppressiva durch Adipositas beeinflusst werden könnte, noch in der Anfangsphase. In dieser Studie wurde mittels einem murinen Modell mit diätetischer Adipositas der Effekt des häufig verwendeten immunsuppressiven Medikaments Rapamycin auf Immunzellen und das Überleben von Hauttransplantaten untersucht.

Nach einer fettreichen Diät wurden adipöse Mäuse einer vollständig Haupthistokompatibilitätskomplex (MHC-) inkongruenten Hauttransplantation unterzogen. Beginnend mit dem Tag der Transplantation wurden die Transplantatempfänger täglich mit 2 mg/kg Rapamycin behandelt. Das Überleben des Transplantats wurde überwacht und an definierten postoperativen Tagen sowie am Tag der Transplantatabstoßung wurden pro- und anti-inflammatorische Zellen, wie myeloide Suppressorzellen (MDSCs), T-Zellen und Makrophagen, mittels Durchflusszytometrie mit zelltypspezifischen Antikörpern quantifiziert. Als Maß für die immunsuppressive Aktivität von MDSCs wurde die Suppression der Proliferation von kokultivierten T-Zellen mit dem Carboxyfluoresceinsuccinimidylester (CFSE)-Proliferationsassay bestimmt. Um Hinweise auf Mechanismen, die den Beobachtungen auf zellulärer Ebene

zugrunde liegen, zu erhalten, wurde die Expression potenziell relevanter mRNAs durch MDSCs mittels qPCR analysiert und die Plasmakonzentrationen ausgewählter Chemokine und Zytokine gemessen.

Die Behandlung mit Rapamycin verlängerte die Überlebenszeit der Hauttransplantate, dieser Effekt war bei adipösen Empfängern signifikant stärker ausgeprägt als bei ihrer schlanken Vergleichsgruppe. Bei adipösen Empfängertieren erhöhte Rapamycin den Anteil der monozytären MDSCs (M-MDSCs) und, was von höherer Bedeutung ist, ebenso deren Fähigkeit, T-Zell-Proliferation zu unterdrücken. Darüber hinaus hatten adipöse Mäuse, die mit Rapamycin behandelt wurden, mehr immunsuppressive regulatorische T-Zellen (Tregs) als entsprechende normalgewichtige Tiere. Mit Rapamycin behandelte adipöse Transplantatempfänger zeigten auch eine veränderte Zusammensetzung der T-Zell- und Makrophagen-Populationen mit einer deutlichen Verschiebung hin zu anti-inflammatorischen Zelluntergruppen. Die Expression bestimmter mRNAs, die für Proteine kodieren, welche an der Immunregulation durch MDSCs beteiligt sind, veränderte sich im Verlauf von der Transplantation bis hin zur Transplantatabstoßung, was sowohl mit der Adipositas als auch mit der Rapamycin-Behandlung assoziiert werden konnte.

Insgesamt geht die Generierung und Aktivierung von immunsuppressiven M-MDSCs in Rapamycin-behandelten adipösen Transplantatempfängern mit einer Zunahme von Tregs und anti-inflammatorischen M2-ähnliche Makrophagen einher, die das verlängerte Überleben des Transplantats zusätzlich begünstigt haben könnten. Diese Ergebnisse liefern erste Hinweise auf Adipositas-spezifische positive Effekte von Immunsuppressiva, die in der klinischen Praxis weit verbreitet sind.

6. Bibliography

Amarnath S, Flomerfelt FA, Costanzo CM, Foley JE, Mariotti J, Konecki DM, et al. 2010. Rapamycin generates anti-apoptotic human Th1/Tc1 cells via autophagy for induction of xenogeneic GVHD. *Autophagy,* 6**,** 523-41.

Arakawa Y, Qin J, Chou HS, Bhatt S, Wang L, Stuehr D, et al. 2014. Cotransplantation with myeloid-derived suppressor cells protects cell transplants: a crucial role of inducible nitric oxide synthase. *Transplantation,* 97**,** 740-7.

Au E, Wong G, Chapman JR 2018. Cancer in kidney transplant recipients. *Nat Rev Nephrol,* 14**,** 508-520.

Ayala Garcia MA, Gonzalez Yebra B, Lopez Flores AL, Guani Guerra E 2012. The major histocompatibility complex in transplantation. *J Transplant,* 2012**,** 842141.

Ballbach M, Hall T, Brand A, Neri D, Singh A, Schaefer I, et al. 2016. Induction of Myeloid-Derived Suppressor Cells in Cryopyrin-Associated Periodic Syndromes. *J Innate Immun,* 8**,** 493-506.

Bao Y, Mo J, Ruan L, Li G 2015. Increased monocytic CD14(+)HLADRlow/- myeloid-derived suppressor cells in obesity. *Mol Med Rep,* 11**,** 2322-8.

Bartels M, Becker T, Klempnauer J 2008. Transplantation. *In:* Bruch HP, Trentz O (ed.) *Chirurgie.* Elsevier, München.

Battaglia M, Stabilini A, Roncarolo MG 2005. Rapamycin selectively expands CD4+CD25+FoxP3+ regulatory T cells. *Blood,* 105**,** 4743-8.

Baumann R 2015. Das Abwehrsystem. *In:* Gekle M, Wischmeyer E, Gründer S, Petersen M, Schwab A, Markwardt F et al. (ed.) *Taschenlehrbuch Physiologie.* Georg Thieme Verlag, Stuttgart, New York.

Bedoya SK, Lam B, Lau K, Larkin J, 3rd 2013. Th17 cells in immunity and autoimmunity. *Clin Dev Immunol,* 2013**,** 986789.

Blenis J 2017. TOR, the Gateway to Cellular Metabolism, Cell Growth, and Disease. *Cell,* 171**,** 10-13.

Boorsma CE, Draijer C, Melgert BN 2013. Macrophage heterogeneity in respiratory diseases. *Mediators Inflamm,* 2013**,** 769214.

Broichhausen C, Riquelme P, Geissler EK, Hutchinson JA 2012. Regulatory macrophages as therapeutic targets and therapeutic agents in solid organ transplantation. *Curr Opin Organ Transplant,* 17**,** 332-42.

Bronte V, Brandau S, Chen SH, Colombo MP, Frey AB, Greten TF, et al. 2016. Recommendations for myeloid-derived suppressor cell nomenclature and characterization standards. *Nat Commun,* 7**,** 12150.

Budhwar S, Verma P, Verma R, Rai S, Singh K 2018. The Yin and Yang of Myeloid Derived Suppressor Cells. *Front Immunol,* 9**,** 2776.

Bustin SA, Benes V, Garson JA, Hellemans J, Huggett J, Kubista M, et al. 2009. The MIQE guidelines: minimum information for publication of quantitative real-time PCR experiments. *Clin Chem,* 55**,** 611-22.

Cai S, Choi JY, Borges TJ, Zhang H, Miao J, Ichimura T, et al. 2020. Donor myeloid derived suppressor cells (MDSCs) prolong allogeneic cardiac graft survival through programming of recipient myeloid cells in vivo. *Sci Rep,* 10**,** 14249.

Cao Q, Wang Y, Wang XM, Lu J, Lee VW, Ye Q, et al. 2015. Renal F4/80+ CD11c+ mononuclear phagocytes display phenotypic and functional characteristics of macrophages in health and in adriamycin nephropathy. *J Am Soc Nephrol,* 26**,** 349-63.

Chang AL, Miska J, Wainwright DA, Dey M, Rivetta CV, Yu D, et al. 2016. CCL2 Produced by the Glioma Microenvironment Is Essential for the Recruitment of Regulatory T Cells and Myeloid-Derived Suppressor Cells. *Cancer Res,* 76**,** 5671-5682.

Chang GR, Chiu YS, Wu YY, Chen WY, Liao JW, Chao TH, et al. 2009. Rapamycin protects against high fat diet-induced obesity in C57BL/6J mice. *J Pharmacol Sci,* 109**,** 496-503.

Cheng CH, Lee CF, Fryer M, Furtmuller GJ, Oh B, Powell JD, et al. 2017. Murine Full-thickness Skin Transplantation. *J Vis Exp*.

Choi JN, Sun EG, Cho SH 2019. IL-12 Enhances Immune Response by Modulation of Myeloid Derived Suppressor Cells in Tumor Microenvironment. *Chonnam Med J,* 55**,** 31-39.

Clements VK, Long T, Long R, Figley C, Smith DMC, Ostrand-Rosenberg S 2018. Frontline Science: High fat diet and leptin promote tumor progression by inducing myeloid-derived suppressor cells. *J Leukoc Biol,* 103**,** 395-407.

Collins S, Martin TL, Surwit RS, Robidoux J 2004. Genetic vulnerability to diet-induced obesity in the C57BL/6J mouse: physiological and molecular characteristics. *Physiol Behav,* 81**,** 243-8.

Condamine T, Dominguez GA, Youn JI, Kossenkov AV, Mony S, Alicea-Torres K, et al. 2016. Lectin-type oxidized LDL receptor-1 distinguishes population of human polymorphonuclear myeloid-derived suppressor cells in cancer patients. *Sci Immunol,* 1.

Condamine T, Mastio J, Gabrilovich DI 2015. Transcriptional regulation of myeloid-derived suppressor cells. *J Leukoc Biol,* 98**,** 913-22.

Cossarizza A, Chang HD, Radbruch A, Akdis M, Andra I, Annunziato F, et al. 2017. Guidelines for the use of flow cytometry and cell sorting in immunological studies. *Eur J Immunol,* 47**,** 1584-1797.

Deissler A, Della Penna A, Van Geffen C, Gonzalez-Menendez I, Quintanilla-Martinez L, Gunther A, et al. 2021. Rapamycin delays allograft rejection in obese graft recipients through induction of myeloid-derived suppressor cells. *Immunol Lett,* 236**,** 1-11.

Delgoffe GM, Kole TP, Zheng Y, Zarek PE, Matthews KL, Xiao B, et al. 2009. The mTOR kinase differentially regulates effector and regulatory T cell lineage commitment. *Immunity,* 30**,** 832-44.

Dibbern J, Eggers L, Schneider BE 2017. Sex differences in the C57BL/6 model of Mycobacterium tuberculosis infection. *Sci Rep,* 7**,** 10957.

Dilek N, Vuillefroy De Silly R, Blancho G, Vanhove B 2012. Myeloid-derived suppressor cells: mechanisms of action and recent advances in their role in transplant tolerance. *Front Immunol,* 3**,** 208.

Elderman M, Van Beek A, Brandsma E, De Haan B, Savelkoul H, De Vos P, et al. 2016. Sex impacts Th1 cells, Tregs, and DCs in both intestinal and systemic immunity in a mouse strain and location-dependent manner. *Biol Sex Differ,* 7**,** 21.

Ellulu MS, Patimah I, Khaza'ai H, Rahmat A, Abed Y 2017. Obesity and inflammation: the linking mechanism and the complications. *Arch Med Sci,* 13**,** 851-863.
Elshal MF, Mccoy JP 2006. Multiplex bead array assays: performance evaluation and comparison of sensitivity to ELISA. *Methods,* 38**,** 317-23.
Erickson MA, Liang WS, Fernandez EG, Bullock KM, Thysell JA, Banks WA 2018. Genetics and sex influence peripheral and central innate immune responses and blood-brain barrier integrity. *PLoS One,* 13**,** e0205769.
Faas M, Vos PD, Melgert B. 2011. *Sex Hormones and Immunoregulation* [Online]. BrainImmune. Available: http://www.brainimmune.com/sex-hormones-and-immunoregulation/ [Accessed 11.11.2020].
Fang Y, Westbrook R, Hill C, Boparai RK, Arum O, Spong A, et al. 2013. Duration of rapamycin treatment has differential effects on metabolism in mice. *Cell Metab,* 17**,** 456-62.
Fantuzzi G 2005. Adipose tissue, adipokines, and inflammation. *J Allergy Clin Immunol,* 115**,** 911-9; quiz 920.
Feuerer M, Herrero L, Cipolletta D, Naaz A, Wong J, Nayer A, et al. 2009. Lean, but not obese, fat is enriched for a unique population of regulatory T cells that affect metabolic parameters. *Nat Med,* 15**,** 930-9.
Friedenreich CM, Ryder-Burbidge C, Mcneil J 2020. Physical activity, obesity and sedentary behavior in cancer etiology: epidemiologic evidence and biologic mechanisms. *Mol Oncol*.
Gabrilovich DI, Nagaraj S 2009. Myeloid-derived suppressor cells as regulators of the immune system. *Nat Rev Immunol,* 9**,** 162-74.
Gekle M 2015. Regulation der Nahrungsaufnahme. *In:* Gekle M, Wischmeyer E, Gründer S, Petersen M, Schwab A, Markwardt F et al. (ed.) *Taschenlehrbuch Physiologie.* Georg Thieme Verlag, Stuttgart, New York.
Graefe KH 2016. Immunsystem. *In:* Graefe KH, Lutz W, Bönisch H (ed.) *Pharmakologie und Toxikologie.* Georg Thieme Verlag, Stuttgart.
Gu L, Deng WS, Sun XF, Zhou H, Xu Q 2016. Rapamycin ameliorates CCl4-induced liver fibrosis in mice through reciprocal regulation of the Th17/Treg cell balance. *Mol Med Rep,* 14**,** 1153-61.
Gulbins E, Lang KS 2019. Immunsystem. *In:* Brandes R, Lang F, Schmidt RF (ed.) *Physiologie des Menschen.* Springer-Verlag, Berlin.
Han X, Shi H, Sun Y, Shang C, Luan T, Wang D, et al. 2019. CXCR2 expression on granulocyte and macrophage progenitors under tumor conditions contributes to mo-MDSC generation via SAP18/ERK/STAT3. *Cell Death Dis,* 10**,** 598.
Heid CA, Stevens J, Livak KJ, Williams PM 1996. Real time quantitative PCR. *Genome Res,* 6**,** 986-94.
Heigl T, Singh A, Saez-Gimenez B, Kaes J, Van Herck A, Sacreas A, et al. 2019. Myeloid-Derived Suppressor Cells in Lung Transplantation. *Front Immunol,* 10**,** 900.
Heinbokel T, Floerchinger B, Schmiderer A, Edtinger K, Liu G, Elkhal A, et al. 2013. Obesity and its impact on transplantation and alloimmunity. *Transplantation,* 96**,** 10-6.
Hellemans J, Mortier G, De Paepe A, Speleman F, Vandesompele J 2007. qBase relative quantification framework and software for management and

automated analysis of real-time quantitative PCR data. *Genome Biol,* 8**,** R19.

Hensel JA, Khattar V, Ashton R, Ponnazhagan S 2019. Characterization of immune cell subtypes in three commonly used mouse strains reveals gender and strain-specific variations. *Lab Invest,* 99**,** 93-106.

Herold G 2017. Adipositas. *In:* Herold, Gerd (ed.) *Innere Medizin.* Gerd Herold, Cologne.

Hill CJ, Courtney AE, Cardwell CR, Maxwell AP, Lucarelli G, Veroux M, et al. 2015. Recipient obesity and outcomes after kidney transplantation: a systematic review and meta-analysis. *Nephrol Dial Transplant,* 30**,** 1403-11.

Hirahara K, Nakayama T 2016. CD4+ T-cell subsets in inflammatory diseases: beyond the Th1/Th2 paradigm. *Int Immunol,* 28**,** 163-71.

Hu CE, Gan J, Zhang RD, Cheng YR, Huang GJ 2011. Up-regulated myeloid-derived suppressor cell contributes to hepatocellular carcinoma development by impairing dendritic cell function. *Scand J Gastroenterol,* 46**,** 156-64.

Iglesias-Escudero M, Sansegundo-Arribas D, Riquelme P, Merino-Fernandez D, Guiral-Foz S, Perez C, et al. 2020. Myeloid-Derived Suppressor Cells in Kidney Transplant Recipients and the Effect of Maintenance Immunotherapy. *Front Immunol,* 11**,** 643.

Jiang M, Chen J, Zhang W, Zhang R, Ye Y, Liu P, et al. 2017. Interleukin-6 Trans-Signaling Pathway Promotes Immunosuppressive Myeloid-Derived Suppressor Cells via Suppression of Suppressor of Cytokine Signaling 3 in Breast Cancer. *Front Immunol,* 8**,** 1840.

Jiang X, Tian W, Sung YK, Qian J, Nicolls MR 2014. Macrophages in solid organ transplantation. *Vasc Cell,* 6**,** 5.

Jing F, Yang F, Cui F, Chen Z, Ling L, Huang X 2017. Rapamycin alleviates inflammation and muscle weakness, while altering the Treg/Th17 balance in a rat model of myasthenia gravis. *Biosci Rep,* 37.

Jose MD, Ikezumi Y, Van Rooijen N, Atkins RC, Chadban SJ 2003. Macrophages act as effectors of tissue damage in acute renal allograft rejection. *Transplantation,* 76**,** 1015-22.

Jung U, Foley JE, Erdmann AA, Toda Y, Borenstein T, Mariotti J, et al. 2006. Ex vivo rapamycin generates Th1/Tc1 or Th2/Tc2 Effector T cells with enhanced in vivo function and differential sensitivity to post-transplant rapamycin therapy. *Biol Blood Marrow Transplant,* 12**,** 905-18.

Kang X, Zhang X, Liu Z, Xu H, Wang T, He L, et al. 2016. CXCR2-Mediated Granulocytic Myeloid-Derived Suppressor Cells' Functional Characterization and Their Role in Maternal Fetal Interface. *DNA Cell Biol,* 35**,** 358-65.

Katoh H, Wang D, Daikoku T, Sun H, Dey SK, Dubois RN 2013. CXCR2-expressing myeloid-derived suppressor cells are essential to promote colitis-associated tumorigenesis. *Cancer Cell,* 24**,** 631-44.

Kay E, Gomez-Garcia L, Woodfin A, Scotland RS, Whiteford JR 2015. Sexual dimorphisms in leukocyte trafficking in a mouse peritonitis model. *J Leukoc Biol,* 98**,** 805-17.

Koehl GE, Andrassy J, Guba M, Richter S, Kroemer A, Scherer MN, et al. 2004. Rapamycin protects allografts from rejection while simultaneously attacking tumors in immunosuppressed mice. *Transplantation,* 77**,** 1319-26.

Kontaki E, Boumpas DT, Tzardi M, Mouzas IA, Papadakis KA, Verginis P 2017. Aberrant function of myeloid-derived suppressor cells (MDSCs) in experimental colitis and in inflammatory bowel disease (IBD) immune responses. *Autoimmunity,* 50**,** 170-181.

Kopf H, De La Rosa GM, Howard OM, Chen X 2007. Rapamycin inhibits differentiation of Th17 cells and promotes generation of FoxP3+ T regulatory cells. *Int Immunopharmacol,* 7**,** 1819-24.

Kumar V, Patel S, Tcyganov E, Gabrilovich DI 2016. The Nature of Myeloid-Derived Suppressor Cells in the Tumor Microenvironment. *Trends Immunol,* 37**,** 208-220.

Lee YS, Zhang T, Saxena V, Li L, Piao W, Bromberg JS, et al. 2020. Myeloid-derived suppressor cells expand after transplantation and their augmentation increases graft survival. *Am J Transplant,* 20**,** 2343-2355.

Lekanne Deprez RH, Fijnvandraat AC, Ruijter JM, Moorman AF 2002. Sensitivity and accuracy of quantitative real-time polymerase chain reaction using SYBR green I depends on cDNA synthesis conditions. *Anal Biochem,* 307**,** 63-9.

Leontieva OV, Paszkiewicz G, Demidenko ZN, Blagosklonny MV 2013. Resveratrol potentiates rapamycin to prevent hyperinsulinemia and obesity in male mice on high fat diet. *Cell Death Dis,* 4**,** e472.

Li J, Li C, Zhuang Q, Peng B, Zhu Y, Ye Q, et al. 2019. The Evolving Roles of Macrophages in Organ Transplantation. *J Immunol Res,* 2019**,** 5763430.

Li W, Zhang X, Chen Y, Xie Y, Liu J, Feng Q, et al. 2016. G-CSF is a key modulator of MDSC and could be a potential therapeutic target in colitis-associated colorectal cancers. *Protein Cell,* 7**,** 130-40.

Li Y, Shi Y, Liao Y, Yan L, Zhang Q, Wang L 2015. Differential regulation of Tregs and Th17/Th1 cells by a sirolimus-based regimen might be dependent on STAT-signaling in renal transplant recipients. *Int Immunopharmacol,* 28**,** 435-43.

Liu YF, Zhuang KH, Chen B, Li PW, Zhou X, Jiang H, et al. 2018. Expansion and activation of monocytic-myeloid-derived suppressor cell via STAT3/arginase-I signaling in patients with ankylosing spondylitis. *Arthritis Res Ther,* 20**,** 168.

Liu Z, Fan H, Jiang S 2013. CD4(+) T-cell subsets in transplantation. *Immunol Rev,* 252**,** 183-91.

Livak KJ, Schmittgen TD 2001. Analysis of relative gene expression data using real-time quantitative PCR and the 2(-Delta Delta C(T)) Method. *Methods,* 25**,** 402-8.

Lopez-Hoyos M, Segundo DS, Fernandez-Fresnedo G, Marin MJ, Gonzalez-Martin V, Arias M 2009. Regulatory T cells in renal transplantation and modulation by immunosuppression. *Transplantation,* 88**,** S31-9.

Lu L, Qian XF, Rao JH, Wang XH, Zheng SG, Zhang F 2010. Rapamycin promotes the expansion of CD4(+) Foxp3(+) regulatory T cells after liver transplantation. *Transplant Proc,* 42**,** 1755-7.

Luan Y, Mosheir E, Menon MC, Wilson D, Woytovich C, Ochando J, et al. 2013. Monocytic myeloid-derived suppressor cells accumulate in renal transplant patients and mediate CD4(+) Foxp3(+) Treg expansion. *Am J Transplant,* 13**,** 3123-31.

Lyons AB, Parish CR 1994. Determination of lymphocyte division by flow cytometry. *J Immunol Methods,* 171**,** 131-7.

Magil AB 2009. Monocytes/macrophages in renal allograft rejection. *Transplant Rev (Orlando),* 23**,** 199-208.

Makki K, Taront S, Molendi-Coste O, Bouchaert E, Neve B, Eury E, et al. 2014. Beneficial metabolic effects of rapamycin are associated with enhanced regulatory cells in diet-induced obese mice. *PLoS One,* 9**,** e92684.

Maurizi G, Della Guardia L, Maurizi A, Poloni A 2018. Adipocytes properties and crosstalk with immune system in obesity-related inflammation. *J Cell Physiol,* 233**,** 88-97.

Meng F, Chen S, Guo X, Chen Z, Huang X, Lai Y, et al. 2014. Clinical significance of myeloid-derived suppressor cells in human renal transplantation with acute T cell-mediated rejection. *Inflammation,* 37**,** 1799-805.

Mercalli A, Calavita I, Dugnani E, Citro A, Cantarelli E, Nano R, et al. 2013. Rapamycin unbalances the polarization of human macrophages to M1. *Immunology,* 140**,** 179-90.

Milner JJ, Beck MA 2012. The impact of obesity on the immune response to infection. *Proc Nutr Soc,* 71**,** 298-306.

Miltenyi S, Muller W, Weichel W, Radbruch A 1990. High gradient magnetic cell separation with MACS. *Cytometry,* 11**,** 231-8.

Moes DJ, Guchelaar HJ, De Fijter JW 2015. Sirolimus and everolimus in kidney transplantation. *Drug Discov Today,* 20**,** 1243-9.

Molinero LL, Yin DP, Lei YM, Chen LQ, Wang Y, Chong AS, et al. 2016. High-Fat Diet-Induced Obesity Enhances Allograft Rejection. *Transplantation,* 100**,** 1015-1021.

Moraes-Vieira PM, Bassi EJ, Larocca RA, Castoldi A, Burghos M, Lepique AP, et al. 2013. Leptin deficiency modulates allograft survival by favoring a Th2 and a regulatory immune profile. [corrected]. *Am J Transplant,* 13**,** 36-44.

Mosser DM, Edwards JP 2008. Exploring the full spectrum of macrophage activation. *Nat Rev Immunol,* 8**,** 958-69.

Mueller NJ 2008. New immunosuppressive strategies and the risk of infection. *Transpl Infect Dis,* 10**,** 379-84.

Mundy-Bosse BL, Lesinski GB, Jaime-Ramirez AC, Benninger K, Khan M, Kuppusamy P, et al. 2011. Myeloid-derived suppressor cell inhibition of the IFN response in tumor-bearing mice. *Cancer Res,* 71**,** 5101-10.

Nagaraj S, Gupta K, Pisarev V, Kinarsky L, Sherman S, Kang L, et al. 2007. Altered recognition of antigen is a mechanism of CD8+ T cell tolerance in cancer. *Nat Med,* 13**,** 828-35.

Nakamura T, Nakao T, Ashihara E, Yoshimura N 2016. Myeloid-derived Suppressor Cells Recruit CD4(+)/Foxp3(+) Regulatory T Cells in a Murine Cardiac Allograft. *Transplant Proc,* 48**,** 1275-8.

Nakamura T, Nakao T, Yoshimura N, Ashihara E 2015. Rapamycin Prolongs Cardiac Allograft Survival in a Mouse Model by Inducing Myeloid-Derived Suppressor Cells. *Am J Transplant,* 15**,** 2364-77.

Nakamura T, Ushigome H 2018. Myeloid-Derived Suppressor Cells as a Regulator of Immunity in Organ Transplantation. *Int J Mol Sci,* 19.

Ng M, Fleming T, Robinson M, Thomson B, Graetz N, Margono C, et al. 2014. Global, regional, and national prevalence of overweight and obesity in children and adults during 1980-2013: a systematic analysis for the Global Burden of Disease Study 2013. *Lancet,* 384**,** 766-81.

Noris M, Casiraghi F, Todeschini M, Cravedi P, Cugini D, Monteferrante G, et al. 2007. Regulatory T cells and T cell depletion: role of immunosuppressive drugs. *J Am Soc Nephrol,* 18**,** 1007-18.

Ohl K, Tenbrock K 2018. Reactive Oxygen Species as Regulators of MDSC-Mediated Immune Suppression. *Front Immunol,* 9**,** 2499.

Okamoto Y, Christen T, Shimizu K, Asano K, Kihara S, Mitchell RN, et al. 2009. Adiponectin inhibits allograft rejection in murine cardiac transplantation. *Transplantation,* 88**,** 879-83.

Okano S, Abu-Elmagd K, Kish DD, Keslar K, Baldwin WM, 3rd, Fairchild RL, et al. 2018. Myeloid-derived suppressor cells increase and inhibit donor-reactive T cell responses to graft intestinal epithelium in intestinal transplant patients. *Am J Transplant,* 18**,** 2544-2558.

Okwan-Duodu D, Umpierrez GE, Brawley OW, Diaz R 2013. Obesity-driven inflammation and cancer risk: role of myeloid derived suppressor cells and alternately activated macrophages. *Am J Cancer Res,* 3**,** 21-33.

Ostrand-Rosenberg S 2018. Myeloid derived-suppressor cells: their role in cancer and obesity. *Curr Opin Immunol,* 51**,** 68-75.

Pawelec G, Verschoor CP, Ostrand-Rosenberg S 2019. Myeloid-Derived Suppressor Cells: Not Only in Tumor Immunity. *Front Immunol,* 10**,** 1099.

Peng D, Tanikawa T, Li W, Zhao L, Vatan L, Szeliga W, et al. 2016. Myeloid-Derived Suppressor Cells Endow Stem-like Qualities to Breast Cancer Cells through IL6/STAT3 and NO/NOTCH Cross-talk Signaling. *Cancer Res,* 76**,** 3156-65.

Pilat N, Wiletel M, Weijler AM, Steiner R, Mahr B, Warren J, et al. 2019. Treg-mediated prolonged survival of skin allografts without immunosuppression. *Proc Natl Acad Sci U S A,* 116**,** 13508-13516.

Porta C, Consonni FM, Morlacchi S, Sangaletti S, Bleve A, Totaro MG, et al. 2020. Tumor-Derived Prostaglandin E2 Promotes p50 NF-kappaB-Dependent Differentiation of Monocytic MDSCs. *Cancer Res,* 80**,** 2874-2888.

Qiao YC, Pan YH, Ling W, Tian F, Chen YL, Zhang XX, et al. 2017. The Yin and Yang of regulatory T cell and therapy progress in autoimmune disease. *Autoimmun Rev,* 16**,** 1058-1070.

Quante M, Dietrich A, Elkhal A, Tullius SG 2015. Obesity-related immune responses and their impact on surgical outcomes. *Int J Obes (Lond),* 39**,** 877-83.

Quante M, Heinbokel T, Edtinger K, Minami K, Uehara H, Nian Y, et al. 2018. Rapamycin Prolongs Graft Survival and Induces CD4+IFN-gamma+IL-10+ Regulatory Type 1 Cells in Old Recipient Mice. *Transplantation,* 102**,** 59-69.

Raber PL, Thevenot P, Sierra R, Wyczechowska D, Halle D, Ramirez ME, et al. 2014. Subpopulations of myeloid-derived suppressor cells impair T cell

responses through independent nitric oxide-related pathways. *Int J Cancer,* 134**,** 2853-64.
Riquelme P, Tomiuk S, Kammler A, Fandrich F, Schlitt HJ, Geissler EK, et al. 2013. IFN-gamma-induced iNOS expression in mouse regulatory macrophages prolongs allograft survival in fully immunocompetent recipients. *Mol Ther,* 21**,** 409-22.
Rojas Marquez JD, Ana Y, Baigorri RE, Stempin CC, Cerban FM 2018. Mammalian Target of Rapamycin Inhibition in Trypanosoma cruzi-Infected Macrophages Leads to an Intracellular Profile That Is Detrimental for Infection. *Front Immunol,* 9**,** 313.
Sakaguchi S, Yamaguchi T, Nomura T, Ono M 2008. Regulatory T cells and immune tolerance. *Cell,* 133**,** 775-87.
Saltiel AR, Olefsky JM 2017. Inflammatory mechanisms linking obesity and metabolic disease. *Journal of Clinical Investigation,* 127**,** 1-4.
Sato A, Kasai S, Kobayashi T, Takamatsu Y, Hino O, Ikeda K, et al. 2012. Rapamycin reverses impaired social interaction in mouse models of tuberous sclerosis complex. *Nat Commun,* 3**,** 1292.
Saxton RA, Sabatini DM 2017. mTOR Signaling in Growth, Metabolism, and Disease. *Cell,* 168**,** 960-976.
Scheurer J, Reisser T, Leithauser F, Messmann JJ, Holzmann K, Debatin KM, et al. 2020. Rapamycin-based graft-versus-host disease prophylaxis increases the immunosuppressivity of myeloid-derived suppressor cells without affecting T cells and anti-tumor cytotoxicity. *Clin Exp Immunol*.
Schmid I, Krall WJ, Uittenbogaart CH, Braun J, Giorgi JV 1992. Dead cell discrimination with 7-amino-actinomycin D in combination with dual color immunofluorescence in single laser flow cytometry. *Cytometry,* 13**,** 204-8.
Schroder M, Krotschel M, Conrad L, Naumann SK, Bachran C, Rolfe A, et al. 2018. Genetic screen in myeloid cells identifies TNF-alpha autocrine secretion as a factor increasing MDSC suppressive activity via Nos2 up-regulation. *Sci Rep,* 8**,** 13399.
Scotland RS, Stables MJ, Madalli S, Watson P, Gilroy DW 2011. Sex differences in resident immune cell phenotype underlie more efficient acute inflammatory responses in female mice. *Blood,* 118**,** 5918-27.
Shi H, Han X, Sun Y, Shang C, Wei M, Ba X, et al. 2018. Chemokine (C-X-C motif) ligand 1 and CXCL2 produced by tumor promote the generation of monocytic myeloid-derived suppressor cells. *Cancer Sci,* 109**,** 3826-3839.
Sica A, Mantovani A 2012. Macrophage plasticity and polarization: in vivo veritas. *J Clin Invest,* 122**,** 787-95.
Sun L, Clavijo PE, Robbins Y, Patel P, Friedman J, Greene S, et al. 2019. Inhibiting myeloid-derived suppressor cell trafficking enhances T cell immunotherapy. *JCI Insight,* 4.
Taki M, Abiko K, Baba T, Hamanishi J, Yamaguchi K, Murakami R, et al. 2018. Snail promotes ovarian cancer progression by recruiting myeloid-derived suppressor cells via CXCR2 ligand upregulation. *Nat Commun,* 9**,** 1685.
Talmadge JE, Gabrilovich DI 2013. History of myeloid-derived suppressor cells. *Nat Rev Cancer,* 13**,** 739-52.
Tannenbaum CS, Rayman PA, Pavicic PG, Kim JS, Wei W, Polefko A, et al. 2019. Mediators of Inflammation-Driven Expansion, Trafficking, and

Function of Tumor-Infiltrating MDSCs. *Cancer Immunol Res,* 7**,** 1687-1699.
Thomson AW, Turnquist HR, Raimondi G 2009. Immunoregulatory functions of mTOR inhibition. *Nat Rev Immunol,* 9**,** 324-37.
Thorn M, Guha P, Cunetta M, Espat NJ, Miller G, Junghans RP, et al. 2016. Tumor-associated GM-CSF overexpression induces immunoinhibitory molecules via STAT3 in myeloid-suppressor cells infiltrating liver metastases. *Cancer Gene Ther,* 23**,** 188-98.
Tremmel M, Gerdtham UG, Nilsson PM, Saha S 2017. Economic Burden of Obesity: A Systematic Literature Review. *Int J Environ Res Public Health,* 14.
Tu S, Bhagat G, Cui G, Takaishi S, Kurt-Jones EA, Rickman B, et al. 2008. Overexpression of interleukin-1beta induces gastric inflammation and cancer and mobilizes myeloid-derived suppressor cells in mice. *Cancer Cell,* 14**,** 408-19.
Walzog B, Fandrey J 2018. Abwehrmechanismen des Körpers. *In:* Pape HC, Kurtz A, Silbernagl S (ed.) *Physiologie.* Georg Thieme Verlag, Stuttgart.
Wang D, Sun H, Wei J, Cen B, Dubois RN 2017. CXCL1 Is Critical for Premetastatic Niche Formation and Metastasis in Colorectal Cancer. *Cancer Res,* 77**,** 3655-3665.
Wei C, Wang Y, Ma L, Wang X, Chi H, Zhang S, et al. 2018. Rapamycin Nano-Micelle Ophthalmic Solution Reduces Corneal Allograft Rejection by Potentiating Myeloid-Derived Suppressor Cells' Function. *Front Immunol,* 9**,** 2283.
Winer S, Chan Y, Paltser G, Truong D, Tsui H, Bahrami J, et al. 2009. Normalization of obesity-associated insulin resistance through immunotherapy. *Nat Med,* 15**,** 921-9.
World Health Organization. 2020. *Obesity and Overweight* [Online]. Available: https://www.who.int/news-room/fact-sheets/detail/obesity-and-overweight [Accessed 09.11.2020].
Wu DA, Robb ML, Forsythe JLR, Bradley C, Cairns J, Draper H, et al. 2019. Recipient Comorbidity and Survival Outcomes after Kidney Transplantation: a UK-wide Prospective Cohort Study. *Transplantation*.
Yang F, Li Y, Wu T, Na N, Zhao Y, Li W, et al. 2016. TNFalpha-induced M-MDSCs promote transplant immune tolerance via nitric oxide. *J Mol Med (Berl),* 94**,** 911-20.
Yang F, Li Y, Zou W, Xu Y, Wang H, Wang W, et al. 2019. Adoptive transfer of IFN-gamma-induced M-MDSCs promotes immune tolerance to allografts through iNOS pathway. *Inflamm Res,* 68**,** 545-555.
Youn JI, Nagaraj S, Collazo M, Gabrilovich DI 2008. Subsets of myeloid-derived suppressor cells in tumor-bearing mice. *J Immunol,* 181**,** 5791-802.
Yu J, Du W, Yan F, Wang Y, Li H, Cao S, et al. 2013. Myeloid-derived suppressor cells suppress antitumor immune responses through IDO expression and correlate with lymph node metastasis in patients with breast cancer. *J Immunol,* 190**,** 3783-97.
Yuan J, Bagley J, Iacomini J 2015. Hyperlipidemia Promotes Anti-Donor Th17 Responses That Accelerate Allograft Rejection. *Am J Transplant,* 15**,** 2336-45.

Zhang C, Wang S, Li J, Zhang W, Zheng L, Yang C, et al. 2017. The mTOR signal regulates myeloid-derived suppressor cells differentiation and immunosuppressive function in acute kidney injury. *Cell Death Dis,* 8**,** e2695.

Zhang C, Wang S, Yang C, Rong R 2016. The Crosstalk between Myeloid Derived Suppressor Cells and Immune Cells: To Establish Immune Tolerance in Transplantation. *J Immunol Res,* 2016**,** 4986797.

Zhang W, Li J, Qi G, Tu G, Yang C, Xu M 2018. Myeloid-derived suppressor cells in transplantation: the dawn of cell therapy. *J Transl Med,* 16**,** 19.

Zhang Y, Bi Y, Yang H, Chen X, Liu H, Lu Y, et al. 2014. mTOR limits the recruitment of CD11b+Gr1+Ly6Chigh myeloid-derived suppressor cells in protecting against murine immunological hepatic injury. *J Leukoc Biol,* 95**,** 961-70.

Zhao Y, Shen XF, Cao K, Ding J, Kang X, Guan WX, et al. 2018. Dexamethasone-Induced Myeloid-Derived Suppressor Cells Prolong Allo Cardiac Graft Survival through iNOS- and Glucocorticoid Receptor-Dependent Mechanism. *Front Immunol,* 9**,** 282.

Zhou L, Miao K, Yin B, Li H, Fan J, Zhu Y, et al. 2018. Cardioprotective Role of Myeloid-Derived Suppressor Cells in Heart Failure. *Circulation,* 138**,** 181-197.

7. Declaration of own contribution / Erklärung zum Eigenanteil

Die Arbeit wurde in der Universitätsklinik für Allgemeine, Viszeral- und Transplantationschirurgie unter Betreuung von Prof. Dr. Alfred Königsrainer durchgeführt.

Die Konzeption der Studie erfolgte durch Dr. Markus Quante, Oberarzt und PD Dr. Saeed Kolahian, wissenschaftlicher Mitarbeiter.

Sämtliche Versuche und Datenanalysen wurden nach Einarbeitung durch PD Dr. Saeed Kolahian, Dr. Markus Quante und Chiel van Geffen von mir eigenständig durchgeführt. Die RNA-Isolation und reverse Transkription für die qPCR-Analysen wurden aus zeitlich-organisatorischen Gründen durch eine studentische Hilfskraft durchgeführt. Die Multiplex-Immunosandwichassay-Experimente (Luminex®) sowie deren Auswertung wurden am Naturwissenschaftlichen und Medizinischen Institut Reutlingen durch Anna Guenther und Dr. Nicole Schneiderhan-Marra durchgeführt. Die statistische Auswertung erfolgte eigenständig durch mich.

Ich versichere, das Manuskript selbständig verfasst zu haben und keine weiteren als die von mir angegebenen Quellen verwendet zu haben.

Tübingen, den 04.01.2023

8. Publication

The results of this work have been published in the following publication:

Astrid Deißler, Andrea Della Penna, Chiel van Geffen, Irene Gonzalez-Menendez, Leticia Quintanilla-Martinez, Anna Günther, Nicole Schneiderhan-Marra, Dominik Hartl, Bernd Nürnberg, Alfred Königsrainer, Saeed Kolahian, Markus Quante – **Rapamycin delays allograft rejection in obese graft recipients through induction of myeloid-derived suppressor cells** – Immunology Letters – 2021 – Volume 236 – Pages 1-11.

9. Acknowledgments

I thank everyone who supported me throughout the different phases of this project from exploring a new field of research *via* conducting the experiments to writing the thesis for making this time worth remembering.

First of all, I want to thank Dr. Markus Quante for the opportunity to contribute to the work on this interesting topic of high clinical relevance, and for his unconditional support regardless of time of day or heavy workload.

I am particularly grateful to PD Dr. Saaed Kolahian for the best possible supervision in the lab, particularly for his advice whenever needed and for valuing my opinions when decisions had to be made.

Special thanks are deserved by Chiel van Geffen for his in many ways helpful support, covering all aspects of this work from its scientific background to plain experimental details. Even more important was his steady encouragement to ensure high motivation even in phases of heavy workload.

I also want to thank Prof. Dr. Alfred Königsrainer for giving me the opportunity to continue my medial training at the Department of General, Visceral and Transplantation Surgery, his general support, and for being a member of the jury evaluating the doctoral thesis. Prof. Dr. Dr. Bernd Nürnberg I thank for the possibility to carry out the experiments in the facilities of the Department of Experimental and Clinical Pharmacology and Pharmacogenomics.

To perform multiplex immunoassays would not have been possible without the enjoyable and productive collaboration with Dr. Nicole Schneiderhan-Marra and Anna Günther (NMI, Reutlingen).

I am grateful to the IZKF of the University of Tübingen, represented by Dr. Inka Montero, for financial and otherwise support through an IZKF fellowship.

I also thank Renate Riehle, Claudia Müller, Dr. Veronika Leiss, Prof. Dr. Sandra Beer-Hammer and all other members of the research groups in the lab who helped to solve technical issues. These include Leon and other students who, in

addition to mutual support, crucially contributed to the always enjoyable working atmosphere.

I am deeply grateful to my parents not only for their ongoing general support, but also for the numerous helpful discussions of scientific and technical questions that came up during the work on this project, and for language polishing of the thesis.

Conscious of the animal sacrifices required, I did my best to perform all experiments in a responsible manner.

Last, but not least, I thank Felix for his patience and ideas.

10. Appendix

Table 8: Postoperative monitoring score sheet.

		points
general condition	clean and shiny fur free body orifices	0
	blunt and ruffled fur dull eyes	1
	stuck and moistened body orifices abnormal posture dehydration	5
	seizures, paralysis breathing sounds cold feeling	20
spontaneous behavior	normal behavior (sleeping, reaction to touching, curiosity, social contacts)	0
	limited motor activity, hyperkinetic back flexion abdomen retraction	1
	isolation pain expression, apathy massive hyperkinetic coordination disorder	5
	automutilation	20
procedure-specific criteria	non-irritant local findings no manipulation signs	0
	suture manipulation hematoma	1
	surrounding erythema secretion	5
	bleeding abscess > 50% allograft rejection	20
body weight	unaffected or weight gain	0
	reduction by 10%	10
	reduction by 20%	20

score	evaluation / measures	
0	no stress	
1-10	low stress	
	1-5	intensification of monitoring
	6-10	supporting measures
11-20	medium stress	
	11-15	consultation of veterinarians
	16-19	medical measures
	20	euthanasia